Mobility of Small Molecules in PEO-PPO-PEO Triblock Copolymer (F127 and P104) Hydrogels

by

Heliasadat Hosseini Nejad

B.Sc, Sharif University of Technology, 2017

M.Sc, University of Victoria, 2021

A Thesis Submitted in Partial Fulfillment
of the Requirements for the Degree of

MASTER OF SCIENCE

in the Department of Chemistry.

Supervisory Committee

Dr. Cornelia Bohne (Department of Chemistry)

Supervisor

Dr. Matthew Moffitt (Department of Chemistry)

Co-Supervisor or Departmental Member

Abstract

Pluronics are triblock copolymers of poly(ethylene oxide) (PEO) and poly(propylene oxide) (PPO) available in different molecular weights and PPO/PEO ratios. Pluronic hydrogels are able to dissolve hydrophobic compounds and they have application in different areas including drug delivery systems and oil recovery. The structure of Pluronic polymers can be designed for specific application by changing the size and ratio of the PPO and PEO blocks. In aqueous environments, the PPO blocks of different unimers form aggregates as they are more hydrophobic compared to the PEO blocks, and in the aggregates the PPOs have less exposure to water. The PEO blocks that are still hydrophilic remain soluble in water and form a shell around the PPO aggregated core. Moreover, some of the Pluronic copolymer aqueous solutions can form hydrogels at elevated temperatures. The aim of this thesis is to study the microheterogeneity of two different Pluronic hydrogels using singlet excited state probes and also study the mobility of small molecules in Pluronic hydrogels using triplet excited state probes.

In the first project, the properties of different microenvironments in Pluronic F127 ($PEO_{99}PPO_{65}PEO_{99}$) were characterized. The quenching of singlet excited state probes was used to determine the number and characteristics of solubilization sites in F127 hydrogels. This method was used to gain information on the accessibility of different quenchers to singlet excited molecules bound to the micellar structures. Singlet excited states are short lived, and these excited states do not move within the gel before their decay to the ground state. The techniques used for these studies were steady-state fluorescence and time-resolved fluorescence spectroscopies. My results showed that there are different solubilization sites in F127 micelles and the accessibility of quenchers to the singlet excited molecules bound to the micellar structure depends on the nature of the quencher and the size of the excited molecules.

In the second project, the different microenvironments in Pluronic P104 ($PEO_{27}PPO_{61}PEO_{27}$) were characterized, and these results were compared with those obtained for the Pluronic F127. Pluronic P104 has similar units of PPO blocks as F127 but different units of PEO blocks which results in different properties between these two

Pluronic copolymers. My results showed that the solubilization sites inside Pluronic micelles changes with the change in PEO/PPO ratio.

In the third project, I studied the mobility of different small molecules between aqueous and micellar environments in the F127 hydrogel by quenching triplet excited state probes. Excited triplet states are suitable for such studies because their lifetimes are longer than the lifetimes for singlet excited states. The laser flash photolysis technique was used for this aim. The results showed that the exit from the micellar environment is slow and depend on the size and hydrophobicity of the probe molecules.

Table of Contents

List of Tables

List of Figures

List of Charts and Schemes

List of Abbreviations

Å	Ångstrom
a_0	Amplitude in absorbance
A_i	Pre-exponential factors for species i
χ^2	Reduced chi-squared parameter
°C	Degree Celsius
cm	Centimeter
CMC	Critical micellization concentration
CMT	Critical micelle temperature
Da	Daltons
ΔA	Change in absorbance
DLS	Dynamic light scattering
DSC	Differential scanning calorimetry
e	Exponential
Eq	Equation
Fig	Figure
g	Gram
γ	Shear strain
G*	Complex modulus
G"	Loss modulus
G'	Storage modulus
h	Hour
HPLC	High-performance liquid chromatography
Hz	Hertz

I_0	Initial intensity
I	Fluorescence intensity
i	Imaginary unit
IRF	Instrument response function
k_0	Diffusion-controlled bimolecular rate constant
k_0^{F127}	Quenching rate constant in F127 micelle in the absence of quencher
k_0^M	Quenching rate constant in the micelle in the absence of quencher
k_{as}	Association rate constant
k_{dis}	Dissociation rate constant
k_{obs}	Observed rate constant
k_q	Quenching rate constant
k_q^{F127}	Quenching rate constant in F127 micelle in the presence of quencher
k_q^M	Quenching rate constant in the micelle in the presence of quencher
K_{SV}	Stern-Volmer constant
LED	Light emitting diode
LFP	Laser flash photolysis
LMW	Low molecular weight
LVR	Linear viscoelastic region
M	Molar
μM	Micromolar
μm	Micrometer
μs	Microsecond
min	Minute
mL	Milliliter

mM	Millimolar
mm	Millimetre
MW	Molecular weight
MΩ	Megaohm
N	Aggregation number
NaI	Sodium iodide
$NaNO_2$	Sodium nitrite
NM	Nitromethane
nm	Nanometer
Np	Naphthalene
2-NpC	2-naphthoic acid
NpOH	R-(-)-1-(2-naphthyl)ethanol
ns	Nanosecond
ω	Frequency
Pa	Pascal
PDI	Polydispersity
PE	Protection efficiency
PEO	Poly(ethylene oxide)
Pht	Phenanthrene
ppm	Parts per million
PPO	Poly(propylene oxide)
$[Q]$	Quencher concentration
s	Second
SANS	Small angle neutron scattering

SAXS	Small angle X-ray scattering
Σ	Sum
sol	Solution
SPC	Single photon counter
t	Time
tanδ	Loss factor
τ_i	Lifetime of emissive species *i*
τ	Fluorescence lifetime
τ_{obs}	Observed lifetime
<τ>	Average lifetime
T_{gel}	Gelation temperature
UV	Ultra-violet
v	Volume
w	Weight
wt	Weight

Acknowledgments

I would like to express my gratitude to Dr. Cornelia Bohne, my supervisor, for all her support, knowledge, dedication, and patience not only during my research but also in the difficult moments of my life. Thanks for all the motivating and I highly appreciate that I had the best mentor during these years to complete my research project and my thesis. I would like to thank Luis Netter for his technical and software support. I appreciate Dr. Suma S. Thomas for training me and her advice through my research and also for analyzing my data in chapter 5.

I also would like to thank my committee member Dr. Matthew Moffitt for his advice and feedback on my research and thesis and also for letting me work in his lab.

I would like to thank the present and previous members of the Bohne group: Mehraveh, Jessy, Kevin, Sree, Ankur, Guan, Alessandra, Amilcar and Stas; for their suggestions and support in many aspects during the past years.

My special gratitude goes to my mom for her endless love and support.

Lastly, I would like to thank PoND, ACS PRF, NSERC and UVic for financial support of my research.

Dedication

To my Mom

1 Chapter 1: Introduction

1.1 Hydrogels

Hydrogels are composite materials made of polymer and water with a three-dimensional network which can absorb large amounts of water or physiological fluids without losing dimensional stability.[1] In 1960, Wichterle and Lim proposed the first hydrogel for soft contact lenses; a copolymer of 2-hydroxyethyl methacrylate with ethylene dimethacrylate.[2] Since then hydrogels have attracted significant attention due to their unique properties.[3]

Smart hydrogels are environmentally responsive materials which can undergo sol-gel phase transition upon changing their environmental conditions such as temperature,[4] pH,[5] light,[6] magnetic fields,[7] electrical fields[8] and chemicals.[9] Hence, in response to external stimuli, stimuli-responsive hydrogels change their structural and phase properties resulting in an enormous potential for various advanced technological applications.[10-11]

1.1.1 Different classes of hydrogels

Hydrogels are classified using several methods and one of them is based on the type of crosslinking. Hydrogel networks are formed through many different processes which are divided into two major classes: physical and chemical categories.

Physical or reversible hydrogels are formed through polymer chains entanglements and/or secondary forces such as hydrogen-bonding, ionic bonding, hydrophobic association, and stereo complexation.[10, 12] The sol-gel transition in physical hydrogels is controlled by environmental conditions, such as pH, temperature and the ionic strength of the solution. Physically crosslinked gels have advantages over chemically crosslinked hydrogels such as the lack of toxic crosslinking agents. Also, the components of physical hydrogels self-assemble to form a gel spontaneously in response to changes in their environmental conditions. Thus, these physical gels have a great potential for application in pharmaceutical and biomedical areas.

Chemically crosslinked or permanent hydrogels have relatively higher mechanical strength, mechanical stability and longer degradation times compared to reversible hydrogels owing to the covalent bonding that exists in the permanent gels.[1] Chemically crosslinked gels can be obtained by polymerization, radiation, small-molecule crosslinking, and polymer–polymer crosslinking. In order to optimize and tune the properties of this type of hydrogels, it is possible to control the degree of crosslinking making these gels suitable for different applications. However, the presence of residual monomers and difficulties in purification of this type of hydrogels have resulted in their limited use for biomedical applications.[13]

There is another class of hydrogels made through self-assembly of small molecules known as low molecular weight (LMW) gels or supramolecular gels. The small molecules self-assemble to form a three-dimensional network of fibers that pack through noncovalent interactions.[14-15] The LMW gels have different mechanical properties compared to other types of hydrogels or biopolymeric gels. In general, for most of LMW gels, the mechanical characteristics are weaker compared to high molecular weight hydrogels or polymeric gels.[16] Some advantages of LMW hydrogels is thermo-reversibility, low minimum concentrations for gel formation, high tolerance to the presence of additives like salts.[17] The twisted fibers which can form a gel network, themselves are made of aggregates. These aggregates are formed through hydrogen bonding, π-π stacking, and hydrophobic interactions.[18-19]

1.1.2 Hydrogel applications

The application of hydrogels involves a wide spectrum of many different fields including engineering, biology and pharmaceutical sciences.[3] Below I described the two examples of polymeric hydrogel applications in solubilizing water-insoluble compounds.

Oily wastewater produced from petroleum industry is environmentally concerning; in this respect polymeric membranes play an important role to separate oil/water emulsion.[20] For instance, poly(ethylene oxide–propylene oxide) block copolymers have been utilized to separate petroleum industry emulsions.[21] On the other hand, oil might be produced along with gas and water. The gas component can form foam with oil and result

in losing precious crude oil. So, the role of defoamers is important to increase the oil recovery and non-ionic surfactants are one of the candidates of defoamers.[22] Polymeric hydrogels can be utilized as plugging agents to plug the large permeable layers of the wells so that water fluid is able to penetrate to the low-permeable layers and sweep the remaining oil to increase the profitability of production.

Hydrogels due to their biocompatibility and the similarity of their physical properties to natural tissue, have a wide variety of applications in the biomedical field such as cell therapeutics, wound healing, cartilage/bone regeneration and for the sustained release of drugs.[12] Injectable and stimuli responsive hydrogels have been used as drug carriers in the body to achieve sustained drug release. These drug carriers have protective effects and are able to release the drug in specific target sites, such as tumor tissue, in response to different stimuli, such as acidic pH or higher temperature which are specific for the tumor tissues.[23]

1.2 Poly-ethylene oxide (PEO)/poly-propylene oxide (PPO) triblock copolymers

Amphiphilic triblock copolymers of PEO_n-PPO_m-PEO_n (the structure is shown in chart 1.1), are commercially known as Pluronics or Poloxamers and have been used in many applications that require solubilization of water-insoluble compounds in aqueous medium because of having both hydrophobic and hydrophilic moieties in Pluronic copolymers and also these copolymers have low toxicity[24-26] they have application in cosmetic products and creams.[27] Some of the Pluronic copolymers have been approved as injectable drug delivery systems for humans by the US Food and Drug Administration. This approval has led to intensive studies on the use of Pluronic as excipients for pharmaceuticals.[24]

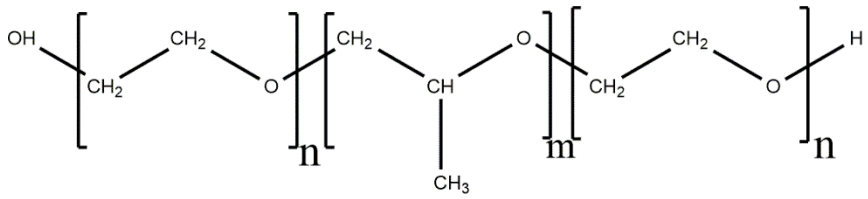

Chart 1.1. The general structure for PEO-PPO-PEO triblock copolymers.

Pluronic copolymers are available in a variety of different compositions and molecular weights through the synthesis of triblock copolymers with various PEO and PPO contents. It should be mention that PPO blocks are more hydrophobic compared to PEO blocks, therefore by changing the length of these two blocks it is possible to achieve copolymers with different characteristics. In this respect, it is possible to design triblock copolymers with optimum properties based on the requirements for a specific application.[25, 28-29]

This class of surfactants have amphiphilic characteristic and they are capable of self-assembling into micelles in aqueous solutions above critical conditions.[30] The other appealing properties of Pluronic copolymers is thermo-reversibility, which has made these polymers suitable for many different applications including drug delivery.[31-32] Some of the Pluronic copolymers are able to form gels depending on various experimental conditions. In the following sections, micellization and gel formation of Pluronic polymers are described further and the studies conducted by other groups to investigate these unique copolymers are mentioned.

1.2.1 Micelle formation in PEO-PPO-PEO triblock copolymers

Temperature and the polymer concentration are two factors which control the formation of thermodynamically stable Pluronic micelles.[28, 33-34] At low temperatures or concentrations, unimers are dispersed in water and surrounded by water molecules forming hydrogen bonds between the unimers and solvent molecules.[34-35] Upon increasing the temperature or polymer concentration, self-assembly occurs (Fig 1.1) where the micelles consist of a PPO dominated core and hydrated-PEO dominated corona.[36] In Pluronic copolymers spherical micelles form in solvents which dissolve one block type better than the other block.[37] For instance, Pluronic L64 spherical micelles were observed using small angle X-ray scattering (SAXS) and small angle neutron scattering (SANS).[38]

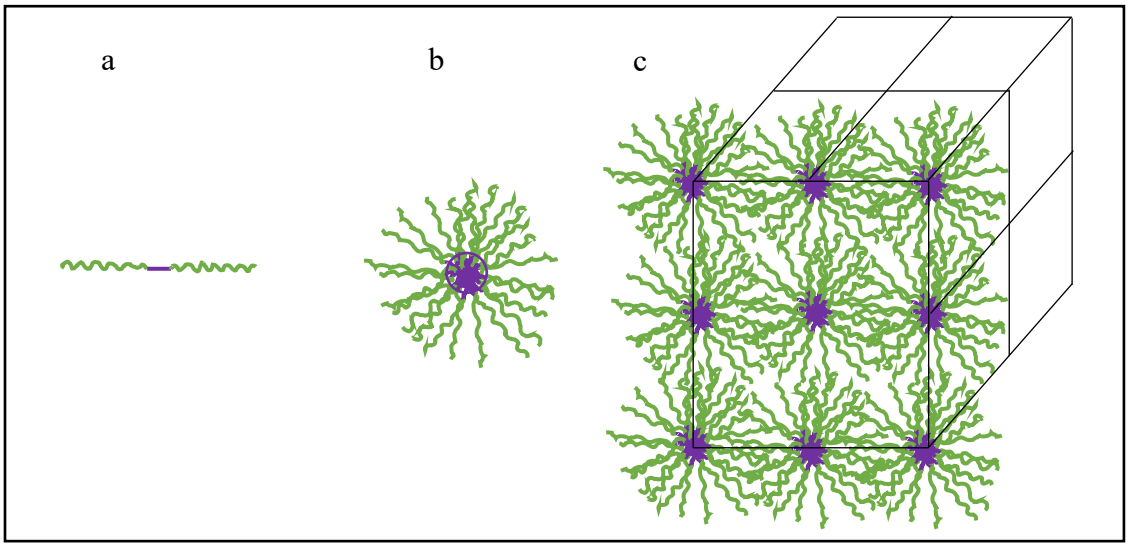

Figure 1.1. Schematic of different phases for Pluronic polymers: a) free unimer b) micelle c) spherical micelles crystallized into a cubic.

The thermodynamically stable spherical micelles form upon increasing temperature of Pluronic aqueous solution, because the more hydrophilic PEO blocks remain soluble in water while the more hydrophobic PPO blocks become less soluble upon heating due to a reduction of the number of hydrogen bonds between water molecules and PPO blocks.[39-40] In this regard, PPO blocks aggregate to have less exposure to water molecules and form the core of the micelles while PEO blocks make the corona shell of the micelles. From the thermodynamic point of view, the reason for micelle formation at elevated temperature is the major role of entropy in the micellization process. Aggregation of unimers in water increases the entropy of the whole system. On the other hand, Pluronic micellar formation is highly endothermic, but enthalpy has a minor role in this process.[33, 39, 41] The other important feature of Pluronic micelles is the thermo-reversibility of micellar formation. In this regard, with decreasing temperature micelles shifts toward the freely dispersed unimers in aqueous solution.[42]

There are critical concentrations and temperature defined for the micellization of Pluronic polymers. Micelles are formed when the polymer concentration is increased above the critical micellization concentration (CMC). The CMC for Pluronic polymers changes with temperature such that increasing temperature decreases the CMC values or, in other

words, heating helps micellar formation at lower concentrations. On the other hand, the critical micelle temperature (CMT) decreases with increasing polymer concentration.[33]

Pluronic polymers show chemical heterogeneity and compositional polydispersity; consequently, the CMC and CMT values for Pluronic block copolymers are not sharp but occur over a range of polymer concentrations and temperatures. Hence, for Pluronic polymers there is a transition temperature range to form micelles during which the equilibrium between micelles and unimers shifts towards micelles.[33-34] Changing the Pluronic copolymer composition (PEO/PPO ratio) alters the CMC and CMT such that both the CMC and the CMT decrease with increasing the PPO block length because the PPO block plays a major role in micellization.[43-44] In this regard, for Pluronics with the same PEO block content but different hydrophobic PPO content, the polymer that has the larger hydrophobic block forms micelles at lower concentrations and lower temperatures. In contrast to the role of PPO blocks on the micellization process, the effect of the length of the hydrophilic PEO block on the micellization process is low.[33]

The Pluronic composition has a direct influence on the molecular weight of the polymer. For polymers with the same PPO/PEO ratio, the polymers with higher molecular weight form micelles at lower concentrations and temperatures.[33] The polarity of the micelles is also affect by the polymer composition of Pluronics . The polarity of different Pluronic micelles has been investigated and it was found that for Pluronic polymers with the same PPO block size, but higher PEO block segments, the micelles are more polar compared to the ones with lower PEO content.[45] A list of different Pluronic polymers with their various physical properties is shown in Table 1.1.[33]

Table 1.1. Physical properties of different Pluronic copolymers.[33]

Polymer	Molecular weight / Da	PPO block weight / Da	PO units	EO units
L64	2900	1740	30	2×13
P85	4600	2300	40	2×26
F88	11400	2280	39	2×103
P104	5900	3540	61	2×27
F108	14600	2920	50	2×132
P123	5750	4025	69	2×19
F127	12600	3780	65	2×100

The structure and phase behavior of Pluronic micelles have been investigated by many researchers.[29, 43-44, 46-48] The micellar size increases with increasing Pluronic concentration above the CMC.[49] Increasing temperatures increase the micellar core size, but the micelle radius remains almost constant.[43, 50] To elaborate more, upon heating, PPO blocks stretch and also PEO blocks at the interface between the core and corona can join the core of the micelle making the core larger, while the corona shell loses water molecules and PEO blocks contract. These two opposing effects lead to little change for the radius of the micelle.[29, 51-53]

For some polymeric aqueous solutions, there is a polymer chain exchange between micelles and the bulk solution.[54] Pluronic micelles also have dynamic characteristic that allows the polymer chains to move between the micelles.[36] For Pluronic polymers, the lifetime of a micelle defined as a time during which the micelle stays intact as an entity with a given aggregation number.[55] The average lifetime of a unimer within a Pluronic (PEO_{28}-PPO_{48}-PEO_{28}) micelle was estimated to be around 1 μs at 20 °C.[56]

The aggregation dynamics of Pluronic copolymers is complex consisting of three relaxation processes as was observed in Pluronic L64 ($PEO_{13}PPO_{30}PEO_{13}$).[55] The complex dynamics of Pluronic micelles is due to the two well-defined regions of core and corona where each region has its own dynamics.

With increasing temperature, during the first relaxation process, unimers aggregate to form micelles resulting in the increase of aggregation number and micellar size. However, these micelles are not thermodynamically stable. The association of unimers to

form micelles is much slower than the diffusion rate constant and increasing the polymer's molecular weight and PEO content can further slow down the first process.[55, 57] During the second relaxation process, with increasing temperature the micellar core becomes dehydrated, and a redistribution of micellar sizes occurs. Increasing the molecular weight makes this relaxation process more complex because of the enhanced entanglements of the PEO chains which makes it difficult for PPO blocks to form the core. In the final relaxation process, micelles form clusters and larger aggregates and also more unimers are incorporated into micelles. During the last process the amount of unimers in solution is very low.[55] Finally, for Pluronic copolymers, the unimers and micelles are always in equilibrium in the solution and increasing temperature leads to decrease in free unimers concentration in the aqueous phase.

1.2.2 Gel formation in PEO-PPO-PEO triblock copolymers

The ordered structure of Pluronic gels is based on the close packing of micelles into a crystalline lattice.[58-59] Differential scanning calorimetry (DSC) measurements were used to study the gelation of PEO-PPO-PEO copolymers. The formation of the stiff gel was explained as a result from the arrangement of the micelles into an ordered network. Indeed, for gel formation a minimum entanglement between PEO chains is required and the gelation temperature increases with increasing PEO content.[60] Moreover, an increase in the polymer concentration leads to a decrease in the gelation temperature.[43] The minimum concentration to form gel decreases with increasing PPO content of the Pluronic.[60]

Not all Pluronic copolymers are able to form gels even at elevated temperatures and polymer concentrations. For these Pluronic polymers, upon increasing temperature or polymer concentration, the micellar solution forms lyotropic liquid crystalline phases such as hexagonal and lamellar. This process leads to the tendency for phase separation and this segregation increases with increasing polymer molecular weight. [29, 59]

Pluronic copolymers with high molecular weight and PEO content are able to form spherical micelles and subsequently form a cubic phase (Fig 1.1) upon increasing the polymer concentration or temperature.[59] The arranged cubic phase leads to formation of a gel network and the tendency of micelles to closely pack into regular cubic structures

increases when the repulsion between the micelles becomes stronger. For example, F127 is one of the Pluronic copolymers with high molecular weight and high PEO content which forms a gel. The gel structure of F127 was shown to correspond to a face-centered cubic structure from SAXS and SANS studies.[53] However, when the repulsion force between micelles is weaker the size of micelles increases as the concentration of polymer is raised and the micelles become elongated without forming cubic lattices.[30]

Formation of micellar cubic structures for Pluronics was further studied using cryogenic temperature transmission electron microscopy, which led to the determination of images for F127 ($PEO_{99}PPO_{65}PEO_{99}$) samples.[29] The ratio of PEO/PPO blocks and polymer molecular weight strongly affect the phase behavior and closed-packing of micellar nanostructures.[29, 59]

1.3 Viscoelastic properties of Pluronic hydrogels

As described above at low polymer concentrations and temperatures, micelles are physically separated and do not interact, however upon increasing these two parameters, close packing of micelles enables them to organize into a lattice and form a soft material that is called a gel. In thermo-reversible Pluronic hydrogels, the gelation temperature is defined as the temperature at which the polymer solution forms a stiff and clear gel.[43, 61-63] The micellar solution of Pluronic polymers at temperatures lower than gelation temperature behave as Newtonian fluid which is a fluid follows Newton's law of viscosity and there is a linear relation between shear stress and shear rate[64], while increasing polymer concentration, enhances viscosity.[65] The sol-gel transition temperature of Pluronic hydrogels can be measured with a number of different techniques such as Fourier transform infrared spectroscopy[62], DSC[43, 62] and rheology.[43, 46, 62, 66] Rheology can be used to study both the viscoelastic behavior of materials and to determine the gelation temperature of hydrogels.[67] In the following, some properties that are specific to viscoelastic materials are described.

Gels are viscoelastic materials which show both viscous and elastic behavior. The viscoelastic property of a gel is studied by rheological tests.[64] In contrast to elastic solids, the shear modulus for viscoelastic materials has a complex form. This shear modulus is

obtained by performing oscillatory measurements on the viscoelastic material. During an oscillatory test, a low frequency stress or strain is applied to the sample and the response stress or strain is recorded. For a perfectly elastic solid, the applied stress and measured strain are in phase. However, for an ideal viscous fluid there is a 90° phase lag between stress and strain. In the case of a viscoelastic material, the phase lag between the stress and strain is in between 0°and 90°.[64, 68] In this regard, the shear modulus has a complex form in viscoelastic materials with real and imaginary terms. The storage modulus (G'), representing the solid-like behavior, measures the stored energy during deformation process and forms the real term of shear modulus. The loss modulus (G"), representing liquid-like behavior, measures the energy dissipated as heat or structural changes in material and forms the imaginary term of shear modulus.[64, 69]

Rheological experiments are used to find the gelation temperature of viscoelastic materials. As an example, the gelation temperature is defined as the temperature for which a measurable yield stress can be determined from the flow curves,[43] or the temperature for which a sharp increase in the shear viscosity appears.[70] A further rheological measurement to define the sol-gel transition temperature is the temperature sweep experiment. During this experiment, G' and G" are measured as a function of temperature. At low temperatures when the material is in the sol state, the liquid-like behavior is dominant and G" is higher than G', while at higher temperature when the material is in the gel state, the solid-like behavior of the material is dominant and G' is higher than G". The sol-gel transition occurs where the material shows equal solid-like and liquid-like behavior, which is when G" equals G'. At this temperature, the ratio of loss modulus to storage modulus which is defined as the loss factor ($\tan\delta = G''/G'$) is equal to one.[64, 71]

There is a relationship between the rheological behavior, the microstructure, and intermicellar interactions of micellar solutions.[50] In this regard, studying the rheological behavior of thermo-reversible Pluronic hydrogels gives important information about the phase behavior and micellar structure.

1.4 Effect of additives on the properties of Pluronic hydrogels

As mentioned in section 1.2 the micellization process of Pluronics is enthalpically unfavorable but entropically favorable. Adding most additives including inorganic salts, into Pluronic solutions results in shifting all the transition temperatures of the copolymer hydrogel such as the CMT and sol-gel transition temperature.[63] For instance, P85 ($PEO_{25}PPO_{40}PEO_{25}$) forms gel at lower temperature and polymer concentration in the presence of potassium chloride and potassium fluoride. Also, the addition of salts increases the aggregation number of Pluronic micelles and can affects the shape and size of these micelles.[72] Moreover, in some cases addition of salts inhibits gel formation.[73]

The different effects observed with the addition of salts to Pluronic hydrogels are due to the different effect that salts have on the water molecules surrounding micelles and located inside the micellar regions defined by the PEO and PPO blocks.[74] Some anions and metal cations have a salting-out effect which leads to the lowering of the transition temperatures in Pluronic micelles.[41, 75] These effects occur because salts can have different effects on the molecular structure of water. Some salts act as water structure makers and enhance the number of hydrogen bonds between water molecules, which leads to the stabilization of the hydrophobic interactions between the hydrophobic molecules in water.[76-77] In the presence of this type of salts, at any given temperature the Pluronic copolymer micelles are more closely packed compared to the micelles in the absence of salt.[73] The addition of salts results in decreasing the solubility of the polymeric chains because the water molecules have more affinity to the ions of salt and the amount of free water molecules in the system decreases fewer hydrogen bonds can be formed with the polymeric chains. Therefore, gelation of Pluronic solutions in the presence of salts occurs at lower polymer concentrations due to the effect of salt on water molecules and the competition that exists between polymeric chains and ions for hydration.

While some salts show salting-out effects in Pluronic micellar solutions, which cause the lowering of the gelation temperature, there are some salts that showing salting-in effects, which can cause an increase of the gelation temperature. For instance, sodium thiocyanate which typically shows salting-in effects, increases the gelation temperature in Pluronic hydrogels.[78]

In general for most of the inorganic salts, the effect of salt addition is similar to the changes observed with increasing temperatures.[72, 79] Addition of salts can dehydrate the PEO corona near the core and increase the size of the core of Pluronic micelles.[80] In the case of L64 micelles, potassium fluoride increased the number of micelles and the size of the micellar core.[79] Some salts are able to enhance the dehydration of the hydrophobic region of Pluronic micelles and the solubility of PPO blocks in the presence of these salts is reduced leading to lower transition temperatures values.[74] The polarity inside of the Pluronic micelles does not change significantly in the presence of added salts. Moreover, the solubility of hydrophobic compounds increases in the presence of salts which is attributed to the increase in the number of Pluronic micelles or the increase of the size of the core.[74]

Addition of salts not only affect the structure of the micelles, but also can affect the behavior of the bulk material like its viscoelastic behavior. The presence of additives in PEO solutions alters the viscoelastic properties of the solution due to a competition between polymer and additives to interact with water molecules. Addition of some salts with salting-out effects, such as sodium chloride, can strengthen the hydrogel and increase the storage modulus.[32, 81-82] The effect of cell-culture media on the viscoelastic properties of F127 hydrogels was studied and it was found that the gelation temperature decreased in the presence of the cell-culture medium.[83] As the gelation temperature is a very important parameter for thermosensitive gels, the changes in gelation temperature after addition of compounds to a hydrogel is usually studied in order to understand the effect of additives on the phase transitions and structure of a gel.

The addition of salt to Pluronic micellar solutions can also impact the solubility of a drug, which is relevant when using these hydrogels as drug delivery systems. For example, the amount of solubilized carbamezapine, which is a poorly water-soluble drug, was either the same or decreased in the presence of sodium chloride.[84] The other possible effect of salt on the drug delivery property of Pluronic copolymers micelles is to change the drug's diffusion behavior out of the Pluronic gels.[75] The application of Pluronic gels for *in vivo* drug delivery is restricted because of the loss of the thermogelation ability due to dilution of the polymer in the body.[85] The presence of some salts can change the gelation

ability of Pluronic hydrogels in the body and this addition reduces the release and diffusion rate of the drug molecules inside the Pluronic gel. This latter effect is due to an increase in the viscosity of the gel because of the water structure is changed leading to an increase in the entanglements between micelles.[75]

1.5 Steady-state and time-resolved fluorescence studies for probes in Pluronic hydrogels

Micellar hydrogels can be used as drug carriers and deliver the drug inside the body and help achieve a sustained release of the drug inside the body. The interaction of drug molecules with polymeric nanoparticles and the location of guest molecules inside the hydrogel has direct impact on the release of the molecule from the hydrogel. For example, the drug molecule located deep inside the micelles needs more time to be released from the hydrogel system compared to the drug attached on the surface of the micelle.[86] Therefore, to better understand the release behavior of drug molecules from hydrogels, the dynamics and location of different small molecules inside the micellar hydrogel is required to be studied.

There have been various physical methods to study the structure and dynamics of self-assembled micellar systems. In this respect, photophysical methods have attracted numerous attentions because of the high sensitivity even at very low concentrations of probe and the broad time scale which allows to study the dynamical processes from picoseconds to microseconds timescale.[87]

The location of fluorescent probes in a heterogeneous micellar system depends on the structural properties of the probe. Studying the fluorescence properties of fluorescent probe molecules gives information on the features of the fluorophore's microenvironment. This is the reason that fluorescence spectroscopy is known as a technique to study various environments in micro-heterogeneous systems such as organized molecular assemblies of micelles.[87-88] In order to understand the micellar structure from a molecular level, it is required to study the photophysical characteristics of the fluorescent probes, such as the fluorescence excitation and emission spectra, relative emission intensities, quantum yields and excited state lifetimes.[87, 89-92] In addition, different information about micelles such as

CMC, microviscosity, polarity of microenvironments, aggregation number, oxygen penetration, the effect of different additives on the permeability of the micelle and micellar dynamics can be obtained from fluorescence measurements.

Probe molecules show different fluorescence spectral changes in different environments of a micellar system.[93] For instance, pyrene is a well-known probe molecule used to study the micropolarity and microviscosity of micellar systems. The fluorescence spectrum of pyrene changes based on the polarity of its microenvironment and can be used as an index to determine the polarity of the pyrene binding site in a micellar system.[94] Excited state pyrene molecules in restricted environments form an excimer, which is a complex consisting of a pyrene in its ground state with a second pyrene in its excited state. Moreover, the formation of pyrene excimers depends on the microviscosity of its environment and the ratio of excimer to monomer fluorescence intensities is a good parameter to determine the microviscosity of the pyrene solubilization site in a micellar system.[95] While steady-state fluorescence measurements are simple from the experimental point of view, time-resolved fluorescence techniques are one of the most powerful techniques to study the microheterogeneity of micellar systems.

Lifetimes of the fluorophores are obtained from time-resolved fluorescence experiments and species of fluorophores in a heterogeneous system can have different lifetimes because of the sensitivity of the fluorophore to its environment. This difference can be used to understand the distribution and location of fluorophore molecules in a micellar system. The fluorescence lifetime of an excited state fluorophore is related to the time that it takes for the singlet excited state molecule to return to the ground state and the lifetime depends on radiative and non-radiative decay processes. The microenvironment of an excited state probe has an effect on the non-radiative decay processes which can lead to changes in the lifetime of the probe.[86, 96] Probe molecules inside of micelles usually have longer lifetimes (still in micro to nanosecond time domain) compared to the excited probe in bulk water because in the micelles the probes are in a more hydrophobic environment and the micelles provide protection for excited state molecules from other molecules located in the aqueous phase that can shorten the lifetime of these excited states.[89]

The fluorescence lifetime of singlet excited state probes is on the nanosecond time scale. If the excited probe molecule locates inside the micelles of a hydrogel, this lifetime is short enough for the singlet excited probe not to be able to exit from the micelle to the aqueous phase of the hydrogel.[90] Therefore, the probe molecule can be viewed as immobile during its singlet excited state lifetime.

Excited states can be deactivated in a process called quenching, which leads to a decrease the fluorescence intensity. There are different mechanisms of quenching singlet excited state molecules and one of them is called dynamic quenching. During this process, the quencher diffuses towards the excited molecule and quenching occurs in the encounter complex resulting in the return of the singlet excited state molecule to its ground state. During this process both the lifetime and fluorescence intensity of the excited state probe decrease. When a probe molecule is quenched in a micellar system through a diffusion-controlled process then the quenching rate constant carries information about the size of probe and quencher, diffusion coefficient, size and structure of micelles.[97]

Micelles are dynamic aggregates which are in equilibrium with dispersed unimers in aqueous solution. The residence time of unimers in micellar aggregates is of the order of microseconds or longer. However, the time scale for quenching of singlet excited state molecules is in the nanosecond time range and micelles can be assumed to be stable for fluorescence quenching experiments.

Fluorescence quenching has been used to characterize the micellar size, dynamics of the micelles and of small guest molecules inside the micelles.[97] From time-resolved fluorescence quenching experiments one can obtain the information about the number of different fluorophore species present in the system which are quenched with different efficiencies and the relative population of each species.[98]

Different fluorophores have been used to characterize the interior of PEO-PPO-PEO hydrogels. These gels have regions with different polarities. The core has the lowest polarity, corona shell with less polarity, and bulk water with highest polarity. The diffusion and solubilization of guest molecules inside the hydrogel depend on the microviscosity and micropolarity of the different environments.[99]

Some examples of using fluorescent probes to investigate Pluronic solutions and gels are described here. The partitioning of two hydrophobic fluorescent molecules (pyrene and diphenylhexatriene) between different phases of Pluronic P85 and F108 polymers was studied using photophysical measurements which gave information on the heterogeneity of these Pluronic micellar systems.[100] There have been several studies on the microviscosity sensed by probes in different regions of Pluronic hydrogels and it has been reported that even when the viscous solution of Pluronic becomes a gel, the microviscosity sensed by probes, such as rhodamine 123[101] and coumarin 343^{-}/ Na^{+}, [102] is similar to the viscosity in water. The effect of electrolytes on the microviscosity and hydration of F127 micelles was investigated using coumarin 153 and coumarin 151 probes.[103] In addition, the location and interaction of telmisartan, which is a hydrophobic drug molecule, within Pluronic F127 and P123 was determined and different microenvironments in the Pluronic micelles were studied using the fluorescence quenching technique.[104] Three different coumarin molecules with different polarities were utilized to probe the heterogeneity of Pluronic hydrogels. The probes based on their polarities located in different regions of micellar system and allowed the determination of the micropolarity and microviscosity of different regions of the Pluronic hydrogel.[102]

In addition, fluorescence spectroscopy has been used to study the dye exchange dynamics in micellar solutions. Different mechanisms have been suggested for solute exchange between micelles.[105] In one mechanism, the exchange process of the probe involves the formation a super-micelle, which is unstable and breaks apart into two separated micelles. In this process, the probe does not become free in the bulk water phase and remains in the micellar phase. The other possible mechanism for the probe exchange between micelles involves the exit of the probe from a micelle into the bulk water before entering the other micelle, where the exit from the first micelle is the rate determining step which usually occurs on the microsecond timescale.

1.6 Study of the mobility of triplet excited state guests in Pluronic F127 hydrogel

Similar to Pluronic micellar monomers, the micelle solubilized additives are not rigidly fixed inside the micelles but these additives can constantly move between the different phases.[105] In order to study the dynamics of small molecules in Pluronic hydrogels several techniques have been used. Fluorescence correlation spectroscopy and single molecule tracking, give information about diffusion rates of single molecules in different environments of the gel and these are precise techniques to track single molecules inside the hydrogel.[106] It is reported that dyes located inside the core of micelles show a more restricted mobility compared to dyes located in the corona due to the presence of compact and highly entangled polymers in the dehydrated core of micelles.[107] On the other hand, NMR diffusion measurements[108-110] and pulsed field gradient methods[111] are used to study the mobility of polymeric macromolecules and to determine the rate of self-diffusion. However, these methods are not suitable to track the motions of single molecules in a microheterogeneous system.

Another photophysical technique to study the mobility of small molecules inside a microheterogenous system is diffuse reflectance flash photolysis, which is based on the measurement of the absorption of transients.[112] This technique has been employed to study the kinetics of transient species, such as triplet excited states, radicals and radical ions on a variety of metal oxide and zeolite supports.[113-117] In our group, laser flash photolysis (LFP) has been used to study the kinetics of association and dissociation between host and guest in supramolecular systems or in complex systems.[98, 118-119]

The time it takes for a probe molecule to exit a micelle is of the order of microseconds to milliseconds.[105] Therefore, typical fluorescence quenching studies are too fast to study the kinetics of the probe dynamics between the different phases of a micellar hydrogel. Triplet excited state probes, in contrast to singlet excited state ones, have longer lifetimes that allow the triplet excited stares to move between different phases inside a micro-heterogenous system, such as micellar hydrogels. In general, the solubility of hydrophobic probe molecules in water increases in the presence of micelles through the incorporation of these probes inside the micelles or by localizing the probes at the surface

of micelles. The localization of the probes depends on the polarity of the probe molecule.[120-122] The residence time of the probe in each phase of the hydrogel depends on the probe's hydrophobicity. For this reason, by studying the kinetics of association and dissociation for triplet excited state molecules within micelles, it is possible to obtain the probe's mobility rate and compare the residence time of small molecules inside different phases of the hydrogel.

For most of the guest molecules in a complex host system, the rate constants for the association and dissociation processes cannot be measured from direct kinetic studies, but quenching experiments make it possible to obtain the guest's exit and entry rate constants.[123] During the quenching process, the excited state probe in the aqueous phase has more exposure to the quencher compared to the excited probe inside the host leading to a differential quenching efficiency for the excited probe in the different environments.[122]

A kinetic model has been proposed to describe the partitioning of a probe between the aqueous and micellar phases and the quenching processes of the excited probes in the different phases.[122] Several assumptions were made for this model. First, the probe molecules should be more soluble in the micellar phase rather than the aqueous phase. Second, the concentration of probe molecules should be low enough to ensure that no self-quenching happens in the system, because two probe molecules are located in one micelle. Third, the quencher has access to the excited state probe molecules in micellar and aqueous phases, but the quenching rate constants are different for each phase. Initially the model assumed that no quenching occurred for the excited probe in the micelle,[122] but in subsequent studies on the dynamics of small molecules in bile salt aggregates the quenching in the aggregates with a lower quenching efficiency than in water was incorporated into the model.[98] I used this model to describe the association and dissociation processes that occur in Pluronic micellar system with small probe molecules.

The reactions that happen in a host-guest system are shown below (Eq. 1.1-1.5) and are also shown in a schematic form in scheme 1.1, which was previously used to illustrate the reactions in different environments of supramolecular host-guest systems.[98] In reactions 1.1 to 1.5, the terms P, P^*, M, Q, and MP^* refer to the probe, excited probe, micelle, quencher, and the micelle containing an excited state probe, respectively. The rate

constant k_{dis} and k_{as} refer to dissociation and association rate constants with the micelle for the triplet excited probe (Eq. 1.1). In equations 1.2-1.5, k_0 and k_0^M are the decay rate constants for the probe in water and in the micelles in the absence of a quencher, k_q and k_q^M are the quenching rate constants for the probe in water and in the micelles in the presence of a quencher, respectively.

$$MP^* \underset{k_{as}}{\overset{k_{dis}}{\rightleftarrows}} M + P^* \qquad 1.1$$

$$P^* \xrightarrow{k_0} P + h\nu \qquad 1.2$$

$$MP^* \xrightarrow{k_0^M} \mathrm{M}P + h\nu \qquad 1.3$$

$$P^* + \mathrm{Q} \xrightarrow{k_q} \text{quenching} \qquad 1.4$$

$$MP^* + \mathrm{Q} \xrightarrow{k_q^M} \text{quenching} \qquad 1.5$$

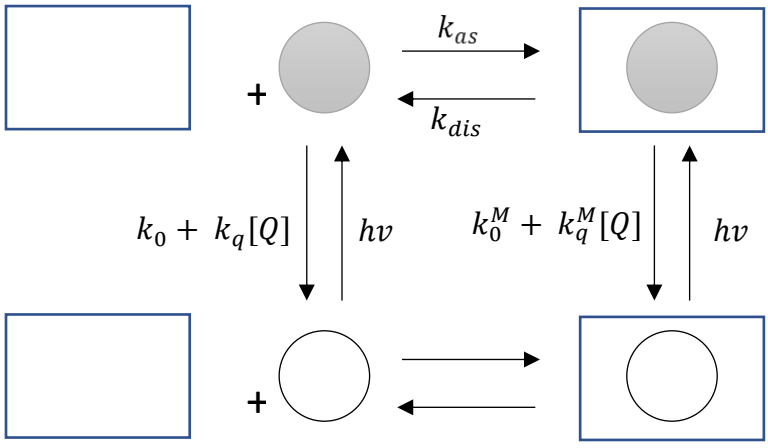

Scheme 1.1. Schematic representation of the reactions for the quenching of triplet excited state probes in different phases of the Pluronic hydrogel. The open and filled circles correspond to the ground- and excited-state probes respectively, and the square corresponds to the micelle.

Quenching of triplet excited state probes was used to understand the factors which control the entry and exit rate of small molecules solubilized in a micellar phase such as structure or polarity of the guest molecules and the results have direct impact on the release behavior of the guest molecules from the hydrogel. Quenching experiments performed on sodium lauryl sulfate micelles yielded the values for exit and entry rates of guest molecules and the results showed that the micelles are more permeable to small size molecules.[124] To show the preferential solubilization in different regions of sodium dodecyl sulfate micelles, phenanthrene triplets were quenched with two quenchers with different hydrophobicity. The higher rate constant for more hydrophobic quencher indicates that phenanthrene prefer to stay in the less polar core of the micelles.[125] In this regard, it is expected that more hydrophobic molecules, tend to stay in the micellar phase more than the aqueous phase of Pluronic micelles.

1.7 Objectives

My project focused on the understanding of the kinetics of guest molecules within gels formed from polymeric PEO-PPO-PEO tri-block copolymers. These Pluronic triblock copolymer hydrogels were chosen because they are materials that solubilize small molecules used in different applications, including drug delivery systems and for oil recovery. To understand the capability of these copolymer gels to solubilize and release small molecules, it is required to understand the properties of the various solubilization sites available to different molecules with different hydrophilicities and the mobility of small molecules in Pluronic hydrogels.

As there are different compositions available for Pluronic polymers, I studied F127 and P104 because they both can form gels at elevated temperatures, they have different PEO contents, but the PPO content is almost the same, which resulted in very different molecular weights for these two polymers. Different composition properties of P104 and F127 Pluronic polymers might change the characteristics of solubilization sites available for different guest molecules in these hydrogels. Hence, I compared the solubilization sites

and the kinetics of quenching for the same probes in F127 and P104 hydrogels through fluorescence spectroscopy measurements.

The mobility of different guest molecules located in different environments of the F127 hydrogel was studied through quenching of the triplet excited states of different probe molecules. The reactions were examined using laser flash photolysis technique.

2 Chapter 2: Experimental

2.1 Materials

Deionized water (Barnstead NANO pure deionizing systems, ≥17.8 MΩ cm) was used to prepare all aqueous solutions. Pluronic F127 (powder, MW 12600, 70 wt% PEO, CMC: 950-1000 ppm ~ 25°C, Sigma-Aldrich), Pluronic P104 (paste, gift from BASF Corp.), polyethylene glycol (40 % w/w in H_2O, average MW 8000, Sigma-Aldrich), polypropylene glycol (average MW 2000, Sigma-Aldrich), polypropylene glycol (average MW 4000, Sigma-Aldrich), methanol (spectral grade, > 99.9%, Fisher), methanol (HPLC grade, Fisher), hexane (HPLC grade, 95%, Fisher), ethanol (Sigma-Aldrich, ≥ 95%), nitromethane (NM, Sigma-Aldrich, ≥ 98.5%), and sodium iodide (NaI, Sigma-Aldrich, ≥ 99.999%) were used without further purification.

Pyrene (Sigma-Aldrich, ≥ 99.0%) was recrystallized twice from ethanol (for purity check see below). Naphthalene (Np, Sigma-Aldrich, ≥ 99%) was purified by vacuum sublimation for fluorescence spectroscopy experiments as described below.

Phenanthrene (Pht, Sigma-Aldrich, ≥ 99.5%), 2-naphthoic acid (2-NpC, Sigma-Aldrich, ≥ 98%), naphthalene (Np, Sigma-Aldrich, ≥ 99%), R-(-)-1-(2-naphthyl)ethanol (NpOH, Fluka, ≥ 99.0%), and glycerol (spectrophotometric grade, ≥99.5%, Sigma-Aldrich) were used without further purification for laser flash photolysis experiments. Sodium nitrite ($NaNO_2$, ACP Chemicals Inc., ≥ 97%) was recrystallized from water once by Dr. Suma S. Thomas.

2.2 Purification Methods

2.2.1 Pyrene recrystallization

In order to purify pyrene to use in photophysical experiments, 1 g of pyrene was dissolved in 150 mL ethanol through sonication at 50 °C. The ethanol solution was left undisturbed until the crystals were formed, which correspond to impurities. These impurity crystals were removed by filtration and discarded. Then, 5 mL of water was added dropwise to the filtrate until the filtrate turned into a milky mixture, after which it was left

on the bench for around 5 min. In the next step, the mixture was filtered by vacuum filtration using a water aspirator and the obtained solid was dried for 1 h. This process was repeated twice to obtain pure pyrene for photophysical experiments. The solid pyrene was kept in a sample vial covered with aluminum foil.

Time-resolved fluorescence spectroscopy was used to test for the purity of pyrene for a sample of 0.5 μM of pyrene in water (Fig. 2.1). The mono-exponential fluorescence decay of pyrene (Eq. 2.1, see below) confirms that pyrene is pure enough for photophysical experiments.

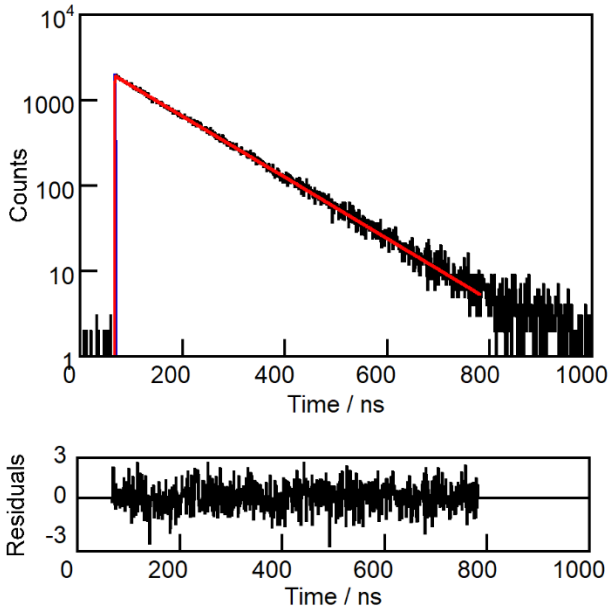

Figure 2.1. Fluorescence decay for 0.5 μM pyrene in water at 30 °C (black) fit to a mono-exponential decay (red). Residuals between calculated and experimental data are shown in the lower panel.

2.2.2 Naphthalene purification

Np used for fluorescence experiments was purified by vacuum sublimation once and kept in a sample vial covered with aluminum foil. To check for the purity of the obtained Np, a 5 μM solution of Np in methanol was used for time-resolved fluorescence spectroscopy. The decay for the emission of singlet excited naphthalene in methanol was mono exponential which confirms the purity of Np (Fig. 2.2).

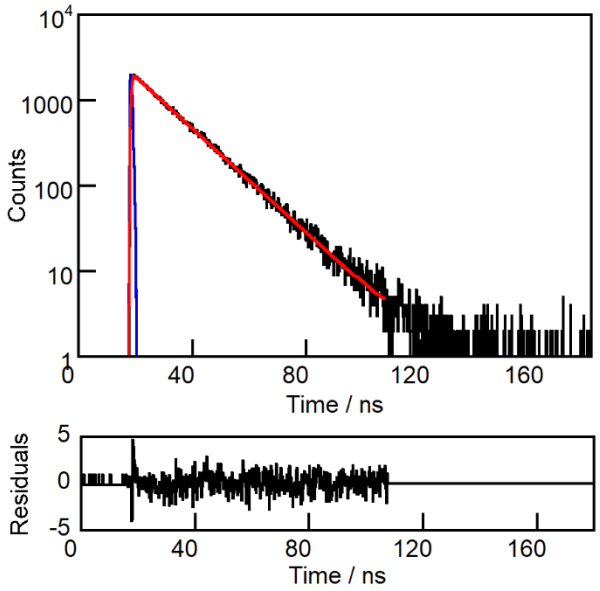

Figure 2.2. Fluorescence decay for 5 µM Np in methanol at 20 °C (black) fit to a mono-exponential decay (red). The instrument response function is shown in blue. Residuals between calculated and experimental data are shown in the lower panel.

2.2.3 F127 purification

Soxhlet extraction was used to eliminate fluorescent impurities in F127 by using hexane as the extraction solvent. The extraction was performed for two time periods of 8 h each and the purity of F127 was checked using steady-state and time-resolved fluorescence spectroscopy. Due to the remaining impurities even after two cycles of Soxhlet purification, a broad peak was observed in the fluorescence emission spectrum of F127 (Fig. 2.3). In figure 2.3, the Raman emission from the solvent was removed from the fluorescence emission spectrum of F127. The lifetimes for these impurities were shorter than 10 ns (Table 2.1). Hence, instead of purifying F127, we developed a method to account for these impurity emissions as described below.

Table 2.1. Fluorescence emission lifetimes and corresponding A values for the impurities in 20% F127 at 30 °C.

τ_1 / ns[a]	τ_2 / ns[a]	τ_3 / ns[a]	A_1[a]	A_2[a]	A_3[a]	χ^2
0.3 ± 0.1	2.3 ± 0.1	8.0 ± 0.2	0.58±0.04	0.37±0.02	0.05±0.01	1.139

[a] The errors represent the standard deviations calculated using the F900 software. The data correspond to one experiment.

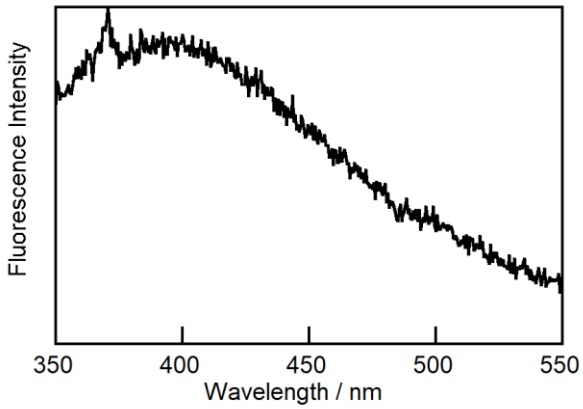

Figure 2.3. Fluorescence emission spectrum for the impurities in 20% F127 at 30 °C.

2.3 Sample Preparation

2.3.1 Preparation of stock solutions

Stock solutions of 500 μM pyrene, 1 mM Np, 3 M NM in spectral grade methanol were prepared by dissolving the solid in methanol. A stock solution of 1 M NaI in water was prepared by dissolving the solid in water. The stock solutions of NM in methanol and NaI in water were kept in the dark and were used right after preparation. The stock solutions of pyrene and Np in methanol were kept in sample vials covered with aluminum foil in the fridge and were used for up to one month.

For laser flash photolysis, the stock solutions of 4 mM Pht, 10 mM 2-NpC, 10 mM Np, 10 mM NpOH in methanol were prepared by dissolving the solids in the alcohol. These stock solutions were covered with aluminum foil and kept in the fridge and were used for up to one month. A stock solution of 1 M $NaNO_2$ in water was prepared and used right after preparation.

2.3.2 Preparation of aqueous solutions of Pluronic F127 and P104

Aqueous solutions of 20% and 30% w/v F127 were prepared by adding 20 mL water to 4 g and 6 g F127 solid, respectively. These solutions were stirred in an ice bath until all the solid was dissolved. The solutions were kept in the fridge overnight to remove bubbles. The aqueous solutions of F127 were used for up to five days after sample

preparation for photophysical experiments. For rheological measurements and dynamic light scattering experiments, the aqueous solutions of F127 were used one day after sample preparation. To prepare other samples containing 20% and 30% w/v F127, I refer to 20% and 30% F127 solutions which correspond to the samples prepared by the above-mentioned procedure.

To prepare aqueous solutions of 34% w/v P104, 6.7 g P104 solid was added to 20 mL water. The next steps of the preparation procedure are as same as the steps described above for the F127 aqueous solution preparation.

2.3.3 Addition of quenchers to Pluronic F127 and P104 solutions to quench impurities

A sample for each quencher concentration was prepared. Appropriate volumes of the NaI stock solution were added to aqueous solution of 20% F127 using a micropipette to achieve final concentrations of NaI between 5 and 70 mM. After addition of NaI, each sample was stirred in an ice bath for 30 min before performing the fluorescence measurements. The same procedure was used for 34% P104 solutions, but the final concentrations of NaI were between 5 and 22 mM. The concentration of NaI was calculated from the dilution of the stock solution. In selected cases, the volumes dispensed by the micropipette were weighted three times and the concentrations were calculated using the density of 1.11 g/mL.[126] The same value within experimental errors was obtained from the calculation based on dilution and by weighing the volume added. The errors for the concentration values are smaller than 0.6 %. The same procedure for concentration determination was used for solution preparations described for the use of NaI below.

A sample for each quencher concentration was prepared. In order to add NM to 20% F127 and 34% P104, appropriate volumes of neat NM liquid (1.127 g/mL) were added to aqueous solutions of 20% F127 and 34% P104 using a micropipette to achieve final concentrations between 15 and 62 mM NM in 20% F127 and 34% P104 aqueous solutions. In the next step, each sample was stirred in an ice bath for 30 min before doing any experiments. The concentrations were always calculated from the weight of the volumes added (average of three volumes weighted), and the error for the concentrations is below

12.7%. The same procedure for concentration determination was used for solution preparations described for the use of NM below.

2.3.4 Addition of pyrene to bulk liquid PPO and PEO blocks

Appropriate volume (200 μL) of the pyrene stock solution was added to 20 mL liquid PEO, PPO 2000, and PPO 4000 using a micropipette to obtain the final concentration of 5 μM pyrene. These solutions were stirred at room temperature for around 3 h. The samples were used one day after preparation.

2.3.5 Quenching of pyrene in water with NM and NaI

An appropriate volume (20 μL) from the pyrene stock solution was added to 20 mL water using a micropipette to reach the final concentration of 0.5 μM pyrene, and this solution was stirred at room temperature for around 2 h. For the following steps, appropriate volumes from the NaI stock solution were added sequentially to the same pyrene aqueous solution using a micropipette at room temperature to reach final concentrations between 4 and 62 mM of NaI. The samples were used right after preparation.

In order to quench the emission of pyrene with NM, appropriate volumes from the NM liquid were sequentially added to the same pyrene aqueous solution using a microsyringe and a micropipette at room temperature to reach final concentrations between 6 and 25 mM of NM. The samples were used right after preparation.

2.3.6 Quenching of pyrene in F127 and P104 with NM

An appropriate volume from the pyrene stock solution (200 μL) was added to 20 mL of 20% and 30% F127 solutions using a micropipette to reach the final concentration of 5 μM pyrene and the solutions were stirred in an ice bath for around 2 h. Appropriate volumes from the NM stock solution were added to the pyrene solution in 20% F127 using a microsyringe to reach final concentrations between 2 and 7 mM NM. Appropriate volumes from the NM liquid were added to pyrene solutions in 20% and 30% F127 using

a microsyringe to reach final concentrations between 15 and 62 mM NM. Each sample was stirred in an ice bath for 30 min before doing the experiments.

The same procedure was followed to study the quenching of 5 μM pyrene in 34% P104 and samples with similar final concentrations between 2 and 62 mM NM were prepared as described above.

2.3.7 Quenching of the singlet excited state pyrene in F127 and P104 with NaI

Appropriate volumes from the NaI stock solution were added to the 20% F127 solution containing 5 μM pyrene using a micropipette to reach final concentrations between16 and 68 mM NaI. Each sample was stirred in an ice bath for 30 min before doing the experiments.

The same procedure was followed to study the quenching of 5 μM pyrene in 34% P104 and samples with final concentrations between 5 and 22 mM NaI were prepared as described above.

2.3.8 Quenching of the singlet excited state of Np in water with NaI

An appropriate volume from the Np stock solution (20 μL) was added to 20 mL water using a micropipette to reach the final concentration of 1 μM Np. This solution was stirred at room temperature for around 2 h. Appropriate volumes from the NaI stock solution were added to the Np aqueous solution using a micropipette at room temperature to reach final concentrations between 5 and 22 mM of NaI. The samples were used right after preparation.

2.3.9 Quenching of the singlet excited state of Np in F127 and P104 with NaI

An appropriate volume from the Np stock solution (100 μL) was added to 20 mL of 20% F127 and 34% P104 solutions using a micropipette to reach the final concentration of 5 μM Np in each solution. Then, the solutions were stirred in an ice bath for around 2 h. Appropriate volumes from the NaI stock solution were added to 20% F127 and 34% P104

solutions containing 5 μM Np using a micropipette to reach final concentrations between 5 and 22 mM NaI. Each sample was stirred in an ice bath for 30 min before doing the experiments.

2.3.10 Preparation of samples for dynamic light scattering measurements

Before sample preparation the cuvette cell was cleaned 6 times with ethanol filtered through two series of Teflon syringe filters with a pore size of 0.2 μm, (National Scientific Company). Then, the cuvette was rinsed 6 times with water filtered through two nylon syringe filters in series with nominal pore sizes of 0.2 μm (National Scientific Company). The samples of 20% F127, 20% F127 + 5 μM pyrene, 20% F127 + 5 μM pyrene + 62 mM NM, and 20% F127 + 5 μM pyrene + 68 mM NaI were diluted using the procedure described below such that the final concentration of F127 in all samples reached to 4% w/v.

To dilute the original samples, water was filtered through two nylon syringe filters after which an appropriate volume of intended sample was added to water using a micropipette. In order to prevent dust entering into the samples, the cuvettes were not shaken after dilution. The diluted samples were kept undisturbed for 5 min before doing the DLS measurement. The samples were prepared and used on the same day.

2.3.11 Quenching of triplet excited state probes in water-glycerol with $NaNO_2$

An appropriate volume of glycerol (24 mL) was added to 9 mL water at the constant temperature of 20 °C (the temperatures of water and glycerol were checked with a thermometer) to reach the same viscosity of 20% F127 at 20 °C. The viscosity of water-glycerol mixture at 20 °C obtained from literature while the viscosity of 20% F127 at 20 °C obtained from viscosity-temperature curve and the values were similar. The calculation of the viscosity of the water-glycerol mixture at 20 °C was done using literature values.[127] Moreover, the viscosity versus temperature curves for 20% F127 solution (Fig 2.4) and prepared water-glycerol mixture confirmed their similar viscosities at 20 °C. The water-

glycerol mixture was stirred for at least 3 h at room temperature. The mixture was used for up to three days after preparation.

Appropriate volumes from the Pht, 2-NpC, Np, or NpOH stock solutions (225, 240, 240, 240 μL, respectively) were added to 30 mL water-glycerol mixtures using a micropipette in order to reach final concentrations of 30 μM, 80 μM, 80 μM, 80 μM for the probes, respectively. Each sample was stirred at room temperature for at least 2 h, stored in the fridge and used for up to three days after preparation. In the case of the sample containing 2-NpC, the pH of the water was measured before preparing the sample and it was 6.2 ± 0.2.

Appropriate volumes from the $NaNO_2$ stock solution were added to each sample using a micropipette to reach final concentrations between 8 and 33 mM $NaNO_2$. Each sample was stirred at room temperature for 30 min before doing the quenching experiments.

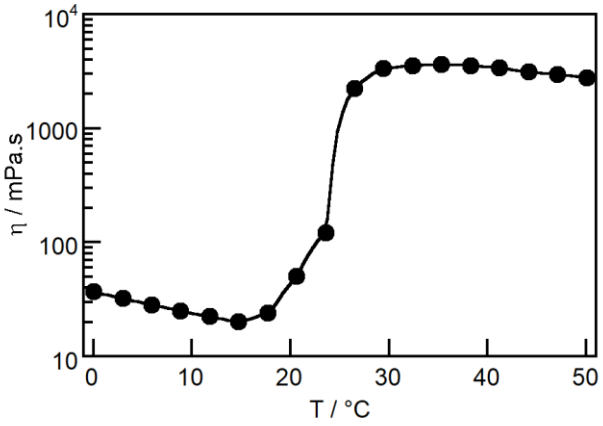

Figure 2.4. Dependence of the viscosity on the temperature for 20% F127. Experiment performed once.

2.3.12 Quenching of triplet excited state probes in F127 with $NaNO_2$

Appropriate volumes from the Pht, 2-NpC, Np, and NpOH stock solutions (750, 480, 480, 480, respectively) were added to 60 mL 20% F127 using a micropipette in order to reach final concentrations of 50 μM, 80 μM, 80 μM, 80 μM in 20% F127, respectively. Each sample was stirred in an ice bath for 2 h, kept in the fridge and used for up to three

days after preparation. In the case of the sample containing 2-NpC, the pH of the F127 solution was measured before preparing the sample and it was 6.5 ± 0.1.

Appropriate volumes from the $NaNO_2$ stock solution were added to each sample using a micropipette to reach final concentrations between 3 and 45 mM $NaNO_2$. Each sample was stirred in an ice bath for 30 min before doing the experiment.

2.4 Equipment

UV-visible spectroscopy: The absorption spectra were recorded from 200−800 nm using a Varian Cary 1 or a Cary 100-Bio UV-Vis spectrometer. The baseline was measured against air. To set the temperature, the sample cuvette was kept in the cuvette holder for at least 10 min before collecting the spectra. The temperature was set using a water bath. The temperature for all hydrogel samples was set to 30 °C and for solutions the temperature was set to 20 °C.

Steady-state fluorescence spectroscopy: Steady-state fluorescence spectra were recorded using a PTI QM-40 spectrofluorimeter. Samples containing pyrene, samples for quenching impurities in F127 with NM and NaI, and samples for quenching impurities in P104 with NM, were excited at 335 nm and the emission spectra were recorded between 350 nm and 550 nm. Samples containing Np, samples for quenching impurities in F127 and P104 with NaI were excited at 266 nm and the emission spectra were recorded between 280 nm and 500 nm. The excitation and emission monochromator bandwidths were set to 0.5 nm for F127 samples containing pyrene while for all other samples the mentioned bandwidths were set to 2 nm. The temperature was set on water bath and samples were kept in the sample holder for around 15 min before performing experiments to ensure the temperature of the samples was constant. The wavelength step-size was 0.5 nm and the integration time was set to 0.25 s. Standard 10 × 10 mm quartz cells were employed. The analysis of the spectra was performed using the Felix32 (version 1.2) software from PTI.

Time-resolved fluorescence spectroscopy: The time-resolved emission decays were recorded using an Edinburgh Instruments OB920 single photon counter (SPC). A 280 nm light emitting diode (LED) was used to excite the samples containing Np, samples of quenching impurities in F127 and P104 with NaI and a 335 nm LED was used to excite

samples containing pyrene, samples for quenching impurities in F127 with NM and NaI, and samples for quenching impurities in P104 with NM. A neutral density filter was used to attenuate the intensity of the light from the LEDs. The emission from the samples containing Np, samples of quenching impurities in F127 and P104 with NaI, was collected at 330 nm. This wavelength was selected by using a monochromator. The emission from the samples containing pyrene, samples for quenching impurities in F127 with NM and NaI, and samples for quenching impurities in P104 with NM was collected at 390 nm. The bandwidth for the emission monochromator was 16 nm.

Standard 10 × 10 mm quartz cells were employed. The number of counts at the channel with maximum intensity was set to 10,000 or 2,000. The number of channels was set to 1,024. The frequency of stop pulses was kept under 2% of the frequency for the start pulses. The temperature was set on a water bath and samples were kept in the sample holder for around 15 min before performing experiments. To measure the instrument response function (IRF), Ludox solutions were used, and the scattering intensity was collected at the same wavelength as the excitation wavelength. To analyze the fluorescence decays with a function corresponding to a sum of exponentials (see below), the F900 software was used and Kaleidagraph software v 4.1.1 was used to generate quenching plots.

Dynamic light scattering (DLS): DLS measurements were carried out using a Brookhaven Instruments Zeta-Pals Analyzer equipped with a solid-state laser (660 nm) with a maximum power output of 35 mW. All DLS measurements were performed at the constant temperature of 20 °C and at the scattering angle of 90°. The hydrodynamic diameter was obtained by the method of cumulant analysis (BIC DLS software). The mean effective hydrodynamic diameters were determined from four measurements of one individually prepared sample, such that the reported errors reflect the error in data collection.

Rheometer: Rheology measurements were performed using an Anton Paar MCR 302 Rheometer. A cone plate geometry with 50 mm diameter, length of 100 mm, and 2° angle was used. A Peltier temperature control system was used, which controls the temperature from the sample base. Sample solutions were loaded onto the geometry base plate using a pipette while the temperature of the base plate was set to 0 °C. Then, the

temperature of the sample base was raised to 30 °C. When the loaded sample gelled, the cone-plate geometry was lowered, and the sample was trimmed at the edges. Paraffin oil along with the solvent trap was used to prevent solvent evaporation from the sample during the experiments. A measuring gap (equivalent to sample thickness) of 211 μm was used.

Strain amplitude sweeps were carried out between 0.01 and 100% at constant temperatures of 20 and 30 °C with a constant frequency of 1 rad/s to determine the linear viscoelastic range for the gel. Dynamic frequency sweep experiments were performed from 0.1 to 100 rad/s at constant shear strain of 0.5% and constant temperature of 23 °C. The viscosity was measured for temperatures in the range of 0–40 °C with a heating rate of 1 °C / min and a constant shear rate of 50 s^{-1}. The shear stress was measured at different shear strain rates (0.1–100 s^{-1}) to generate the flow curves at 20 °C. Temperature ramp tests were performed at constant shear strain and angular frequency of 0.5% and 1 rad/s, respectively. With these parameters the gel remains in the linear viscoelastic region. The temperature was increased from 10 to 35 °C with a rate of 0.5 °C/min to study the sol-to-gel transition and determine the sol-to-gel transition temperature. The reproducibility of the data was checked by performing experiments for at least two independently prepared samples.

Laser flash photolysis (LFP): The LFP system was previously described.[118, 128] The samples were excited at 266 nm using a Quanta Ray Lab 130-4 pulsed Nd:YAG laser from Spectra Physics with a 4 Hz pulse frequency. A Xe-arc lamp was used as monitoring beam to measure the transient decays and spectra. At least 6 kinetic traces were averaged for each measurement. The transient absorption changes were detected on two oscilloscopes. The temperature for F127 samples was set to 20 °C or 30 °C using a Unisoko cryostat.[129] The temperature of the water-glycerol samples was set at 20 °C. All experiments were initiated 15 min after placing the cells in the sample holder inside the cryostat to ensure that the temperature of the sample was constant. Samples were contained in 7 mm × 7 mm quartz cells and the transient absorption was monitored at 415 nm for NpOH, at 490 nm for Pht, and at 420 nm for Np and 2-NpC. The experiments were performed for at least 2 independently prepared samples and the averaged values are reported.

pH measurement: pH measurements were done using an Eutech pH-meter. The pH-meter was calibrated by using three standard buffer solutions of pH 4.01, 7.00 and 10.01.

For each sample, the measurements were done three times and the average values are reported.

2.5 Methods

2.5.1 Determination of the I/III ratio for pyrene

In the fluorescence emission spectrum of pyrene, the third peak is not sensitive to the polarity of pyrene microenvironment, while the first one is sensitive.[130-131] In order to determine the I/III ratio of pyrene, the fluorescence emission spectrum of pyrene was normalized such that the third peak is equal to one and first peak indicates the I/III value. For example, for the fluorescence emission spectrum of pyrene in water (Fig 2.5), the third peak, which occurred at 379 nm, was normalized to one and the first peak, which occurred at 369 nm was 1.9, leading to a I/III ratio of 1.9. The wavelengths for the peaks varied slightly for different days and can be slightly different from the published values because of the calibration during set-up of the emission monochromator. In this regard, I measured the maximum value of intensity for each peak and the peak wavelength could change by up to 1 nm between experiments done on different days with different monochromator calibrations.

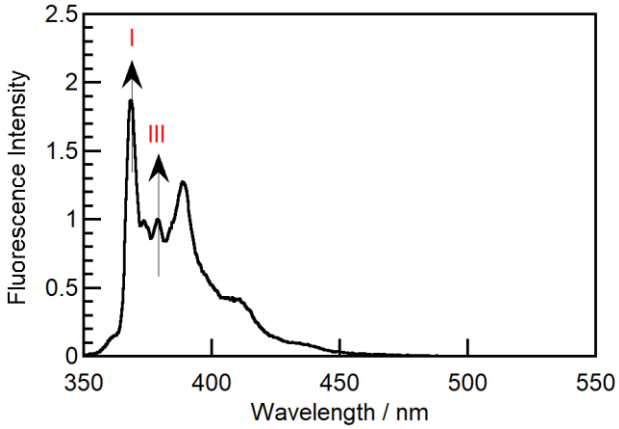

Figure 2.5. Normalized fluorescence emission spectrum of 0.5 μM pyrene in water. The I/III ratio for pyrene in water is 1.9.

2.5.2 Fitting of time-resolved fluorescence decays

An exponential fit to the fluorescence decay curve *I(t)* gives the fluorescence lifetime τ (Eq. 2.1), where I_0 is the intensity at time $t = 0$. However, if more than one fluorophore is present in the solution or if there are different populations of the same fluorophore, then a more complex fluorescence decay curve occurs, which is fit by a sum of exponentials (Eq. 2.2); where A_i is the pre-exponential factor related to the population of fluorescent species and τ_i is the lifetime for each species. The sum of the pre-exponential factors equals one.[96]

$$I(t) = I_0\, e^{-t/\tau} \tag{2.1}$$

$$I(t) = \sum_{i=1}^{n} A_i e^{-t/\tau_i} \tag{2.2}$$

The quality of the fits was judged based on the randomness of the residuals between the data and the fit, and the χ^2 values that should be between 0.9 and 1.2. To analyze the decay and obtain the lifetimes for the fluorophore, the software reconvolutes the IRF with the calculated fit to account for the contribution of instrument response to the experimental decay. The IRF is the response of the SPC instrument to a zero-lifetime sample. The IRF curve is collected using a colloidal silica solution (Ludox) which scatters light and represents the response time of the SPC instrument. The IRF limits the shortest lifetime that can be measured with the SPC system. Reconvolution of the IRF is required when the width of the IRF is significant compared to the time scale of the decay, and reconvolution was used when the total collection time for the decay was 500 ns or less. When the collection is longer the IRF is narrow and is not included in the fit, which is called a tail fit. As an example, the decay profile of Np in methanol fits well to a mono-exponential decay (Eq. 2.1) as shown by the random residuals between the experimental and calculated data (Fig. 2.2).

2.5.3 Data analysis for singlet excited state quenching

In the case of collisional quenching, where both the intensity and lifetime of the singlet excited state fluorophore decrease, the Stern-Volmer equation shows the relationship between intensities, lifetimes and quencher concentration:

$$\frac{I_0}{I} = \frac{\tau_0}{\tau} = 1 + K_{SV}[Q] = 1 + k_q\tau_0[Q] \quad (2.3)$$

In equation 2.3, I and τ are intensities and lifetimes in the presence of quencher, I_0 and τ_0 are the intensity and the lifetime in the absence of quencher, $[Q]$ is the quencher concentration, K_{SV} is the Stern-Volmer constant, and k_q is the quenching rate constant.[96] From time-resolved quenching experiments we can obtain lifetimes for each species of fluorophore and subsequently we can calculate the quenching rate constant for each species of fluorophore (Eq. 2.4).[96-97] The observed rate constant, k_{obs} corresponds to the inverse of the observed lifetime, τ_{obs}.

$$k_{obs} = k_0 + k_q[Q],\ k_{obs} = \frac{1}{\tau_{obs}} \quad (2.4)$$

The total fluorescence emission intensity obtained from steady-state spectroscopy is related to the integral below the decay curve of the singlet excited state decay. The amplitude-averaged lifetime (Eq. 2.5, where A_i is the pre-exponential factor and τ_i is the lifetime that corresponds to each species) was used to check the mechanism of quenching. An equality between the intensity and average lifetime ratios indicates that the quenching occurs through the collision of the excited state and quencher. This mechanism is also named dynamic quenching.[96]

$$<\tau> = \frac{\sum_{i=1}^{n}\tau_i A_i}{\sum_{i=1}^{n} A_i} \quad (2.5)$$

2.5.4 Method to account for the impurity emission of F127 and P104 in time-resolved studies

I was unable to remove the emissive impurities from F127 and P104. The following method was developed to account for the lifetimes data analysis and to account for the impurity emission when analyzing F127 and P104 samples containing pyrene or Np. In this respect, I studied the quenching of the impurity emission in both F127 and P104 samples with the same concentrations of quenchers used to quench the singlet excited state of the probes. The assumption made is that the lifetimes for the emission of the impurities do not change after addition of probes and that the impurities have no interaction with the

probe molecules. Based on this assumption, the lifetimes for the impurities determined from the decay in the absence of pyrene (Table 2.2) were fixed when analyzing the emission decay for pyrene in the F127 (Table 2.3) or P104 samples.

Table 2.2. Fluorescence emission lifetimes and corresponding A values for the quenching of the impurities in 20% F127 with NM at 30 °C.

[NM]/mM	τ_1 / ns[a]	τ_2 / ns[a]	τ_3 / ns[a]	A_1[a]	A_2[a]	A_3[a]	χ^2
0	0.3±0.1	2.3±0.1	8.0±0.2	0.58±0.04	0.37±0.02	0.05±0.01	1.139
15.4	0.2±0.1	1.9±0.1	5.8±0.2	0.61±0.08	0.33±0.02	0.06±0.01	1.026
30.8	0.3±0.1	1.8±0.1	5.0±0.2	0.60±0.05	0.35±0.02	0.06±0.01	0.837
46.2	0.3±0.1	1.6±0.1	4.4±0.2	0.59±0.04	0.35±0.02	0.06±0.01	0.921
61.5	0.2±0.1	1.3±0.1	3.5±0.2	0.7±0.1	0.26±0.03	0.05±0.01	1.021

[a]The errors correspond to standard deviations calculated with the F900 software. The data correspond to one experiment.

Table 2.3. Fluorescence emission lifetimes and corresponding A values for the quenching of the excited state of 5 μM pyrene with NM in 20% F127 at 30 °C.

[NM] / mM	τ_1 /ns[a]	τ_2 /ns[a]	τ_3 /ns[a]	τ_4 / ns[b]	A_1[b]	A_2[b]	A_3[b]	A_4[b]	χ^2
0	0.3	2.3	8.0	180±1	0.30±0.03	0.08±0.03	0.03±0.01	0.59±0.02	1.182
15.4	0.2	1.9	5.8	45±1	0.44±0.06	0.15±0.08	0.08±0.04	0.3±0.2	1.051
30.8	0.3	1.8	5.0	27±1	0.2±0.3	0.13±0.04	0.12±0.03	0.33±0.08	1.101
46.2	0.3	1.6	4.4	20±1	0.51±0.02	0.07±0.01	0.12±0.01	0.30±0.01	1.082
61.5	0.2	1.3	3.5	16±1	0.57±0.02	0.04±0.01	0.14±0.01	0.25±0.01	1.134

[a] Lifetimes corresponding to the F127 impurities were fixed.
[b]The errors represent the standard deviations calculated with the F900 software. The data correspond to one experiment.

2.5.5 Rheological measurement: determination of the complex modulus

The relationship (Eq. 2.6)[64] between complex modulus (G^*), loss modulus (G"), and storage modulus (G') leads to the absolute value of the complex modulus (Eq. 2.7):

$$G^*(\omega) = G' + iG" \tag{2.6}$$

$$|G^*| = \sqrt{G'^2 + G"^2} \tag{2.7}$$

2.5.6 Data analysis for triplet excited state quenching

In the LFP system, the sample is excited with one pulse of the laser beam. The absorption changes as a function of time are measured by comparing the light intensity before and after exciting the sample. The triplet excited state probe decay profile was fit to

a mono-exponential function (Eq. 2.8), where a_0 and k_{obs} are the amplitude in absorbance change and rate constant for the decay. This fit used a custom software[118, 128] and led to the determination of the lifetimes of the triplet excited state probe. The quality of the decay is judged based on the randomness of the residuals between the data and fit. Figure 2.6 shows an example of fitting the decay profile of triplet excited state of Np in water-glycerol mixture.

$$\Delta A = a_0 e^{-k_{obs}t} \tag{2.8}$$

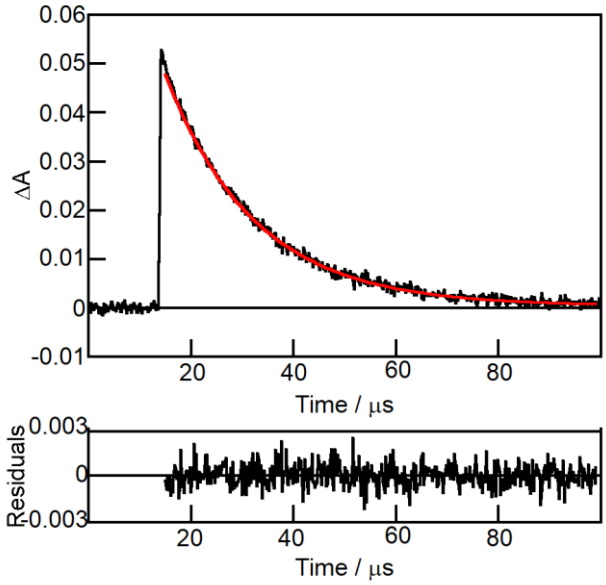

Figure 2.6. Triplet excited state decay for 80 μM Np in water-glycerol at 20 °C (black) fit to equation 2.8 (red). Residuals between calculated and experimental data are shown in the lower panel.

Based on the model described in the previous chapter (see section 1.6), the data for the quenching in F127 samples were fit to equation 2.9,[122] where k_0, k_0^{F127}, k_q and k_q^{F127} are known, while $k_{as}[F127]/N$ and k_{dis} are unknown. This equation assumes that the decays are monoexponential in the presence of all quencher concentrations. At very high concentrations of quencher, the second term of equation 2.9 became insignificant and the equation is reduced to equation 2.10.[98] The value of k_q^{F127} was obtained from the slope of the linear dependence at high quencher concentrations. The value for the quenching in the absence of F127, k_q, was obtained from the quenching studies in water-glycerol (Eq. 2.4).

$$k_{obs} = k_0^{F127} + k_{dis} + k_q^{F127}[Q] - \frac{k_{dis}\, k_{as} \frac{[F127]}{N}}{k_{as} \frac{[F127]}{N} + k_0 + k_q[Q]} \quad (2.9)$$

$$k_{obs} = k_0^{F127} + k_{dis} + k_q^{F127}[Q] \quad (2.10)$$

In order to find the unknown parameters (k_{as}[*F127*]/*N* and k_{dis}), the quenching plots, which correspond to the dependence of k_{obs} on the quencher concentration, were fit to equation 2.9 using the Kaleidagraph software v.4.1.1. The quality of the fits was determined based on nonlinear regression value between 0.98 and 0.99. The quenching plot for the quenching of triplet excited state of Np in 20% F127 hydrogel fit to equation 2.9 is shown as an example (Fig. 2.7).

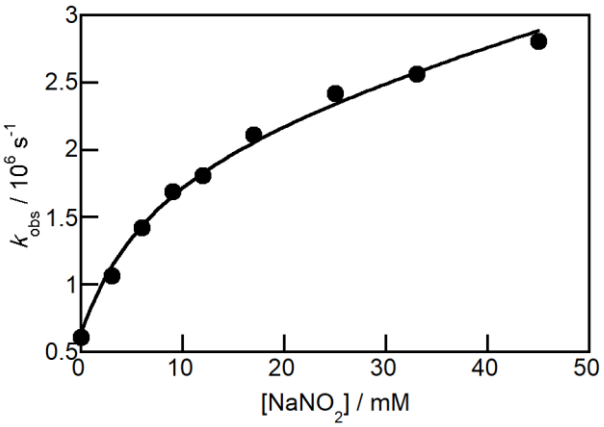

Figure 2.7. Quenching plot for the quenching by nitrite anions of triplet excited Np in 20% F127 at 30 °C.

3 Chapter 3: Studying the Microenvironments in F127 Hydrogel Using Fluorescence Probes

3.1 Introduction

3.1.1 Background

Pyrene (Chart 3.1) is a suitable fluorophore to study heterogenous systems, such as polymeric hydrogels, because of pyrene's sensitivity to the polarity around its microenvironment.[130] The fluorescence emission spectrum of pyrene consists of five vibronic bands. The third vibronic band is not sensitive to the polarity of environment, but the first one is sensitive. In this regard, the ratio of the first to the third vibrionic bands (I/III) is related to the polarity sensed by pyrene and is known as the pyrene scale. The I/III ratio is high in polar solvents and low in non-polar solvents.[131] In addition, the pyrene fluorescence emission spectrum can show a broad peak around 460 nm that corresponds to the pyrene excimer emission. The excimer forms when an excited monomer encounters a ground state monomer, which can occur at high concentrations of pyrene or when two pyrene molecules are in a confined microenvironment.[132] Pyrene molecules are highly hydrophobic and therefore in the presence of surfactants in water the pyrene molecules are more likely to reside in the hydrophobic domains of the surfactant micelles. The location of pyrene can be confirmed from the measurement of I/III values. Besides the solubilization site for pyrene, the value of the I/III ratio in the presence of surfactants is also affected by factors such as compactness of the micelles and the water penetration into the micelles.[133]

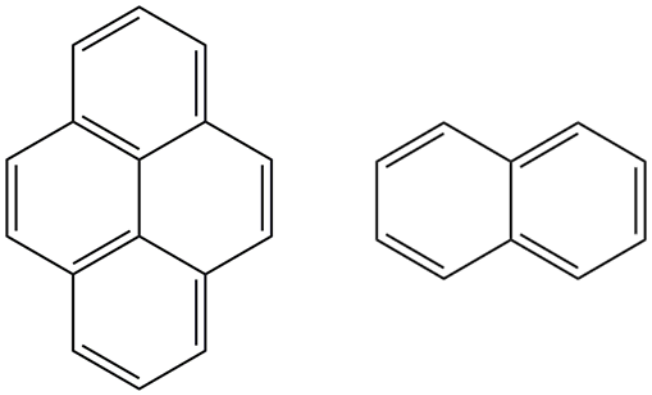

Chart 3.1. Pyrene (left) and naphthalene (right) used as fluorescent probes.

According to the literature, pyrene fluorescence has been used frequently to probe micelles[133-139] including PEO-PPO-PEO triblock copolymer micelles and it was assumed that pyrene locates in the core of the micelles due to the highly hydrophobic nature of pyrene.[45, 140] However, there is a lack of solid explanation to show that pyrene only locates in the core region of Pluronic micelles. To study Pluronic micelles, pyrene fluorescence has been used to determine the aggregation number for these micelles.[141] This emission also has been used to study the effect of temperature on the polarity of Pluronic micellar solutions and to determine the polarity of the core region of Pluronic micelles.[140] Finally, the hydration and microviscosity of Pluronic F127 sol and gel also was studied using pyrene as a fluorescent probe.[142]

Naphthalene (Np, Chart 3.1) is another fluorophore which has been widely used to study the properties of supramolecular and micellar systems. Np is a smaller molecule compared to pyrene. Np has a crystalline unit cell[143] of 362 $Å^3$ while the volume of the pyrene crystalline unit cell[144] is 1035 $Å^3$. Np can form excimers at elevated concentrations in aqueous solution or in restricted environments such as inside the micelles with a peak appearing at 394 nm in the Np fluorescence emission spectrum.[145-146] Np solubility in water increases in the presence of PEO-PPO-PEO triblock copolymers even below CMC and Np solubility have been used to determine the CMC of these micelles.[147]

Pluronic F127 ($(PEO_{99}PPO_{65}PEO_{99})$ is a well-known Pluronic with usage in drug delivery systems. The thermo-reversibility of gel formation and high molecular weight (~12,600 Da) make this polymer a good candidate to carry nonpolar drug molecules.[148] This triblock copolymer forms thermo-reversible gels above a certain concentration.[43] F127 has a low CMC which leads to the formation of micelles at room temperature at very low concentrations of polymer (CMC at 20 °C is 4% w/v).[33] A 20% (w/v) solution of F127 forms a transparent gel state at 30 °C, while decreasing the temperature to 20 °C causes it to reverse back to the solution state, also called sol. There have been several studies on the heterogeneity of F127 micelles using fluorescent probes.[101-102, 104, 149] Studies on the micropolarity and microviscosity of F127 using Nile red as a fluorescence probe showed that in F127 hydrogels there are three regions with different polarities: 1) bulk water, 2) the less polar corona region that consists of hydrated PEO chains and 3) the non-polar core

region made of hydrophobic PPO chains.[99] Different small guest molecules are able to locate in different regions in a Pluronic hydrogel based on the characteristics of the small molecule.

Different additives show a variety of changes in F127 micelles and gels. There have been several studies on the effect of electrolytes on micellization, structure and viscoelastic properties of F127 hydrogels because of the usage of F127 as a drug delivery system and the presence of different electrolytes inside the human body.[150-152] For instance, different ions might locate in different regions of the micellar system, where Na^+ ions were shown to locate deeper inside the corona compared to Li^+ ions locate near the surface. Moreover, different electrolytes can alter the micellar interactions differently, such as LiCl, which cause formation of F127 micellar clusters while NaCl does not show the same effect. Finally, some electrolytes cause dehydration of the corona shell of micelles such as LiCl and NaCl.[103]

F127 hydrogels can be used as an injectable drug delivery system due to its thermo-reversible characteristics. In this respect, the viscosity and moduli are significant for the injection process and cellular responses. Additives can change the sol-gel transition temperature and mechanical properties of Pluronic hydrogels. Therefore, the effect of electrolytes[153], cell-culture media[83], alcohols[151] on the gelation temperature and the rheological behavior of the F127 hydrogel are important properties to be characterized.

In order to better understand the effect of additives on structural change and the bulk properties of hydrogels, the viscoelastic properties of the hydrogel were measured. Heating the aqueous solution of F127 results in aggregation and further increasing the temperature cause F127 gelation around 22-30 °C. Additional heating leads to degelation of F127 and a reversal back to the sol state (around 50-60 °C), and finally at very high temperatures the system reaches the cloud point and phase separation occurs. At elevated temperatures, dehydration of PEO chains in the corona results in the lowering of the volume fraction of the micelles inhibiting the entanglements that form the gel structure.[154]

At low temperatures F127 solutions behave like a Newtonian fluid[71] and its viscosity depends on temperature and concentration of polymer, but with increasing

temperature the viscosity abruptly increases when the gel structure is formed. F127 gels show a significant yield stress and some protocols for finding the gelation temperature define gelation temperature at which the yield stress appears.[65] The protocol that is used in this chapter to define the gelation temperature, is the temperature at which the storage modulus and the loss modulus become equal in the temperature sweep rheology experiments. In addition, frequency sweep experiments were performed to further confirm the state of the viscoelastic material.

The accessibility of a molecule to the excited probe in the various environments of the gel was studied by adding excited state quenchers to the solution. NM was used as a quencher that is sufficiently polar to be located in water and still has access to the interior of the micelles. Two mechanisms has been suggested for quenching singlet excited state pyrene with NM but the most energetically feasible one consists of formation of pyrene-NM ion pair.[155] NM was previously shown to quench the singlet excited state of pyrene in water and also quench this excited state when pyrene was incorporated into micellar systems. These studies were used to infer the solubilization sites for pyrene in the micelles.[139, 156-157]

The other quencher I used to quench the singlet excited states of both pyrene and Np was NaI. Iodide ions are able to quench the excited states of pyrene monomer and excimer emissions.[137, 158-159] Quenching pyrene with iodide ions in an amphiphilic dendro-calixarene indicated the existence of two species of guest in the micellar system; one bound to the micelles and the other where pyrene stayed in the aqueous phase.[137] The binding sites for probes in sodium cholate aggregates were determined using fluorescence quenching of different probes including pyrene and naphthalene with iodide ions. In these studies, the protection efficiency and accessibility of the quenchers to different guest molecules binding to supramolecular aggregates were compared, and information was obtained as to the different environments in which the probes were located in these aggregates.[160] There have been several studies on probing the different regions of PEO-PPO-PEO triblock copolymer micelles using fluorescence probes.[102, 149]

3.1.2 Objectives

In this chapter, steady-state and time-resolved fluorescence spectroscopy were used to study the different probe interaction sites in F127 sol and gel using singlet excited state pyrene and Np as probes. Based on the different sizes of pyrene and Np, I expect that Np will locate in a more protected environment than pyrene in the polymeric micelles for the interaction with quencher molecules that primarily reside outside of the micelles. In this regard, pyrene was quenched with quenchers which have different hydrophilicities to determine the regions in the micelles and gels in which pyrene was located and to compare the accessibility of the different quenchers to the excited state pyrene molecules in different regions. Subsequently, the singlet excited state of Np was quenched with NaI to compare the quenching of two different fluorophores, their location in micelles, and the protection provided by F127 micelles for these two different probe molecules.

After addition of fluorescence probes and quenchers I had to determine if changes to the structure of the F127 hydrogels occurred. To this effect the hydrogel viscoelastic behavior and structure of the micelles were studied using rheology and DLS techniques in the absence and presence of probes and quenchers.

3.2 Results

3.2.1 Steady-state and time-resolved fluorescence spectroscopy for pyrene in F127 hydrogel

The fluorescence spectroscopy of pyrene was used to probe for the polarity of the environments in F127 in which pyrene is located. The normalized fluorescence emission spectrum of pyrene (Fig. 3.1) after addition of F127 polymer showed a 1 nm wavelength shift. No emission was observed around 460 nm which confirms that no excimer was formed, indicating that pyrene molecules were not located in close proximity in the gel. The I/III value decreased in 20% F127 hydrogel compared to water (Fig. 3.1, Table 3.1), and the I/III values remained constant (Fig. 3.2) for F127 concentrations above the CMC[161] (0.008 wt% at 30 °C). At concentrations of 5 and 10% (w/v) and at 30 °C, F127 is in solution state but at concentrations of 20 and 30% (w/v) at 30 °C, F127 is in gel state.

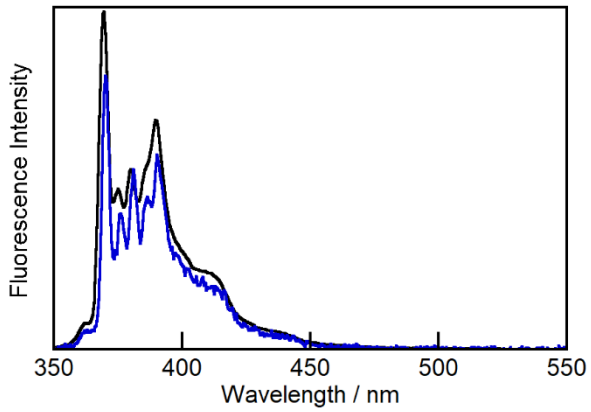

Figure 3.1. Normalized fluorescence emission spectra at 381 nm of pyrene in water (0.5 μM, black) and pyrene in 20% F127 hydrogel (5 μM, blue) at 30 °C.

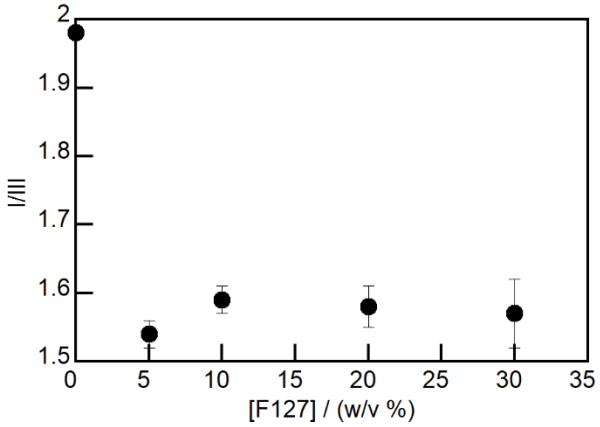

Figure 3.2. I/III ratios for the pyrene emission at different concentrations of F127 at 30 °C. The data correspond to averages for three independent experiments. The error bars correspond to standard deviations, error bars smaller than the symbols are not shown.

Excited state lifetime measurements are used to identify fluorophores in different environments of the gel, since the lifetimes for the same fluorophore are frequently different in the different environments of a microheterogeneous or compartmentalized systems.[37] In order to better understand the features of different regions of the F127 hydrogel, I performed steady-state and time-resolved fluorescence studies for pyrene in bulk liquid PPO with different molecular weights and bulk liquid PEO at 30 °C, which correspond to the individual constituents of F127. The temperature of 30 °C was chosen

because at this temperature 20% F127 is in the gel state. Only one lifetime corresponding to pyrene found in the liquid polymers at 30 °C as demonstrated in table 3.1. In the F127 hydrogel, the pyrene lifetime (Table 3.1) was lengthened compared to water and was similar to the lifetimes in PPO, while the pyrene lifetime was longer in PEO. The I/III ratios were the same for pyrene in PEO and water and lower, but the same, for pyrene in F127 and PPO (Table 3.1).

Table 3.1. I/III ratios and lifetimes (τ) for the singlet excited state of pyrene in different solutions at 30 °C.[a]

Solutions	I/III	τ / ns
Water	2.0 ± 0.1 (3)	120 ± 1 (2)
20% F127	1.6 ± 0.1 (4)	180 ± 3 (4)
PPO (MW:2000)	1.5 ± 0.1 (2)	150 ± 2 (2)
PPO (MW:4000)	1.4 ± 0.1 (3)	180 ± 6 (3)
PEO (40% w/w in H_2O)	2.1 ± 0.1 (2)	210 ± 6 (2)

[a] The number of independent experiments is shown in parenthesis. For two experiments the errors correspond to average deviations and for more than two experiments the errors correspond to standard deviations.

The I/III ratios were measured for pyrene in 20% F127 at different temperatures spanning the CMT of around 10 °C[74, 162] and the sol-to-gel-transition temperature of 23 °C for 20% F127[65] (Table 3.2). The I/III ratios did not change at different temperatures. The 20% F127 is in gel state above 25 °C.

Table 3.2. The I/III ratio for 5 μM pyrene in 20% F127 at different temperatures.[a]

T / °C	I/III
15	1.6 ± 0.1
20	1.7 ± 0.1
25	1.6 ± 0.1
30	1.6 ± 0.1
35	1.5 ± 0.1

[a]The data correspond to two independent experiments and the errors correspond to average deviations.

3.2.2 Quenching of pyrene in F127 with different concentrations of NM

The fluorescence intensity for pyrene decreases with increasing NM concentrations (Fig. 3.3), showing that quenching of excited pyrene by NM occurred in the hydrogel (Fig.

3.3a) and in the sol state (Fig. 3.3b). At all NM concentrations, the pyrene spectra corresponded to the monomer emission and no excimer emission was observed. The I/III ratios for the pyrene emission in the F127 hydrogel were constant with increasing NM concentrations (Fig. 3.4a), while in the sol state the I/III ratios decreased with increasing NM concentrations (Fig. 3.4b).

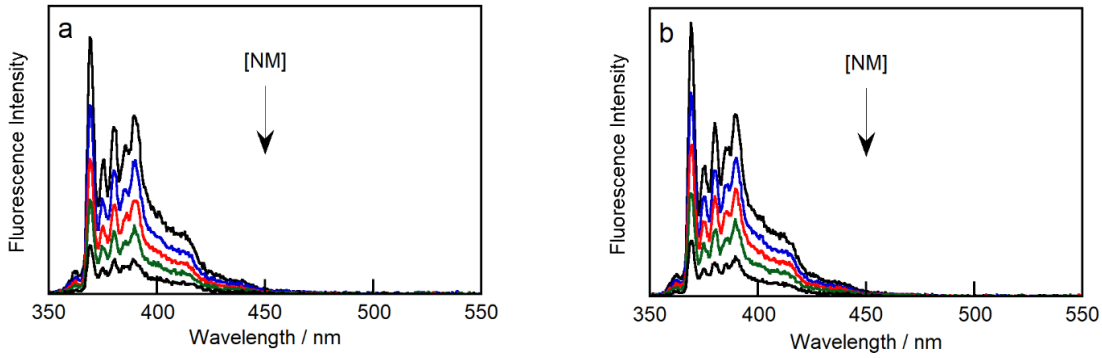

Figure 3.3. Fluorescence emission spectra for 5 μM pyrene in 20% F127 quenched with NM ([NM] = 0-6.5 mM) at a) 30 °C and b) 20 °C.

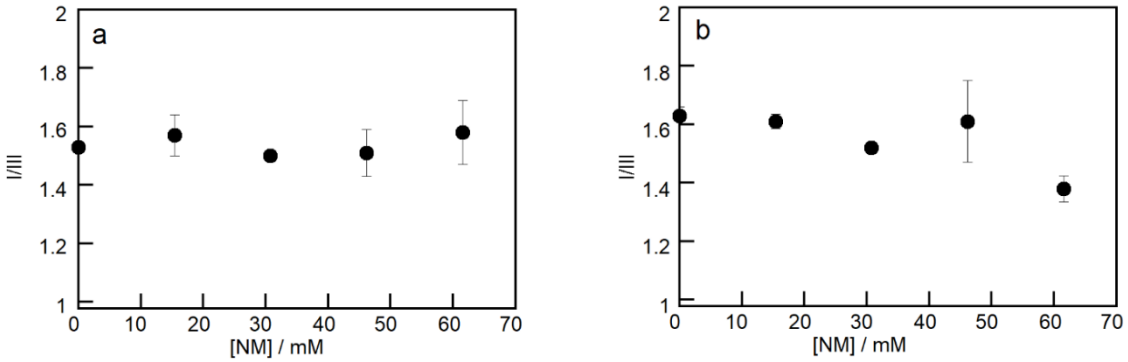

Figure 3.4. I/III ratios for 5 μM pyrene in 20% F127 at different concentrations of NM at a) 30 °C and b) 20 °C. The data correspond to averages for two independent experiments. The error bars correspond to average deviations, error bars smaller than the symbols are not shown.

The decays for the singlet excited state pyrene emission in water in the presence of NM were adequately fit to a monoexponential function (Table 3.3). In contrast, for pyrene in 20% F127 hydrogel the decays were fit to a sum of exponentials (Eq. 2.2, Fig 3.5). In the presence of F127 the emission decay contains components due to the impurity emission from F127 (Fig 3.6). The lifetimes for the impurities in the presence of the various NM

concentrations were determined independently (see 2.5.4, Tables 2.2-2.3) and were fixed for the analysis of the decays in the presence of pyrene (Tables 7.1-7.4 in the Appendix). Only the lifetimes for the pyrene emission will be presented and analyzed here.

Table 3.3. Fluorescence emission lifetimes and corresponding A values for 0.5 μM pyrene quenching with NM in water at 30 °C.

[NM] / mM[b]	τ / ns[a]	χ^2
0	120.7 ± 0.4	0.984
6.01 ± 0.01	14.4 ± 0.2	0.838
12.01 ± 0.01	8.6 ± 0.1	0.899
19.5 ± 0.2	5.7 ± 0.1	1.007
25.3 ± 0.2	4.3 ± 0.1	1.092

[a]The errors correspond to standard deviations obtained from the fit using the F900 software. The data correspond to one experiment.
[b]See 2.3.3 and 2.3.5 for method in the determination of the NM concentration and quenching pyrene in water.

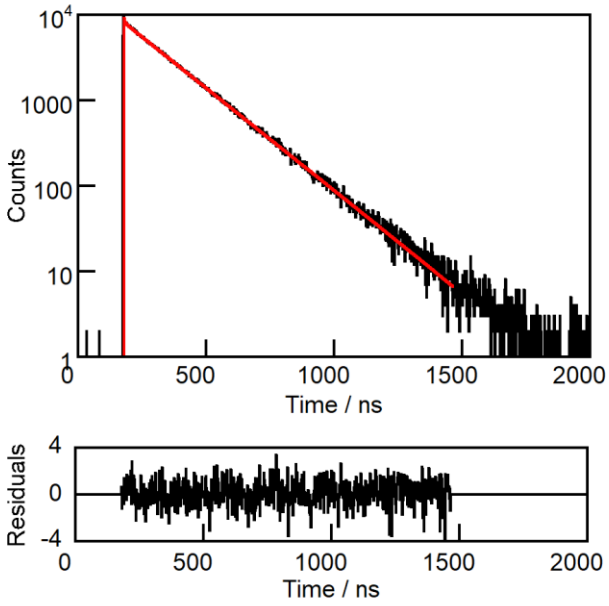

Figure 3.5. Fluorescence decay for 5 μM pyrene in 20% F127 at 30 °C (black) fit to a sum of exponentials decay (red) using a tail fit. Residuals between calculated and experimental data are shown in the lower panel.

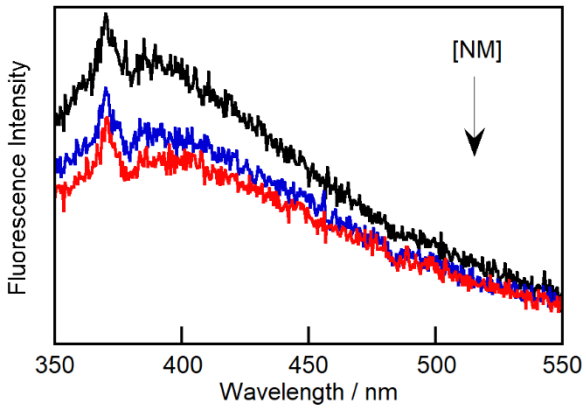

Figure 3.6. Fluorescence emission spectra of impurities in 20% F127 quenched with NM ([NM] = 0-31 mM) at 30 °C.

The decay profiles of excited state pyrene in 20% F127 hydrogel at different concentrations of NM are illustrated in figure 3.7a-e. In 20% F127 gel, only one lifetime corresponding to pyrene was found as indicated in tables 7.1-7.2 (in the Appendix). On the other hand, the decay profiles of excited state pyrene in 20% F127 sol at different concentrations of NM are illustrated in figure 7.1 a-e (in the Appendix). In F127 sol at 20 °C after the addition of NM two lifetimes correspond to pyrene were found as shown in tables 7.3-7.4 (in the Appendix); one lifetime component of pyrene decays faster than the other. With increasing concentrations of NM, the relative population of short lifetime component increases and the relative population of long lifetime component decreases, table 7.3 (in the Appendix). For the second quenching experiment in F127 sol, this trend is observed, table 7.4 (in the Appendix).

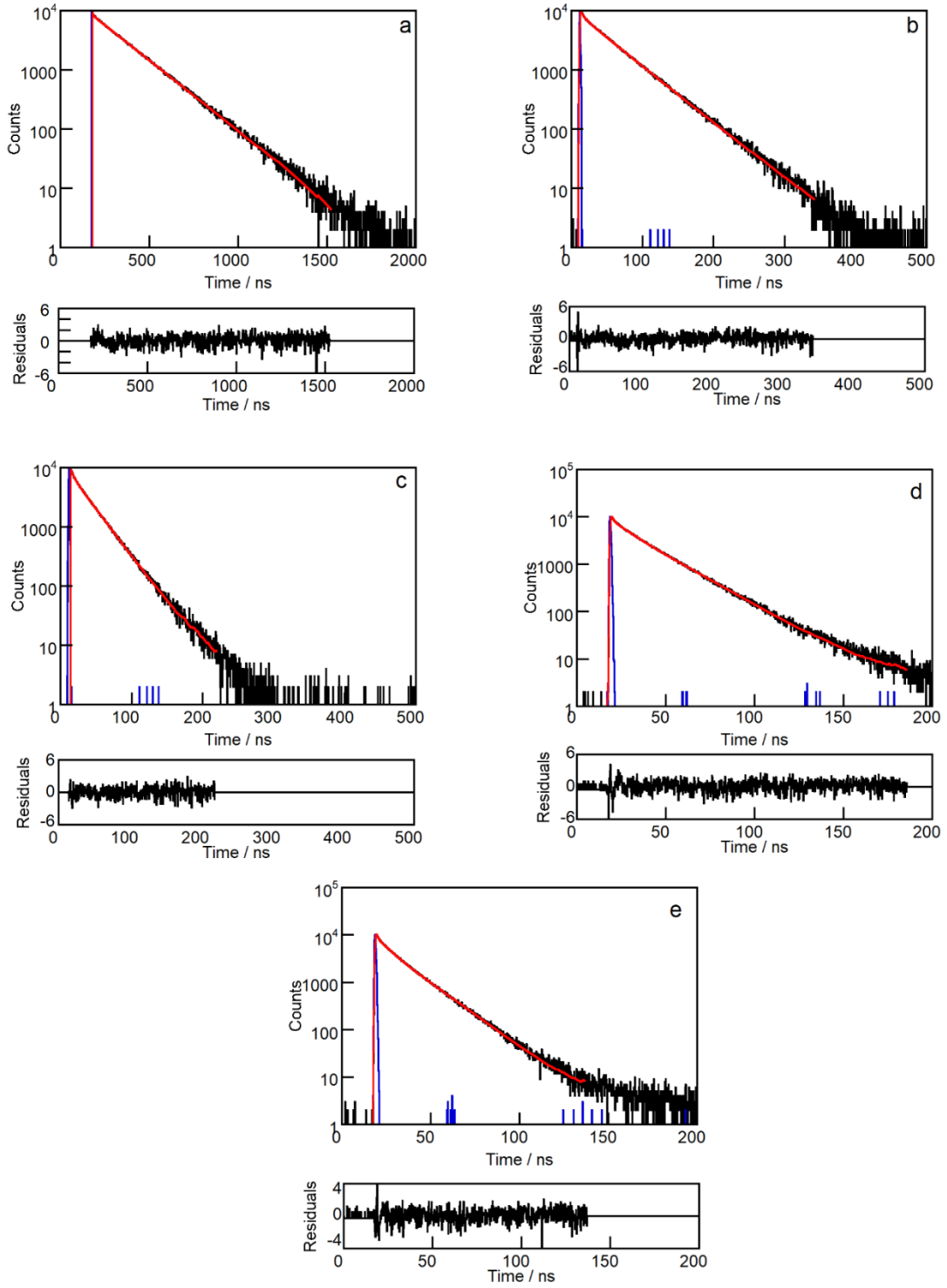

Figure 3.7. Fluorescence decay for 5 µM pyrene in 20% F127 at 30 °C (black) fit to a sum of exponentials decay (red) with IRF shown in blue. The different concentrations of NM are a) 0 mM, b) 15.4 mM, c) 30.8 mM, d) 46.2 mM, and e) 62.5 mM. Residuals between calculated and experimental data are shown in the lower panels.

Quenching experiments were performed for higher concentration of F127. In 30% F127 at 30 °C, only one lifetime corresponding to pyrene was found as shown in table 7.5 (in the Appendix). Decreasing the temperature to 20 and 10 °C led to the appearance of the second species of pyrene with a faster lifetime component (Tables 7.6-7.7 in the Appendix). Again, it was observed that increasing the concentration of NM led to an increase in the relative population of fast lifetime component and decreased the relative population of slow lifetime component.

The mechanism of quenching was inferred from the analysis of figures 3.8a-b where the lifetime ratios and intensity ratios for 5 μM pyrene in F127 hydrogel and sol in the presence and absence of quencher are shown. Quenching plots for the quenching of excited pyrene in 20% F127 gel (Fig 3.8a) and sol (Fig 3.8b) are linear. The intensity ratios and lifetime ratios in the absence and presence of quencher are the same at different concentrations of quencher which shows that the quenching plots follow the Stern-Volmer equation (Eq 2.3). The plot of k_{obs} which correspond to the longer lifetime of pyrene species and intensity ratios in the absence and presence of quencher versus NM concentration were linear for quenching pyrene in 20% F127 gel (Fig 3.9a-b) and sol (Fig 3.10). The k_{obs} correspond to the shorter lifetime of pyrene in 20% F127 at 20 °C, is plotted in figure 7.2 (in the Appendix). The value of k_q for the shorter lifetime correspond to the other species of pyrene (Table 7.3 in the Appendix) is $(8.9 \pm 0.1) \times 10^8$ $M^{-1}s^{-1}$.

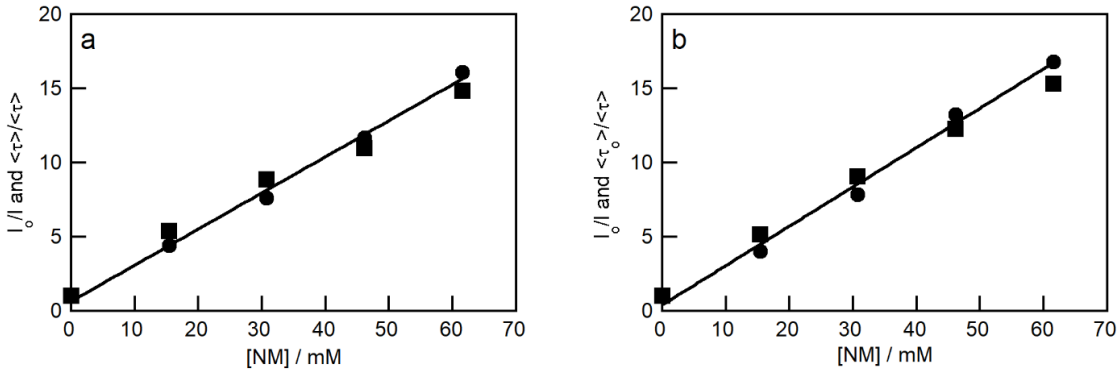

Figure 3.8. Dependence of the intensity ratio (circle) and average lifetime ratio (square) on the quencher concentration corresponding to quenching 5 μM pyrene in 20% F127 by NM at a) 30 °C and b) 20 °C. Data correspond to one experiment.

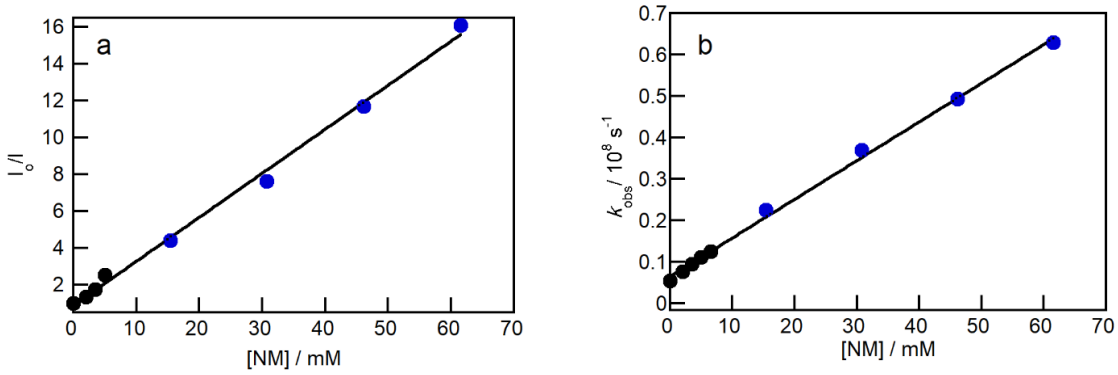

Figure 3.9. Quenching plots for 5 μM pyrene in 20% F127 at 30 °C quenched by NM a) intensity ratio in the absence and presence of quencher, b) dependence of k_{obs} for pyrene with the NM concentration. Black and blue symbols correspond to different set of experiments. All the experiments were performed once.

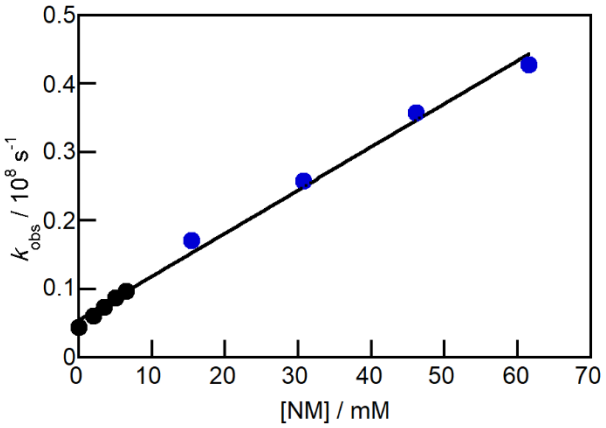

Figure 3.10. Quenching plot for 5 μM pyrene in 20% F127 at 20 °C quenched by NM (k_{obs} correspond to longer lifetime of singlet excited pyrene). Black and blue symbols correspond to different set of experiments. All the experiments were performed once.

The quenching rate constants and Stern-Volmer constants for the quenching of pyrene in different concentrations of F127 at different temperatures are shown in table 3.4. The value of k_q (all reported k_qs in table 3.4 correspond to longer lifetime for pyrene), and K_{sv} in water is significantly higher than when pyrene is located in F127. Nonetheless, the values of k_q at different concentrations of F127 at similar temperatures, are very close. Upon increasing temperature, the value for k_q increases. Moreover, the value for k_q for the

shorter lifetime of pyrene species is higher compared to k_q for another pyrene species with longer lifetime in 20% F127 at 20 °C.

Table 3.4. Quenching rate constant (correspond to longer lifetime of singlet excited pyrene) and Stern-Volmer constant for the quenching of 5 μM pyrene with NM in F127 and quenching with NM of 0.5 μM pyrene in water.[a]

Sample	T / °C	k_q / 10^8 $M^{-1}s^{-1}$	K_{sv}/ 10^2 M^{-1}
Water	30	81 ± 9 (2)	10 ± 2 (2)
20% F127	20	6.0 ± 0.2 (2)	2.7 ± 0.1 (2)
20% F127	30	9.1 ± 0.3 (3)	2.9 ± 0.5 (3)
30% F127	10	4.7 (1)	1.9 (1)
30% F127	20	6.5 (1)	2.2 (1)
30% F127	30	8.8 ± 0.3 (2)	3.7 ± 0.4 (2)

[a]The number of independent experiments is shown in parenthesis, for two experiments the errors correspond to average deviations and for more than two experiments the errors correspond to the standard deviations.

3.2.3 Quenching of pyrene in F127 with different concentrations of NaI

Figure 3.11a-b illustrates the reduction in fluorescence intensities of excited state pyrene with increasing the concentration of NaI in the F127 gel (Fig 3.11a) and sol (Fig 3.11b). This reduction shows the quenching of excited pyrene. With increasing concentrations of NaI, the lifetime of excited state pyrene is shortened, and the quenching plots are linear in F127 gel and sol (Fig 3.12a-b). The fluorescence emission spectra the quenching of the F127 impurities with NaI shown in figure 3.13. The decay profiles for quenching pyrene in F127 hydrogel in different concentrations of NaI is shown in figure 3.14, where the decays are fit to a sum of exponentials function to obtain the lifetime of excited pyrene (Fig 7.3 a-e in the Appendix). In order to obtain the lifetime of pyrene, the impurities in F127 polymer quenched with NaI must be accounted for, and the lifetimes for the impurities are shown in table 3.5. The lifetimes of for the impurity emission were fixed and the lifetimes of excited pyrene in F127 gel (Table 7.8 in the Appendix) and sol (Table 7.9 in the Appendix) were obtained. With increasing the concentration of NaI only one lifetime corresponding to excited pyrene is observed in F127 sol and gel using time-resolved quenching measurements (Tables 7.8-7.9 in the Appendix).

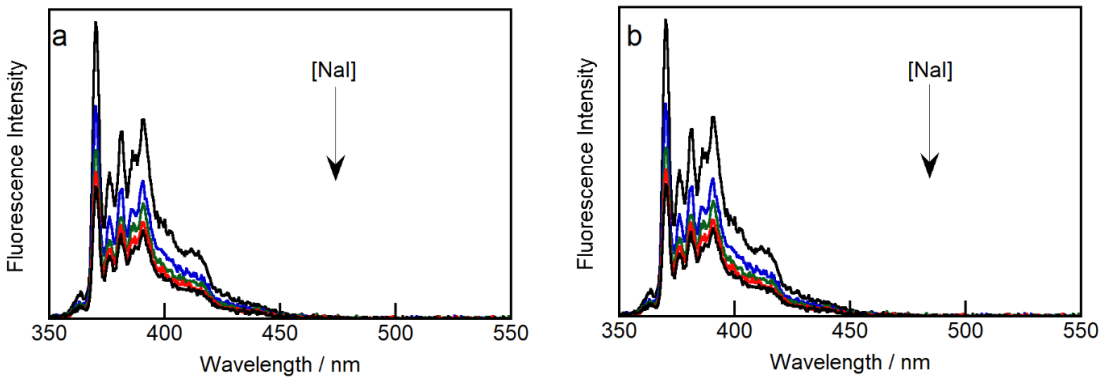

Figure 3.11. Fluorescence emission spectra for 5 μM pyrene in 20% F127 quenched with NaI ([NaI] = 0-62 mM) at a) 30 °C and b) 20 °C.

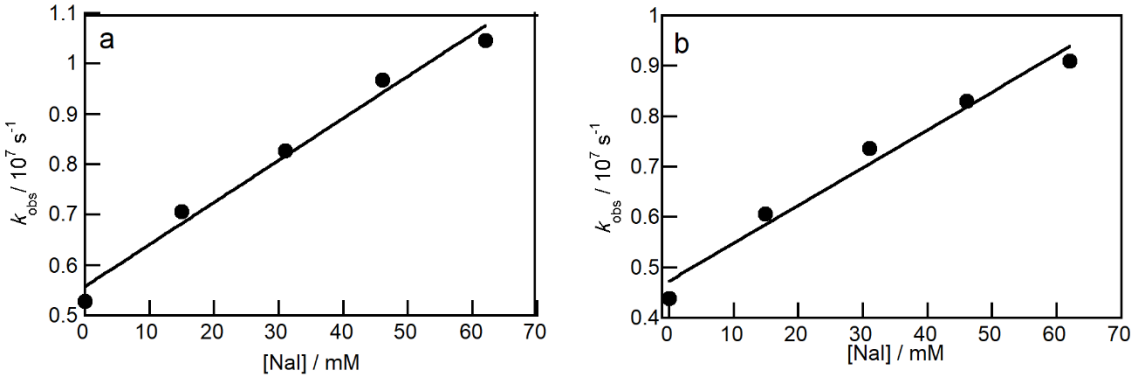

Figure 3.12. Quenching plots for 5 μM pyrene in 20% F127 at 30 °C quenched by NaI a) at 30 °C b) at 20°C. The data correspond to one experiment.

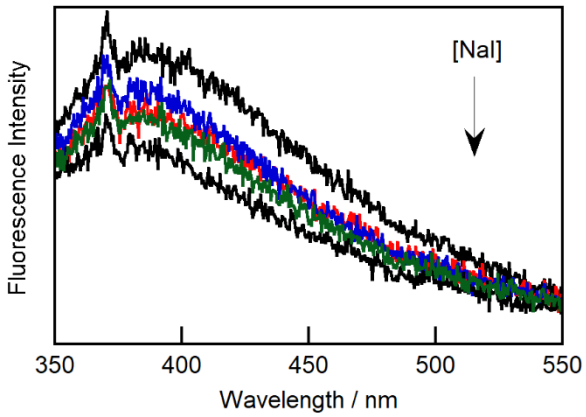

Figure 3.13. Fluorescence emission spectra of impurities in 20% F127 quenched with NaI ([NaI] = 0-62 mM) at 30 °C.

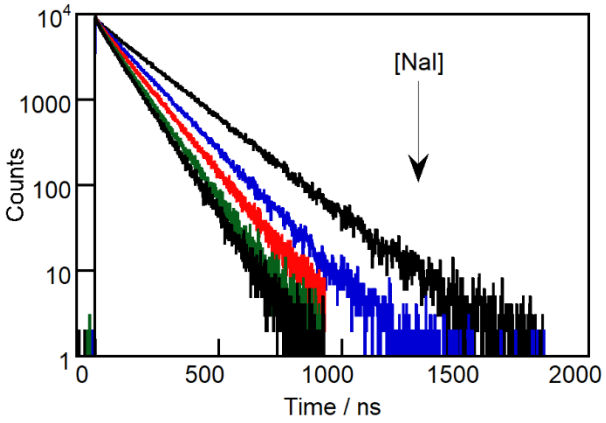

Figure 3.14. Fluorescence decays for 5 μM pyrene in 20% F127 at 30 °C fit to a sum of exponentials decay at different concentrations of NaI (0-62 mM).

Table 3.5. Fluorescence emission lifetimes and corresponding A values for the quenching of impurities in 20% F127 with NaI at 30 °C. (The excitation wavelength was 335 nm).

[NaI] / mM[b]	τ_1/ns	τ_2 / ns[a]	τ_3 / ns[a]	A_1[a]	A_2[a]	A_3[a]	χ^2
0	0.2	2.3±0.1	9.1±0.3	0.8±0.1	0.22±0.02	0.03±0.01	0.993
14.9 ± 0.1	0.2	2.2±0.1	9.0±0.2	0.8±0.1	0.20±0.01	0.02±0.01	1.015
30.8 ± 0.1	0.2	2.2±0.1	8.7±0.2	0.7±0.2	0.26±0.04	0.03±0.01	1.073
45.7± 0.1	0.3	2.2±0.1	8.6± 0.2	0.7±0.3	0.27±0.04	0.03±0.01	0.843
61.7 ± 0.1	0.2	2.1±0.1	8.2±0.2	0.8±0.1	0.22±0.02	0.03±0.01	0.990

[a]The errors represent the standard deviations calculated using the F900 software. The data correspond to one experiment.

[b]See 2.3.3 for method in the determination of the NaI concentration.

I/III ratios for excited pyrene molecules inside the F127 gel, do not change with increasing NaI concentrations as shown in figure 3.15. The ratio of fluorescence intensities and lifetimes in the absence and presence of quencher are equal at different concentrations of NaI (Fig. 3.16). This result is similar to the results of quenching pyrene with NM in F127 hydrogels, which also followed the Stern-Volmer equation.

In the presence of F127 micelles, quenching rate constants for the quenching of excited pyrene probe with NaI decreased significantly compared to the quenching of this probe in water (Table 3.6), which is consistent with the quenching results for NM quencher as demonstrated above.

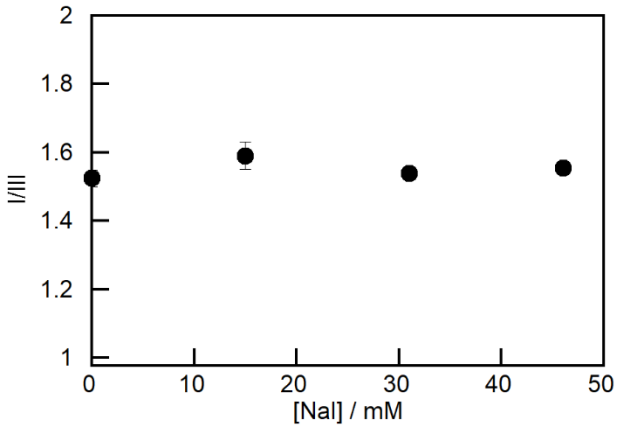

Figure 3.15. I/III ratios for 5 μM pyrene in 20% F127 at different concentrations of NaI at 30 °C. The data correspond to averages for two independent experiments. The error bars correspond to average deviations.

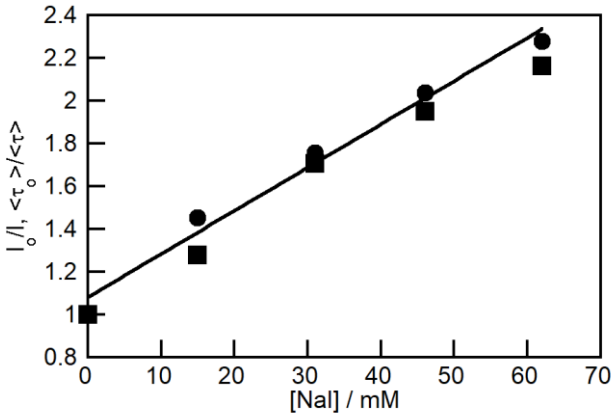

Figure 3.16. Intensity ratio (circle) and average lifetime ratio (square) versus NaI concentration corresponding to quenching 5 μM pyrene in 20% F127 at 30 °C. Data correspond to one experiment.

Table 3.6. Quenching rate constants for quenching 5 μM pyrene in 20% F127 and 0.5 μM pyrene in water with NaI at different temperatures.[a]

Sample	T / °C	k_q / 10^7 $M^{-1}s^{-1}$
Water	30	120 (1)
Water	20	100 (1)
20% F127	20	7.4 ± 0.5 (2)
20% F127	30	8.3 ± 0.5 (2)

[a] The number of independent experiments is shown in parenthesis, for two experiments the errors correspond to average deviations.

3.2.4 Quenching of Np in F127 with different concentrations of NaI

The other probe which is used to study the microheterogeneity of F127 hydrogels is Np, with the objective of comparing the protection efficiency for Np with that for pyrene. The concentration of Np and pyrene are the same and this concentration is much lower than the concentration of micelles. Np was quenched with NaI in water and in the F127 hydrogel. After addition of different concentrations of NaI, no excimer peak was observed in the fluorescence emission spectra of Np in F127 sol and gel, figure 3.17. The linear quenching plot for Np with NaI in water at 30 °C is demonstrated in figure 3.18a. The mechanism of quenching Np with NaI is known to be the dynamic mechanism. The quenching rate constant in water (Table 3.8) is similar to the values reported in literature and lifetime of singlet excited state of Np in water is close to the reported values in literature[163-164], the linear quenching plot for Np in water is demonstrated in figure 7.4 (in

the Appendix). In the presence of F127 micelles, the quenching plot for Np is also linear (Fig 3.18b).

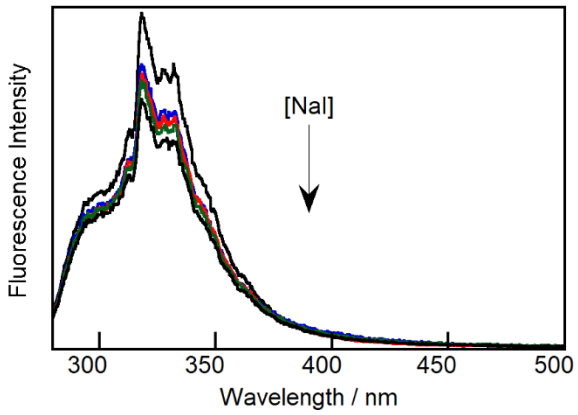

Figure 3.17. Fluorescence emission spectra for 5 μM Np in 20% F127 quenched with NaI ([NaI] = 5-20 mM) at 30 °C.

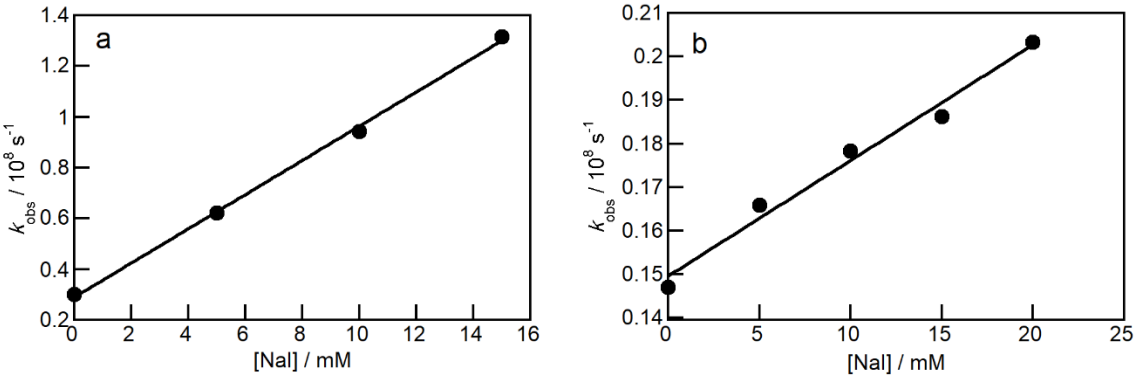

Figure 3.18. Quenching plots for 5 μM Np at 30 °C quenched by NaI in a) water b) 20% F127. The data correspond to one experiment.

The lifetimes of Np in F127 hydrogel obtained from the analysis of time-resolved fluorescence measurements are shown in table 3.7. The impurities of F127 were quenched and the lifetimes were obtained by exciting the sample at the same wavelength as Np was excited. The results for the lifetimes recovered from the quenching of impurities are shown in table 7.10 (in the Appendix). After fixing the lifetimes for the impurities for samples containing Np, only one lifetime corresponding to singlet excited Np in F127 hydrogel was found (Table 3.7). The relative population of Np did not change with increasing NaI

concentration. The quenching rate constants of Np in water and F127 hydrogel with NaI are reported in table 3.8.

Table 3.7. Fluorescence emission lifetimes and corresponding A values of for the quenching of 5 μM Np with NaI in 20% F127 at 30 °C.

[NaI] / mM[b]	τ_1/ns [a]	τ_2 /ns[a]	τ_3 /ns[a]	τ_4 / ns[c]	A_1[c]	A_2[c]	A_3[c]	A_4[c]	χ^2
0	0.4	4.1	12.1	68±1	0.83±0.01	0.13±0.01	0.02	0.02	1.087
4.8±0.1	0.4	4.1	11.7	60±1	0.83±0.01	0.13±0.01	0.02	0.02	1.159
10.2±0.1	0.4	3.9	11.0	56±1	0.82±0.02	0.14±0.01	0.02	0.02	1.138
14.9±0.1	0.4	3.8	10.9	54±1	0.83±0.01	0.13±0.01	0.02	0.02	1.029
19.9±0.1	0.4	3.8	11.0	49±1	0.82±0.02	0.14±0.01	0.02	0.02	1.108

[a]Lifetimes correspond to F127 impurities were fixed.
[b]See 2.3.3 for method in the determination of the NaI concentration.
[c]The errors represent the standard deviations calculated using the F900 software. The data correspond to one experiment.

Table 3.8. Quenching rate constants of for the quenching of 5 μM Np in 20% F127 and 1 μM Np in water with NaI.[a]

Sample	T / °C	k_q / 10^8 $M^{-1}s^{-1}$
Water	30	67 (1)
20% F127	30	2.8 ± 0.1 (2)

[a] The number of independent experiments is shown in parenthesis, for two experiments the errors correspond to average deviations.

3.2.5 Structural and viscoelastic behavior of F127 hydrogel in the presence of different additives

The size of F127 micelles in the presence of different additives, such as pyrene and the highest concentrations of NM and NaI was studied. The polydispersity index and hydrodynamic diameter of F127 micelles did not change significantly after addition of different additives as shown in table 3.9.

Table 3.9. Hydrodynamic diameter and polydispersity of F127 micelles in the presence of different additives at 20 °C.[a]

Sample	Hydrodynamic diameter / nm	PDI
F127	11 ± 1	0.18 ± 0.02
F127_pyrene	11 ± 1	0.16 ± 0.03
F127_pyrene_ NaI	10 ± 2	0.18 ± 0.04
F127_ pyrene_ NM	12 ± 4	0.20 ± 0.04

[a] Measurements were done four times and errors correspond to standard deviations.

The linear viscoelastic region (LVR) is defined when G' and G" are constant with the applied strain or stress during the measurement. In this region the deformations in the material are reversible. At higher shear strains or shear stress, the material deviates from the linear region and the deformations are not reversible leading to a decrease of both G' and G". LVR are defined as the region where both G' and G" do not deviate more than 5% around the plateau.[64, 165] Hence, before performing oscillatory measurements I checked the LVR for the F127 hydrogels.

Figure 3.19 shows the strain sweep tests performed on F127 hydrogels containing different additives. Addition of pyrene did not change the extend of the LVR for F127 hydrogel. However, after addition of 62 mM NaI the LVR of the sol state sample shortened compared to pure F127 sol; the values are presented in table 3.10. At the shear strain (γ) of 0.5% all samples are in the LVR. For temperature sweep experiments, I chose γ of 0.5% to remain in LVR and decrease the signal to noise ratio that caused by the low-torque limit of rheometer.

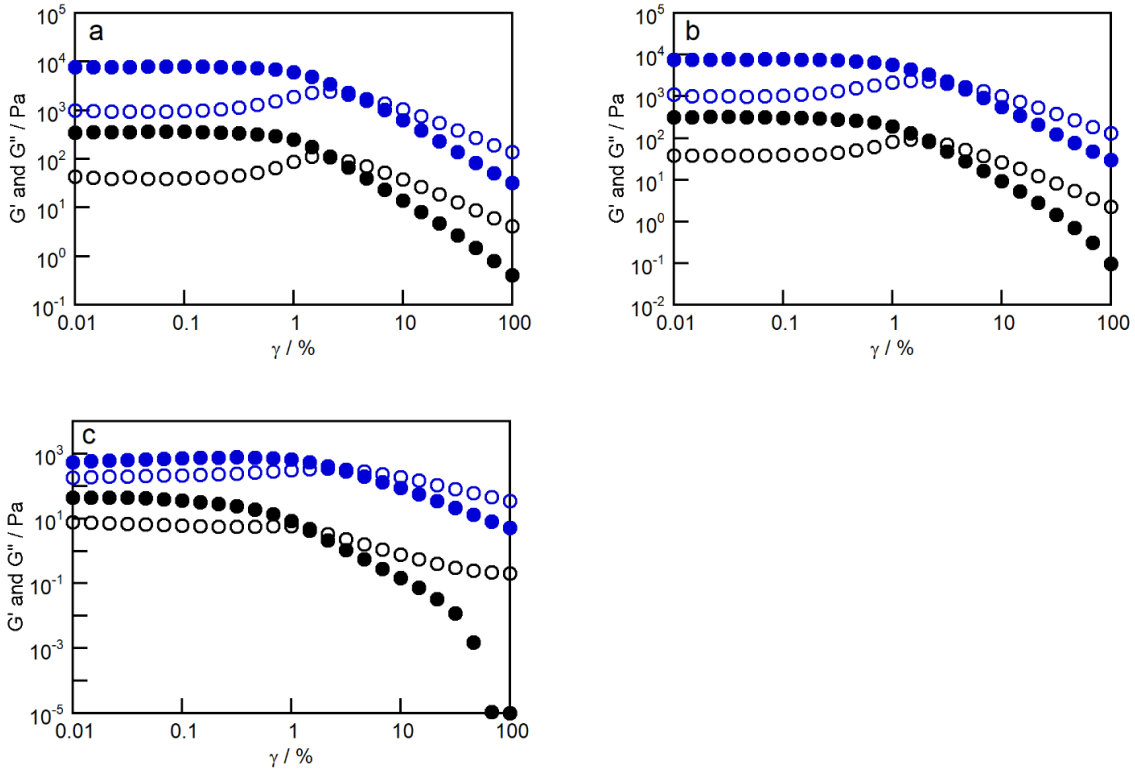

Figure 3.19. Dependence of G′ (filled symbols) and G″ (open symbols) on shear strain at the angular frequency of 1 rad/s at 20 °C (black), and 30°C (blue) for a) 20% F127 b) 20% F127 + 5 μM pyrene, and c) 20% F127 + 5 μM pyrene + 62 mM NaI.

Table 3.10. The LVR for different samples at 30 °C.[a]

Sample	γ / %
20% F127	1.1 ± 0.4
20% F127_5 μM pyrene	1.2 ± 0.2
20% F127_5 μM pyrene_62 mM NaI	1.3 ± 0.2

[a], The measurements were performed for two independent experiments and errors correspond to average deviation.

Temperature sweep experiments can give information about the phase transitions and the transition temperatures for the gel. Pluronic F127 hydrogel forms gel over a narrow temperature range. At low temperatures, F127 samples are in the sol state and have low viscosity. In the sol state G" is higher than G', the G' is too low to be measured by rheology. The scatter observed for G' at low temperatures occurs because the measurements are close

to the low-torque limit of the instrument.[71] The shear strain of 0.5% was the best choice to the lower noise for the temperature sweep measurements.

There are sol-gel and gel-sol phase transitions for F127 hydrogel upon heating which are defined from temperature sweep experiments of gels.[67, 71] At very high temperatures, F127 gel melts[67] so I did not increase the temperature further to enter the gel-sol phase transition region in F127 hydrogel. Upon heating, the F127 moduli increase slowly until a characteristic temperature when both moduli start increasing sharply. The gelation occurs over a narrow temperature range when G' and G" starts increasing abruptly. To define the gelation temperature (T_{gel}), I considered the temperature at which tan(δ) is equal to one.[166] For different samples, T_{gel}s were measured from temperature sweep tests as shown in figure 3.20 for F127 hydrogels containing additives like pyrene and the highest concentrations of quenchers used for the excited state pyrene quenching experiments (see 3.2.2 and 3.2.3 sections). T_{gel} for different samples are reported in table 3.11, which indicates that even at highest concentrations of quenchers the viscoelastic behavior of F127 hydrogels did not change and gel is formed at roughly the same T_{gel} as observed for the pure F127 hydrogel. To further confirm that at 30 °C all the samples are in the gel state, frequency sweep tests were performed. For all samples at 30 °C as illustrated in figure 3.21, G' is higher than G" and the samples demonstrate a solid-like behavior.

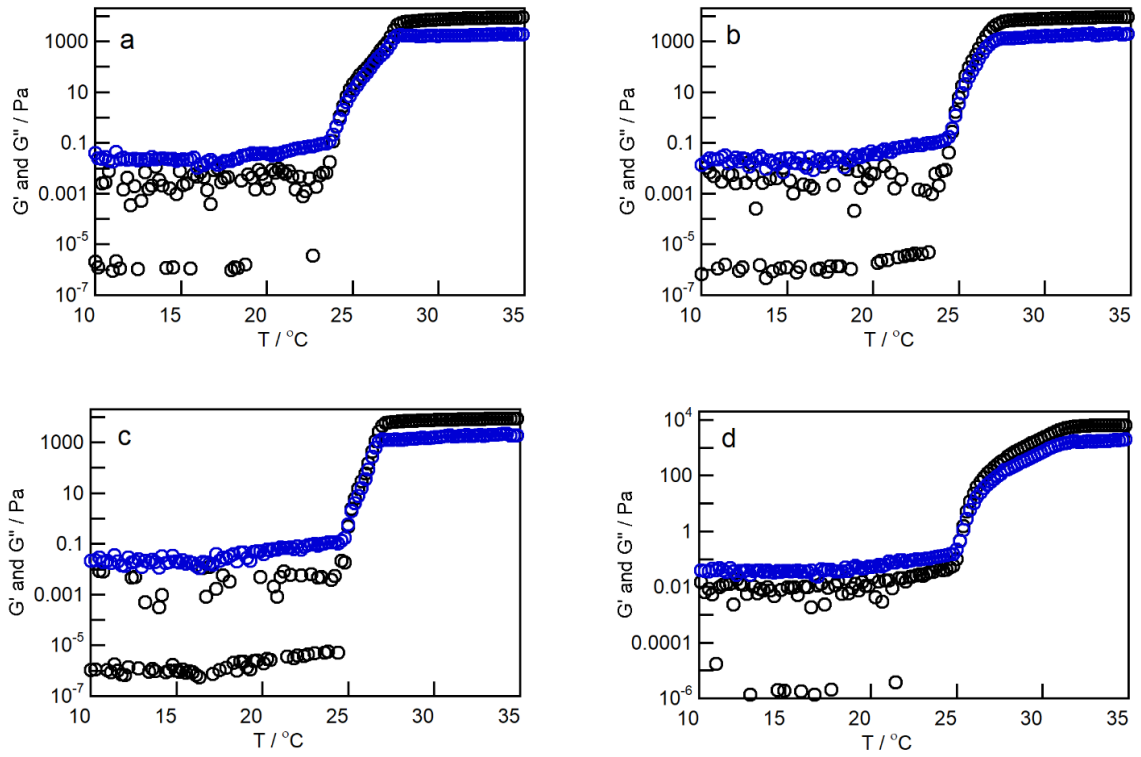

Figure 3.20. Dependence of G′ (black circles) and G″ (blue circles) on temperature at the angular frequency of 1 rad/s and shear strain of 0.5% for a) 20% F127 b) 20% F127 + 5 μM pyrene, c) 20% F127 + 5 μM pyrene + 61.5 mM NM, and d) 20% F127 + 5 μM pyrene + 62 mM NaI.

Table 3.11. Gelation temperatures of 20% F127 in the presence of different additives with heating rate of 0.5 °C/min, ω of 1 rad/s, and γ of 0.5%.[a]

Sample	T_{gel} / °C
20% F127	23.5 ± 0.1
20% F127_5 μM pyrene	24.8 ± 0.1
20% F127_5 μM pyrene_62 mM NaI	25.5 ± 0.5
20% F127_5 μM pyrene_61.5 mM NM	21.6 ± 1.9

[a], The measurements were performed for three independent experiments and errors correspond to standard deviation.

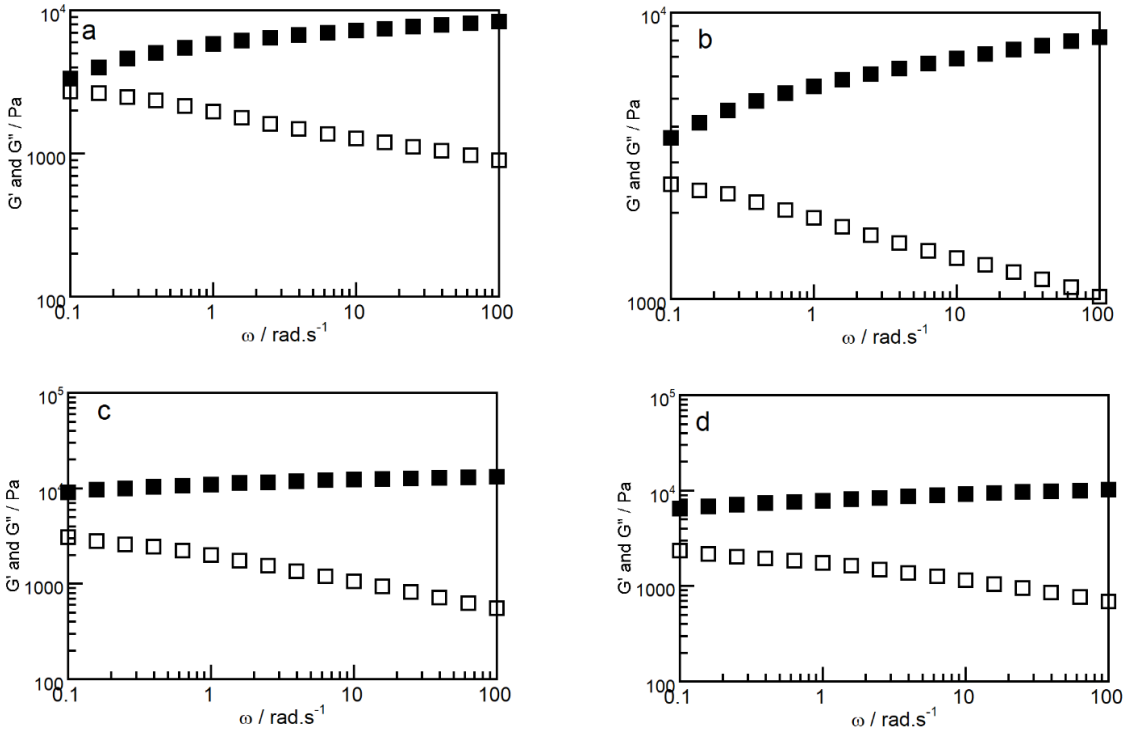

Figure 3.21. Dependence of G′ (closed symbols) and G″ (open symbols) on angular frequency at the constant shear strain of 0.5% at 30 °C for a) 20% F127 b) 20% F127 + 5 μM pyrene, c) 20% F127 + 5 μM pyrene + 61.5 mM NM, and d) 20% F127 + 5 μM pyrene + 62 mM NaI.

The changes of the complex modulus with temperature for F127 hydrogels containing different additives is depicted in figure 3.22. This plot allows the comparison of the overall mechanical characteristics of the samples. The complex modulus increases with increasing temperatures until a sharp increase in G^* occurs at the T_{gel}. After gel formation, all hydrogel samples show similar G^* values at elevated temperatures.

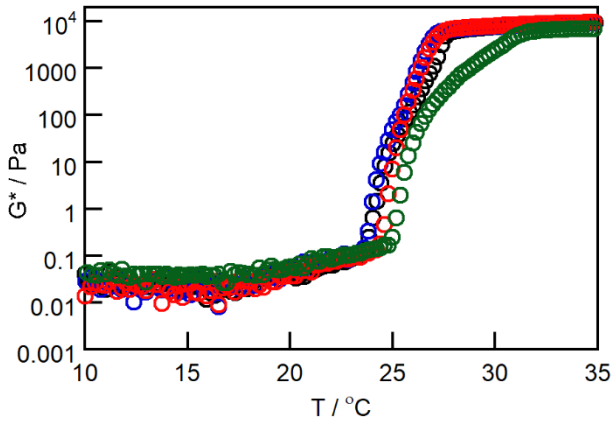

Figure 3.22. Dependence of G^* on temperature for 20% F127 (black), 20% F127 + 5 μM pyrene (blue), 20% F127 + 5 μM pyrene + 62 mM NaI (green), 20% F127 + 5 μM pyrene + 61.5 mM NM (red).

3.3 Discussion

3.3.1 Effect of additives on Pluronic F127

In this chapter, the microheterogeneity of F127 hydrogels is determined using fluorescence quenching measurements on different probes with different quenchers. In addition, these measurements made it possible to characterize the solubilization sites inside F127 micellar system. However, the important point in these experiments is that after addition of probes and quenchers, the structure of the micelles does not change. Therefore, fluorescence spectroscopy findings are applicable to F127 hydrogel that do not contain additives. The control experiments on the size of F127 micelles and the viscoelastic properties of F127 hydrogels in the absence and presence of different additives support the conclusion that the additives do not change the properties of the micelles. These experiments were done only with the addition of pyrene since this probe is larger when compared to Np. The highest concentrations of quenchers were also added since if these concentrations show no drastic effect on properties of the F127 micelles then no effects would be expected for the lower quencher concentrations.

The hydrodynamic diameter of the F127 micelles at 20 °C is close to the reported values in literature.[148, 167] Addition of small molecules such as hydrophobic drugs can increases the size of F127 micelles, because the micelles swell and become larger when the drugs enter the micelles.[148] On the other hand, salts can enlarge the size of the core region

of micelles. For example NaCl, enlarged the core of F127 micelles.[151] Thus, addition of pyrene and quenchers might have had the same effect and could have changed the micellar size or even the micellar shape. However, these additives did not change the size and polydispersity of F127 micelles, so they did not alter the structure of F127 micelles. To confirm this claim, rheological measurements were also performed.

The sol-gel transition temperature did not significantly change in the presence of different additives showing that these additives could not inhibit gel formation of F127. Moreover, because gelation of F127 occurs in a short-range temperature, it is possible to assume that T_{gel} of F127 remained almost constant in the presence of the different additives. The addition of pyrene and quenchers did not change the phase transitions and stiffness of F127 hydrogel. Therefore, based on these control experiments it was shown that addition of probe and quenchers did not change the rheological properties of the F127 hydrogel. In addition, because any change in the structure of micelles could be revealed from the rheological behavior of the bulk material, it is possible to conclude that the micelles remained intact after addition of probe and quenchers.

3.3.2 Steady-state fluorescence spectroscopy for pyrene in F127 hydrogel

I/III ratios give information on the average location of pyrene molecules in the hydrogel. In the presence of F127 aggregates pyrene molecules entered the F127 micelles because I/III of pyrene decreased significantly in the presence of F127 micelles. Increasing the concentration of the F127 polymer has no effect on the I/III ratio of pyrene, which shows that increasing the number of micelles does not change the polarity of the microenvironment around pyrene after the micelles are formed. In the presence of micelles, a higher amount of pyrene could be solubilized because pyrene is highly hydrophobic, and the micelles help to solubilize a higher amount of pyrene in aqueous solution.

The molecular weight of PPO blocks in F127 is around 3780 Da.[28] To understand the average location of pyrene molecules inside the micelles, the I/III ratios of pyrene in bulk PEO and PPO blocks with similar molecular weight to this block in F127 polymer were compared. This comparison showed that a higher portion of pyrene molecules are located inside the hydrophobic region of Pluronic micelles because the I/III ratio in F127

is close to that observed in liquid PPO blocks. Moreover, the I/III values in F127 sol and gel were similar meaning that the average location of pyrene does not change with increasing temperature and phase transition of F127 from the sol to the hydrogel. All these findings from studying the I/III ratios of pyrene illustrate that pyrene molecules are located inside the micelles. Also, only monomer emission was seen because pyrene could enter the micelles and even at the much higher concentration of pyrene in F127 hydrogel compared to water (5 μM in F127 solution and 0.5 μM in water), no excimer emission observed at longer wavelengths.

3.3.3 Quenching of pyrene in F127 hydrogel with NM

Incorporation of pyrene inside supramolecular or micellar systems leads to a lengthening of the lifetime for the singlet excited state pyrene compared to the lifetime of this excited state in aqueous solution. The excited state pyrene in the micelles is in a different environment and it can be protected from possible quenchers inside the aqueous phase such as oxygen.[137] The lifetime of the singlet excited state of pyrene lengthened in the presence of F127 micelles compared to water. Additionally, only one lifetime was observed for the excited state pyrene in F127 sol and gel indicating that there is at least one species of pyrene inside the micelles. However, from time-resolved fluorescence spectroscopy experiments in the absence of quencher it is not possible to determine the number of different species of the excited state of the probe that exist in different regions of the micellar system. This may occur because the lifetimes of these different species might be similar in the absence of quencher making it impossible to differentiate between them. After increasing the quencher concentration, different species of excited probe, which have different accessibility to the quencher due to their location, will exhibit different lifetimes. This differentiation is a consequence of the different quenching efficiencies. In conclusion, use of the quenching methodology enables the determination of the number of different solubilization sites in the F127 hydrogel. For example, different binding sites in sodium cholate aggregates were found through fluorescence quenching of different probes based on naphthalene derivatives.[98] In another studies, the solubilization sites in amphiphilic diblock copolymers and the kinetics of the release of fluorescent probes were determined using quenching experiments. Based on fluorescence quenching results,

a three-region model for the solubilization of hydrophobic guest molecules in these micelles was suggested. The regions are namely core, inner corona, and outer corona.[168]

Different quenchers might access different species of pyrene and quench them with different rate constants, which would result in different lifetimes corresponding to excited pyrene molecules in different regions of the F127 micellar phase. More importantly, the lifetime of singlet excited state pyrene is not long enough to allow it to exit from the micelles during the excited state lifetime. Therefore, it is possible to obtain information on the interaction sites in F127 micelles from quenching experiments.

Singlet excited states of pyrene were quenched in F127 hydrogel by NM. This quenching leads to both the fluorescence intensities and lifetimes of excited pyrene decreasing with increasing the NM concentration, showing that mechanism of quenching is the dynamic quenching mechanism. This conclusion is supported by the linear quenching plots and equal intensities and lifetimes ratios in the presence and absence of quencher which indicates that the dynamic mechanism operated for the quenching of pyrene with NM. The dynamic quenching mechanism is consistent with a previous report.[169] The quenching mechanism in water was also dynamic as was previously described in the literature. The lifetime of pyrene in water and the quenching rate constant value for quenching of pyrene with NM in water were very close to the reported values by other researchers.[134, 170]

Excited state pyrene molecules should be protected from quenchers in the aqueous phase in the presence of polymeric micelles. Because of the hydrophobicity of pyrene molecules, they enter into the micellar phase and have less accessibility to NM molecules which are relatively hydrophilic molecules. The higher k_q value in water compared to F127 supports the suggestion of the better protection provided for pyrene by the F127 micelles.

The I/III ratios for pyrene in 20% F127 gel (30 °C) at different concentrations of NM were constant. However, when the temperature is decreased to 20 °C, where 20% F127 is in sol state, the I/III ratio for pyrene in 20% F127 sol showed a declining trend with increasing the concentration of NM. This result suggests that there might be different microenvironments for pyrene species in 20% F127 sol compared to 20% F127 gel.

After addition of pyrene, it was assumed that the distribution and lifetimes of impurities in F127 do not change and that the impurities do not interact with pyrene molecules. In this regard, the lifetimes correspond to F127 impurities were found at different concentrations of NM and were fixed for the analysis of the decay in the presence of pyrene. This procedure increases the precision for the determination of the lifetime components that correspond to singlet excited pyrene. Only one lifetime corresponding to pyrene was found in the gel state of 20% F127 at 30 °C, which means that pyrene at 30 °C exist in only one region of the F127 micelles. The binding of pyrene is assigned to the hydrophobic interior of the micelles. The increasing concentrations of NM did not cause a change in the location of excited pyrene molecules inside the micelles. In addition, quenching pyrene at a higher concentration of F127 polymer (30% w/v) at 30 °C with NM revealed only one species of pyrene which is again located in the hydrophobic region of the micelles.

Decreasing the temperature to 20 °C revealed two different lifetime components correspond to pyrene in 20% F127 sol after addition of NM. The longer lifetime component is similar to the one found at 30 °C. Therefore, this species of pyrene is located in the hydrophobic region of the micelles which has less accessibility to NM molecules. On the other hand, the shorter lifetime component corresponds to the species of pyrene that has higher accessibility to NM molecules. This species of pyrene could be located in a more hydrophilic region of the micelles. The relative populations of these two species of pyrene change with increasing NM concentration which means that excited pyrene can move between hydrophilic and hydrophobic regions of the micelle during its lifetime. At higher concentrations of NM, the population of pyrene species in the hydrophilic region is higher than the population in the hydrophobic region. This result indicates that of singlet excited pyrene moves to the hydrophilic part of the micelles where more NM molecules exist.

The time-resolved fluorescence experiments for quenching pyrene in 30% F127 with NM at 20 °C and 10 °C showed similar results as discussed above for 20% F127. Thus, increasing the polymer concentration did not affect the location of pyrene molecules in the system. The only factor which affects the location of pyrene inside the micelles is temperature.

The ratio of quenching rate constants in the absence and presence of the micelles (k_{q0}/k_q) is defined as the protection provided by the micelles for excited guest molecules from quencher and this ratio is called protection efficiency or PE.[98] The PE for pyrene molecules did not change at different concentrations of F127. Hence, as long as pyrene molecules are inside the micelles the protection that is provided for excited pyrene does not change by increasing the number of micelles.

As the mechanism of quenching is dynamic, it means that a collision must happen between quencher and probe. In this respect, the quencher should diffuse towards the probe to become close enough until the process of electron transfer occurs.[96] In this case, increasing the temperature can increase the diffusion rate of molecules and subsequently can increase the k_q for dynamic quenching process.[171]

3.3.4 Quenching of pyrene in F127 hydrogel with NaI

The other quencher which I used to quench excited state pyrene molecules was the iodide ion. Pyrene was quenched with the different concentrations of NaI in 20% F127 in the solution and gel states. Because the F127 concentration did not affect the results for the quenching of pyrene with NM, I only studied the quenching of pyrene in 20% F127. It is reported in the literature that pyrene is quenched with iodide ions through a collisional mechanism.[158] Upon increasing the concentration of NaI, both the lifetimes and fluorescence intensities of excited pyrene decreased. From the linear quenching plots following the Stern-Volmer equation it can be concluded that iodide ions quenched pyrene in F127 micelles through dynamic mechanism.

The constant I/III ratios for pyrene in 20% F127 sol and gel at different concentrations of NaI indicate that on average there is one microenvironment sensed by pyrene when it was quenched with NaI. This result suggest that excited pyrene species did not move between different microenvironments inside the micelle with increasing the concentration of NaI.

In the presence of different concentrations of NaI, only one lifetime for excited pyrene was found in F127 sol or gel. Even decreasing temperature did not result in observing another pyrene species. Some salts have the same effect as changes in

temperature on Pluronic micelles. Some salts enlarge the size of the core region of Pluronic micelles as a result of dehydrating the PEO blocks by a salting out mechanism.[172] Consequently in the presence of NaI, pyrene molecules in the hydrophilic region of micelles would reside in the hydrophobic region of micelles and that is the reason I observed only one species of excited pyrene molecules for the quenching studies with NaI.

The quenching rate constant for the quenching of pyrene with NaI in water is similar to the reported value in the literature.[160] The PE values in 20% F127 gel for pyrene at 30 °C in the case of NM quencher is 9.8 ± 0.3, while in the case of NaI this PE is 14.5 ± 0.8. Accordingly, the better protection provided for excited pyrene from iodide ions means that iodide ions have less access to excited pyrene molecules inside F127 micelles compared to NM molecules. The size of iodide ions and NM molecules is very similar, and it is difficult to deduce that size is the relevant parameter for the different PEs.[173-174] However, the hydrophobicity of these quenchers is the important parameter responsible for observing a higher PE in the case of NaI, because NM molecules are slightly hydrophobic allowing them to enter faster into the hydrophobic interior of the micelles.

3.3.5 Quenching of Np in F127 hydrogel with NaI

Np with a smaller molecular size was the other probe I used to study the heterogeneity of the F127 hydrogel. No emission corresponding to excimer or aggregation was observed for Np in the F127 hydrogel. The high micelle to probe concentration ratio ensures that Np can enter the micelles and a higher concentration of Np was dissolved in aqueous solution in the presence of micelles (5 μM Np in 20% F127) than in water (1 μM Np in water).

Time-resolved fluorescence quenching studies of Np with NaI in 20% F127 gel, resulted in finding one species of Np probably located in the hydrophobic region of the micelles due to the hydrophobicity of the Np molecules and their small size. The PE provided by F127 micelles for singlet excite Np at 30 °C, is 24.8 ± 0.9 while this value for pyrene at same temperature was 14.5 ± 0.8, showing that a lower PE occurs for larger molecules such as pyrene. In previous studies the quenching efficiency for Np and pyrene with iodide ions was compared in the presence of bile salt aggregates. It was reported that

because of Np's smaller size the bile salt molecules were able to closely pack around the Np.[160]

3.4 Conclusions

In summary, fluorescence spectroscopy experiments showed that pyrene was located inside the hydrophobic region of the micelles in the F127 hydrogel. Quenching studies of singlet excited pyrene with NM revealed another possible location of pyrene in the micelles for the sol phase, which is likely at the interface between the hydrophilic side of the micelle and the hydrophobic core. Lower accessibility of iodide ions to pyrene compared to NM displays that pyrene molecules exist in the hydrophobic interior of the micelles. Lower protection provided for pyrene is due to the larger size of this probe compared to the smaller Np guest, suggesting that the polymer aggregates tightly surround Np molecules and protect them better from quenchers. Since addition of pyrene and quenchers did not change the structure and mechanical properties of F127, it can be concluded that fluorescence quenching results give information about the possible solubilization sites for small molecules inside F127 micelles and that photophysical experiments provide information that is relevant for the gel without any additives. As F127 is a popular Pluronic polymer in the field of drug delivery, characterizing different probable solubilization sites for drug molecules, paves the way for predicting the release of the drug from F127 micellar systems.

4 Chapter 4: Studying the Microenvironments in P104 Hydrogel Using Fluorescence Probes

4.1 Introduction

4.1.1 Background

Pluronic polymers can have different molecular weights and PPO/PEO ratios leading to the formation of micelles with different sizes. To probe a heterogeneous system like the F127 hydrogel, it is required to compare it with a similar Pluronic system that has a different micellar structure. In the previous chapter it was found that pyrene molecules might be locate in two different regions of the F127 micelles including the hydrophobic core region of the micelle and a more hydrophilic region which is probably the micellar corona. The P104 polymer with an average molecular weight of 5900 Da has a lower MW compared to F127 (~12600 Da), but the length of PPO blocks in the two polymers is similar (F127; $PEO_{99}PPO_{65}PEO_{99}$ and P104; $PEO_{27}PPO_{61}PEO_{27}$). The other difference is in the PEO content. P104 has 40 wt.% PEO and F127 has 70 wt.% PEO, so the ratio of PEO/PPO blocks is higher in F127 compared to P104.[28, 175] The content of PPO and PEO blocks in Pluronic polymers is an important attribute which affects directly the shape of the micelles and the aggregation number.[29] Although the molecular weights of Pluronic P104 and F127 are different, the molecular weights of the PPO block segment in both polymers are very similar, such that the PPO MW in P104 is 3540 Da while in F127 it is 3780 Da.[33] The schematic of the two different Pluronic micelles is shown in chart 4.1.

Chart 4.1. F127 micelle (left) and P104 micelle (right). PEO corona shells are shown in black.

The PEO content in Pluronic polymers determines the cloud point of Pluronic which is the temperature above which phase segregation happens and micellar solution transforms to a two-phase system.[33, 176] Higher PEO content copolymers have a solid shape and dissolve in water faster due to higher hydrogen bonding with water molecules. CMC and CMT are parameters that are affected by the molecular weight and PEO/PPO ratio of the copolymer. The CMC value for P104 at 20 °C is 2 wt% and at 30 °C it is 0.04 wt%, while the CMC for F127 at 20 °C is 4 wt% and at 30 °C it is 0.1 wt%.[33] Both F127 and P104 polymers are able to form gels at elevated temperatures and high concentrations. For example, 34% P104 is in sol state at 20 °C but forms gel at 30 °C. The P104 micelles have smaller shell thickness due to the shorter length of PEO block when compared to F127 micelles.[29, 177] In addition, P104 can be used as a drug delivery system to dissolve water-insoluble drug molecules in aqueous solutions.[178] The rheological behavior of P104 micelles changes in the presence of an aromatic amino acid, which was used in synthesizing sedative drugs. The hydrodynamic diameter of P104 micelles increased upon addition of anthranilic acid and induced a micellar transition in P104.[179]

In another study, the effects of different phenolic antioxidants on the CMC and CMT was investigated and it was determined that addition of these molecules lowers the CMC and CMT for P104. Moreover, the locations of these antioxidants in P104 micelles were studied using 2D NMR. The solubilization site of guest molecules inside P104 micelles was shown to depend on the structure and hydrophobicity of the antioxidants.[178]

The aqueous solution of P104 behaves like a Newtonian fluid at low temperatures but with increasing temperature the behavior of the material becomes non-Newtonian.[179] For 25 wt% P104, T_{gel} was measured from temperature sweep experiments and it was determined to be 26 °C.[180] The size and properties of P104 micelles change in the presence of different additives.[177, 179]

4.1.2 Objectives

In this chapter, similar fluorescence measurements as performed for the F127 hydrogel were carried out with the 34% P104 sol and gel to characterize the different solubilization sites in the P104 micellar system. The results are compared to those obtained with the F127 polymer in order to understand the differences between microenvironments where the probe is located for these two Pluronic micelles. In addition, I studied the effect of different additives on the rheological behavior of the 34% P104 hydrogel.

4.2 Results

4.2.1 Quenching of pyrene in P104 with different concentrations of NM

A different Pluronic polymer is studied in this chapter. Pyrene probe is quenched with NM in P104 polymer to probe the microheterogeneity of a different PEO-PPO-PEO triblock copolymer. The concentration of pyrene and NM in the P104 micellar system is the same as the concentrations used for probing the F127 gel. The fluorescence studies were performed in both in the sol and gel states of P104.

Before carrying out the fluorescence studies on pyrene in the P104 hydrogel, the absorption spectrum of pyrene in the P104 hydrogel was determined. Figure 4.1 demonstrates the absorption spectra of 5 μM pyrene in 34% P104 hydrogel (black), and in 20% F127 hydrogel (blue) at 30 °C. There is a broad peak around 300 nm in 34% P104 hydrogel which might correspond to the impurities in this polymer. Different impurities in these two polymers caused the difference in the absorption spectra for pyrene in F127 and P104 gels.

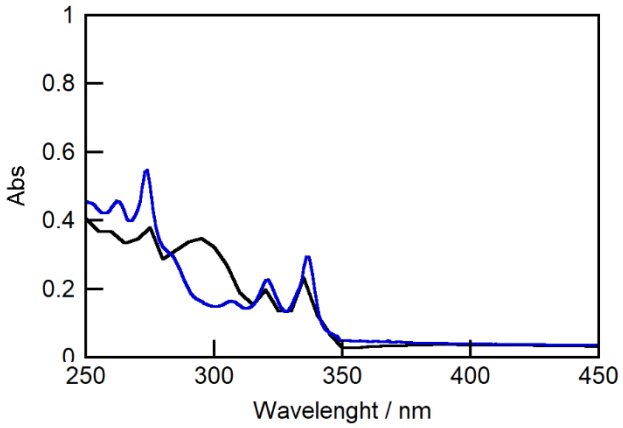

Figure 4.1. UV-vis absorption spectra for 5 μM pyrene in 34% P104 (black line), and in 20% F127 (blue line) at 30 °C.

The fluorescence emission intensities of excited pyrene decreased upon addition of NM in both the P104 gel (Fig 4.2a) and sol (Fig 4.2b). Additionally, the pyrene excimer peak was not observed in both the P104 sol and gel even at high concentrations of NM. The I/III ratio for pyrene in the presence of P104 micelles decreased to the value of 1.5 ± 0.1 which is very similar to the value in the presence of F127 micelles and liquid PPO blocks (Table 3.1).

The I/III ratios for pyrene at different concentrations of NM were roughly constant when this probe was quenched in 34% P104 gel (Fig 4.3a) and sol (Fig 4.3b). The plots described in figure 4.3a-b are similar to the plot of I/III ratios for pyrene in 20% F127 gel versus different concentrations of NM (Fig 3.4a). However, in 20% F127 sol state a decrease in the I/III ratios for pyrene upon increasing the NM concentration (Fig 3.4b) was observed, while in the case of 34% P104 sol state, such result was not observed, figure 4.3b.

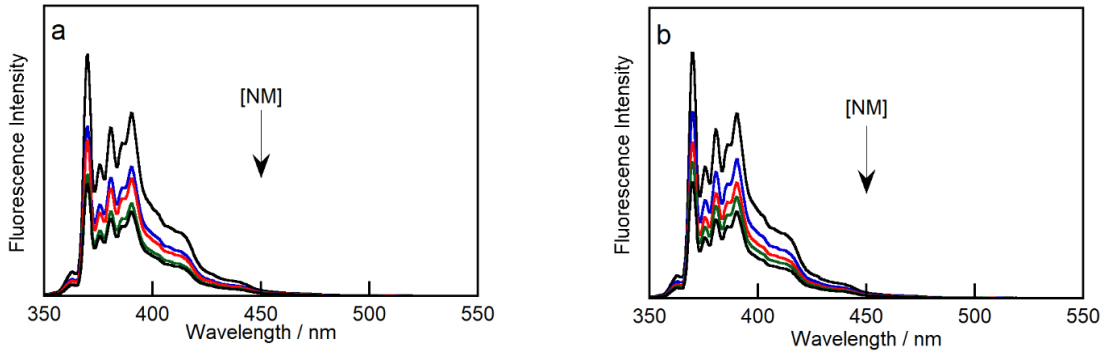

Figure 4.2. Fluorescence emission spectra for 5 μM pyrene in 34% P104 quenched with NM ([NM] = 0-6.5 mM) at a) 30 °C and b) 20 °C.

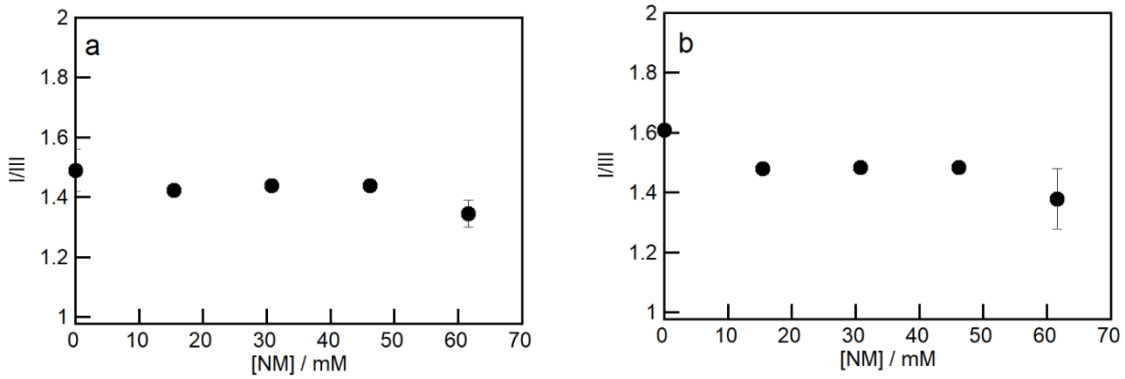

Figure 4.3. I/III ratios for 5 μM pyrene in 34% P104 at different concentrations of NM at a) 30 °C and b) 20 °C. The data correspond to averages for two independent experiments. The error bars correspond to average deviations, error bars smaller than the symbols are not shown.

The plots of k_{obs} and intensity ratios in the absence and presence of quencher versus the NM concentrations were linear for the quenching of pyrene in 34% P104 gel at 30 °C (Fig 4.4a-b). As displayed in figure 4.5, the intensity ratio and average lifetime ratio in the absence and presence of quencher (I_0/I, $\langle\tau_0\rangle/\langle\tau\rangle$), at different concentrations of quencher, are equal and follow the Stern-Volmer equation (Eq 2.3).

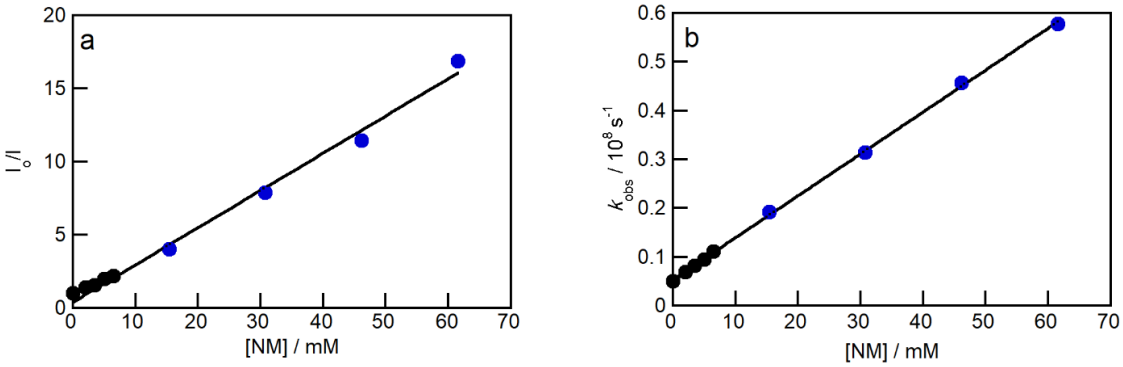

Figure 4.4. Quenching plots for 5 μM pyrene in 34% P104 at 30 °C quenched by NM a) intensity ratio in the absence and presence of quencher, b) dependence of k_{obs} for pyrene with the NM concentration. Black and blue symbols correspond to different sets of experiments. All the experiments were performed once.

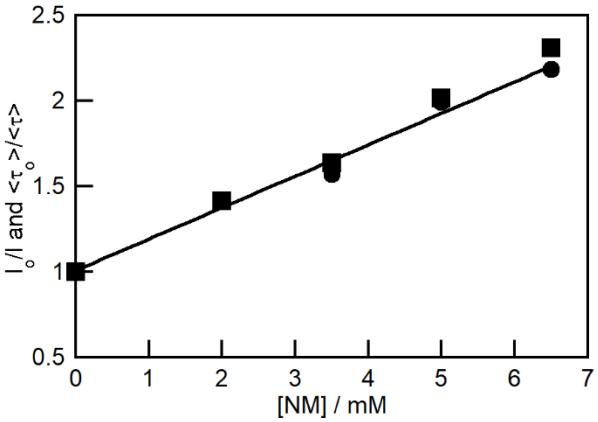

Figure 4.5. Intensity ratio (circle) and average lifetime ratio (square) versus NM concentration corresponding to quenching 5 μM pyrene in 34% P104 at 30 °C. Data correspond to one experiment.

I followed the same approach used in the previous chapter to determine the lifetimes for the singlet excited state of pyrene in 34% P104. Subsequently, the emission due to impurities in 34% P104 were quenched with NM. The lifetimes for the impurity emissions were fixed and the lifetime corresponding to excited state pyrene in P104 hydrogel were determined. The results from the time-resolved fluorescence quenching studies of the impurities in P104 are shown in table 4.1 and the fluorescence emission spectrum for the impurities in this polymer at different concentrations of NM are shown in figure 7.5 (in the

Appendix). Only one lifetime relating to excited state pyrene in 34% P104 gel at 30 °C was found as shown in table 7.11 (in the Appendix). The relative population of pyrene species did not change with increasing NM concentration. Figure 4.6 illustrates the decay of excited state pyrene in 34% P104 gel which is fit to sum of exponentials (Eq. 2.2).

Quenching of excited pyrene in 34% P104 sol state at 20 °C with NM, revealed only one lifetime which corresponds to excited pyrene (Table 7.13 in the Appendix), a result that contrasts with the case of the F127 polymer (Table 7.3 in the Appendix). The lifetimes of impurities were measured at different concentrations of NM at 20 °C (Table 7.12 in the Appendix). Figure 4.7 shows the linear quenching plot corresponding to pyrene in the 34% P104 sol. Overall, changing the Pluronic polymer from F127 to P104 shows that at 20 °C, there are two different species of pyrene in 20% F127 while this second species does not exist in 34% P104 at 20 °C.

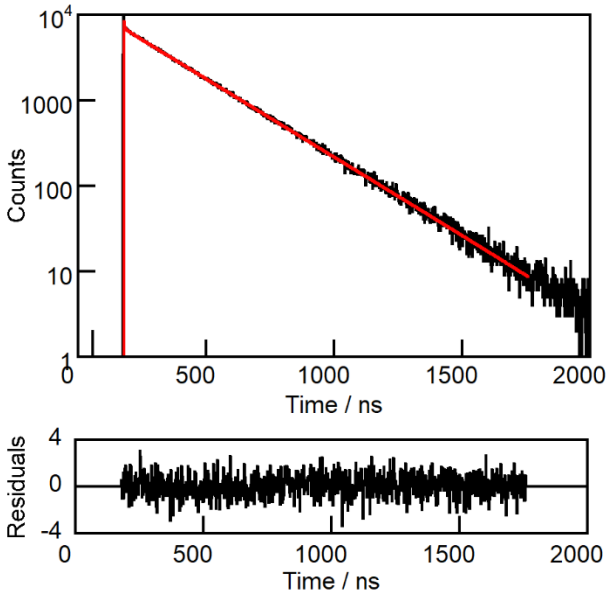

Figure 4.6. Fluorescence decay for 5 µM pyrene in 34% P104 at 30 °C (black) fit to a sum of exponentials decay (red) using tail fit. Residuals between calculated and experimental data are shown in the lower panel.

Table 4.1. Fluorescence emission lifetimes and corresponding A values for the quenching of the impurities in 34% P104 with NM at 30 °C.

[NM] / mM[b]	τ_1 / ns[a]	τ_2 / ns[a]	τ_3 / ns[a]	A_1[a]	A_2[a]	A_3[a]	χ^2
0	0.3±0.1	2.2±0.1	8.9±0.2	0.48±0.05	0.47±0.02	0.05±0.01	1.009
15.4±0.2	0.4±0.1	2.0±0.1	5.6±0.2	0.45±0.03	0.48±0.02	0.07±0.01	0.931
30.8±0.2	0.3±0.1	1.7±0.1	4.4±0.2	0.53±0.08	0.39±0.03	0.08±0.01	0.988
46.2±0.3	0.3±0.1	1.6±0.1	4.3±0.2	0.53±0.06	0.40±0.02	0.07±0.01	0.928
61.5±0.7	0.2±0.1	1.3±0.1	3.3±0.1	0.53±0.06	0.37±0.03	0.10±0.02	0.990

[a]The errors represent the standard deviations calculated using the F900 software. The data correspond to one experiment.
[b]See 2.3.3 for method in the determination of the NM concentration.

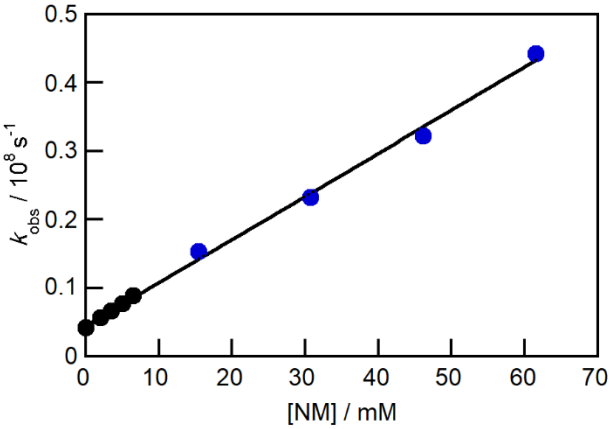

Figure 4.7. Quenching plot for 5 μM pyrene in 34% P104 at 20 °C quenched by NM. Black and blue symbols correspond to different sets of experiments. All the experiments were performed once.

The lifetime of pyrene changes when there is a change in the microenvironment around this excited molecule and in the presence of Pluronic micelles, the lifetime of pyrene lengthens compared to water. The quenching rate constants shown in table 4.2 is related to the pyrene species in Pluronic gels at 30 °C. The k_q values for quenching pyrene with NM in F127 and P104 gels are the same.

Table 4.2. Lifetimes (τ) for singlet excited state pyrene in different media and quenching rate constants for the quenching 5 μM pyrene in 20% F127 and P104 hydrogels and 0.5 μM pyrene in water with NM at 30°C.[a]

Media	τ / ns	k_q / 10^8 $M^{-1}s^{-1}$
Water	120 ± 1 (2)	81 ± 9 (2)
20% F127	180 ± 4 (4)	9.1 ± 0.3 (3)
34% P104	200 ± 3 (3)	9.0 ± 0.3 (2)

[a]The number of independent experiments is shown in parenthesis. For two experiments the errors correspond to average deviations and for more than two experiments the errors correspond to standard deviations.

4.2.2 Quenching of pyrene in P104 with different concentrations of NaI

The other quencher utilized to quench the pyrene probe in order to study the solubilization sites in P104 was NaI. In the previous chapter, I determined that quenching pyrene in F127 hydrogel with NaI shows only one species of pyrene in the F127 micellar system when it is either in the sol or gel states. I quenched pyrene again in both the 34% P104 gel and sol states to compare how the two polymers protect the singlet excited pyrene probe from reaction with the quencher. Figure 4.8 shows the reduction of fluorescence intensity for pyrene in 34% P104 gel (Fig 4.8a) and sol (Fig 4.8b) with increasing NaI concentrations. In the case of quenching pyrene with NaI in 34% P104 gel, the I/III ratios for pyrene did not change with increasing NaI concentration (Fig. 4.9) which is similar to the quenching results with the other quencher molecules (NM). This result is also in consistence with the quenching results observed in the F127 hydrogel (Fig 3.14).

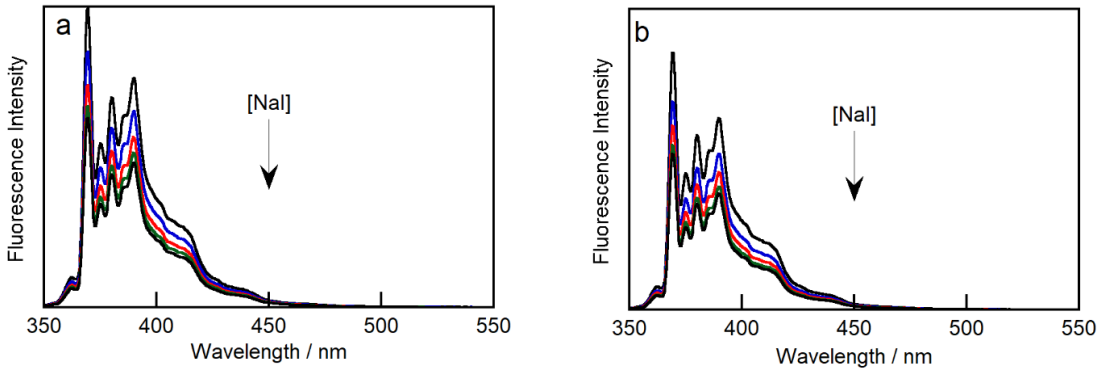

Figure 4.8. Fluorescence emission spectra for 5 μM pyrene in 34% P104 quenched with NaI ([NaI] = 0-20 mM) at a) 30 °C and b) 20 °C.

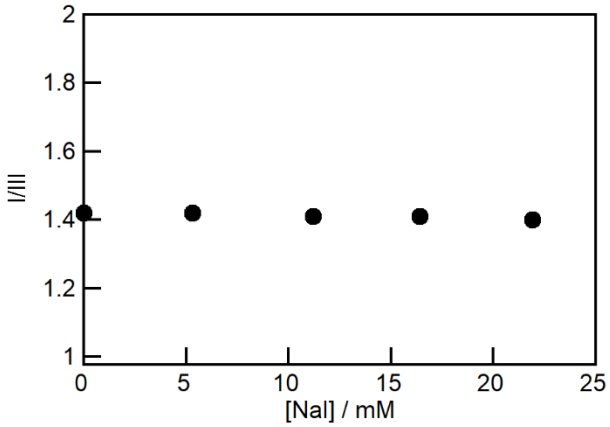

Figure 4.9. I/III ratios for 5 μM pyrene in 34% P104 at different concentrations of NaI at 30 °C. The data correspond to one experiment.

Figure 4.10 a-b shows the linear quenching plots for the quenching of pyrene with NaI in 34% P104 at 30 °C. Figure 4.11 shows that the intensity ratio and lifetime ratio in the absence and presence of NaI are the same at all NaI concentrations indicating that the collisional quenching mechanism occurs in the P104 gel. As reported in table 7.14 (in the Appendix), only one species of pyrene was found in 34% P104 gel when pyrene was quenched with NaI.

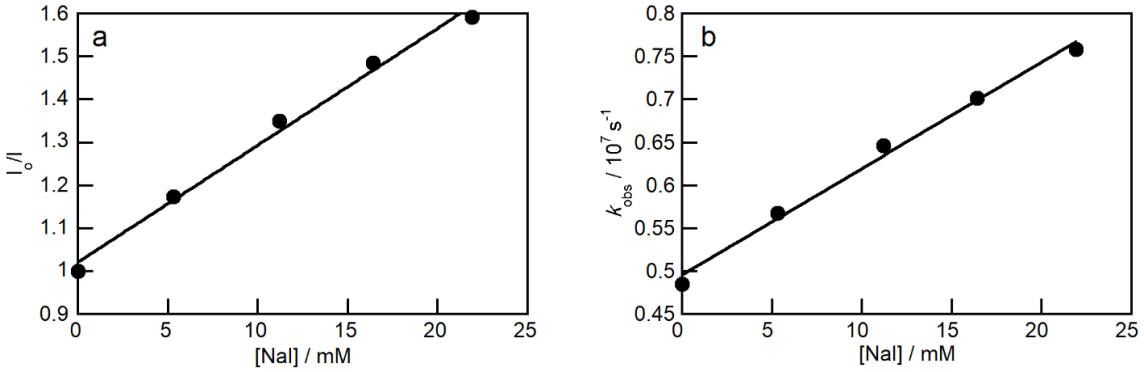

Figure 4.10. Quenching plots for 5 μM pyrene in 34% P104 at 30 °C quenched by NaI a) intensity ratio in the absence and presence of quencher, b) dependence of k_{obs} for pyrene with the NaI concentration. The data correspond to one experiment.

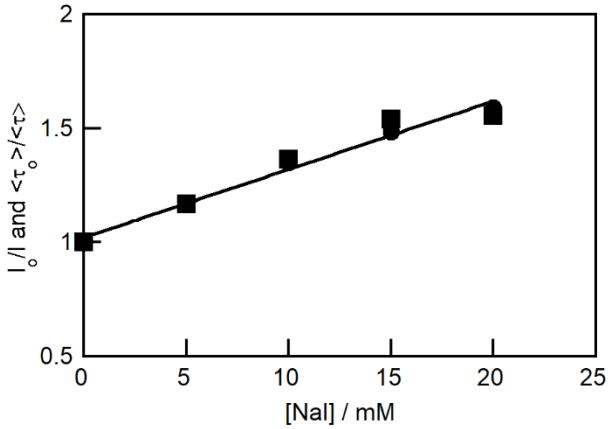

Figure 4.11. Intensity ratio (circle) and average lifetime ratio (square) versus NaI concentration corresponding to quenching 5 μM pyrene in 34% P104 at 30 °C. Data correspond to one experiment.

Decreasing the temperature to 20 °C, did not affect the quenching plots for excited pyrene with NaI in the P104 sol (Fig. 4.12). At 20 °C, one lifetime corresponds to excited pyrene observed in 34% P104 sol (Table 7.15 in the Appendix). Table 4.3 summarized the quenching rate constants for pyrene with different quenchers in 20% F127 and 34% P104 gels. The values of k_q for same quenchers in P104 and F127 hydrogels are the same within experimental errors.

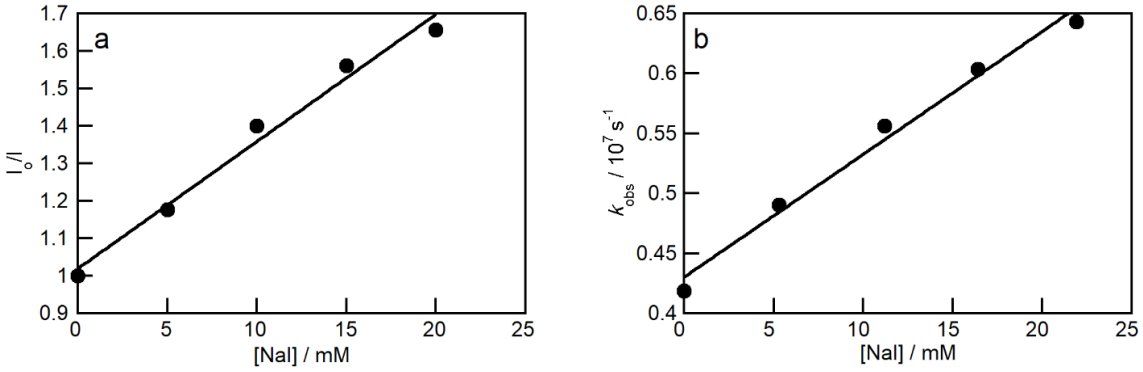

Figure 4.12. Quenching plots for 5 μM pyrene in 34% P104 at 20 °C quenched by NaI a) intensity ratio in the absence and presence of quencher, b) dependence of k_{obs} for pyrene with the NaI concentration. All the experiments were performed once.

Table 4.3. Quenching rate constant for quenching 5 μM pyrene with different quenchers in different hydrogels at 30 °C.[a]

Hydrogel	Quencher	k_q / 10^8 $M^{-1}s^{-1}$
20% F127	NM	9.1 ± 0.3 (3)
34% P104	NM	9.0 ± 0.3 (2)
20% F127	NaI	0.8 ± 0.1 (2)
34% P104	NaI	1.4 (1)

[a] The number of independent experiments is shown in parenthesis. For two experiments the errors correspond to average deviations and for more than two experiments the errors correspond to standard deviations.

4.2.3 Quenching of Np in P104 with different concentrations of NaI

The other probe molecule used to study P104 hydrogel was Np that was quenched with NaI. Fluorescence emission spectra for Np in 34% P104 gel at different concentrations of NaI are shown in figure 4.13. These spectra do not have the broad peak around 300 nm observed for the emission of Np in 20% F127 gel (Fig 3.16). From time-resolved measurements only one lifetime was found for the singlet excited state of Np in 34% P104 gel at different concentrations of NaI (Table 7.16 in the Appendix). The quenching plot for Np was linear (Fig 4.14) and the quenching rate constant in the case of P104 polymer was somewhat higher than for the F127 polymer (Table 4.4).

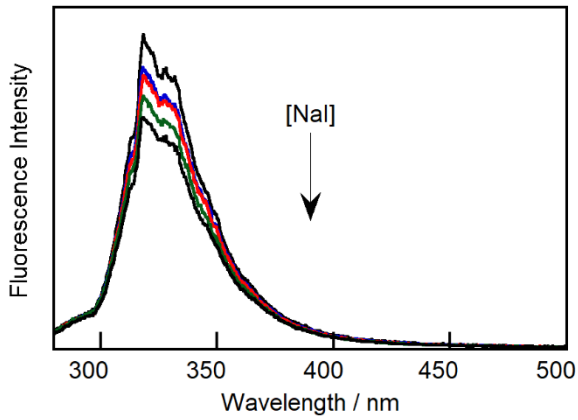

Figure 4.13. Fluorescence emission spectra for 5 μM Np in 34% P104 quenched with NaI ([NaI] = 0-20 mM) at 30 °C.

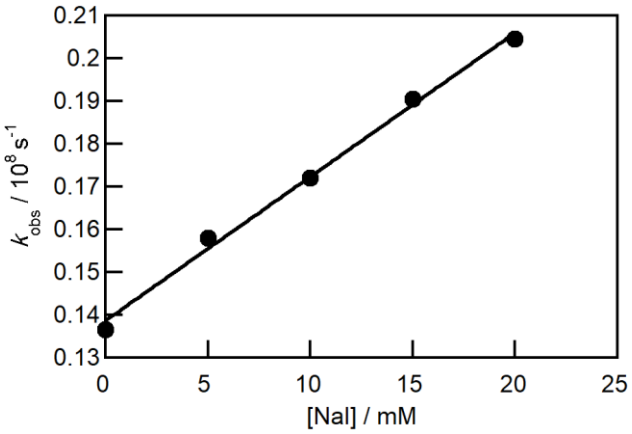

Figure 4.14. Quenching plots for 5 μM Np in 34% P104 quenched by NaI at 30 °C. Data correspond to one experiment.

Table 4.4. Quenching rate constants for quenching 5 μM Np with NaI in different hydrogels at 30 °C.[a]

Hydrogel	k_q / 10^8 $M^{-1}s^{-1}$
20% F127	2.8 ± 0.1 (2)
34% P104	3.4 (1)

[a]The number of independent experiments is shown in parenthesis. For two experiments, the errors correspond to average deviations.

4.2.4 Viscoelastic behavior of P104 in the presence of different additives

The LVR for 34% P104 hydrogel was determined from strain sweep test as indicated in figure 4.15. In the previous chapter, it was shown that additions of pyrene and the highest concentrations of NM and NaI do not change the LVR region of 20% F127 hydrogel (Fig 3.18, Table 3.10). The same type of experiments were performed for P104.

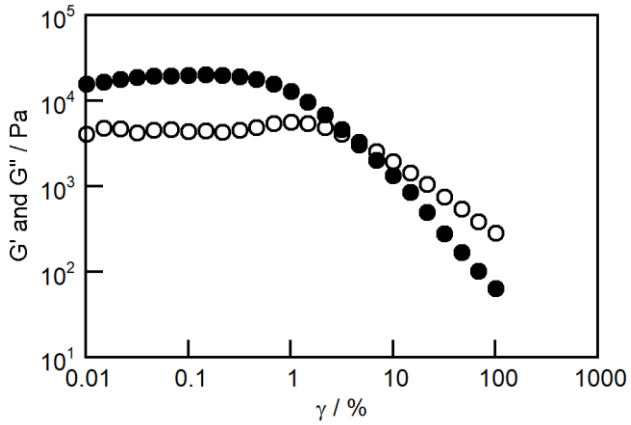

Figure 4.15. Dependence of G' (filled symbols) and G'' (open symbols) with the shear strain (γ) at the angular frequency of 1 rad/s at 30°C for 34% P104.

The effect of additives on the T_{gel} of 34% P104 hydrogel was studied through temperature sweep tests (Fig. 4.16). The highest concentrations of NM and NaI for fluorescence experiments were 62 and 20 mM, respectively. Addition of pyrene and the highest concentrations of quenchers did not change the T_{gel} for 34% P104 hydrogel significantly as shown in table 4.5. The effect of these additives on the mechanical properties of the bulk gel studied through the changes of G^* over different temperatures is shown in figure 4.17. Changing the polymer from F127 to P104 did not result in changes of the rheological behavior of these gels in the presence of additives.

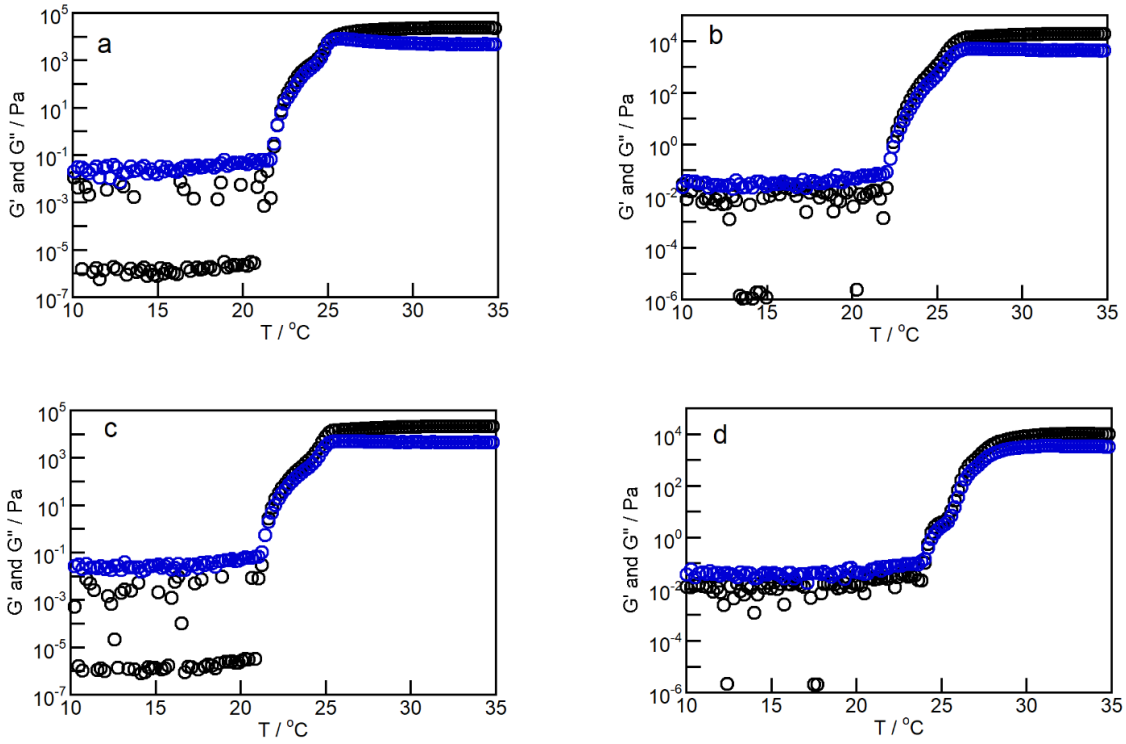

Figure 4.16. Dependence of G′ (black circles) and G″ (blue circles) on temperature at angular frequency of 1 rad/s and γ of 0.5% for a) 34% P104 b) 34% P104 + 5 μM pyrene, c) 34% P104 + 5 μM pyrene + 61.5 mM NM, and d) 34% P104 + 5 μM pyrene + 20 mM NaI.

Table 4.5. Gelation temperatures for 34% P104 in the presence of different additives with heating rate of 0.5 °C/min, angular frequency of 1 rad/s, and shear strain of 0.5%.[a]

Sample	T_{gel} / °C
34% P104	22.3 ± 0.3 (2)
34% P104_5 μM pyrene	22.1 ± 0.1 (2)
34% P104_5 μM pyrene_61.5 mM NM	21.4 (1)
34% P104_5 μM pyrene_20 mM NaI	24.0 (1)

[a]The number of independent experiments is shown in parenthesis. For two experiments, the errors correspond to average deviations.

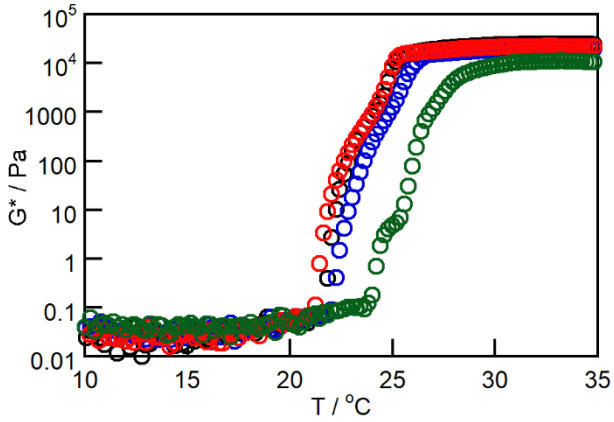

Figure 4.17. Dependence of G^* on temperature for 34% P104 (black), 34% P104+5 µM pyrene (blue), 34% P104+5 µM pyrene+ 61.5 mM NM (red), 34% P104 + 5 µM pyrene + 20 mM NaI (green).

4.3 Discussion

In this chapter, the microheterogeneity of the P104 hydrogel was studied and the differences between the solubilization site properties in F127 and P104 micelles are compared. This comparison helps to understand the effect of the molecular weight and the PPO/PEO ratio of Pluronic polymers on the solubilization sites for a hydrophobic guest in these micelles. For this purpose, fluorescence quenching experiments analogous to the experiments described in chapter 3 were carried out using the 34% P104 hydrogel. The effect of the addition of the fluorescent probe and quenchers on the mechanical properties of the bulk P104 hydrogel was studied in order to relate the results of the photophysical experiments to the P104 hydrogel without any additives.

Addition of pyrene and quenchers did not cause any extra phase transitions in the P104 hydrogel and the T_{gel} for P104 did not change significantly in the presence of these additives. This result indicates that P104 is still in the sol state at 20 °C and in the gel state at 30 °C in the presence of these additives. The overall mechanical properties of P104 hydrogel did not change in the presence of different additives as indicated from the dependence of G^* on temperature for different samples. Hence, the stiffness and flexibility of P104 gels did not change in the presence of pyrene and quenchers. To summarize, the fluorescence quenching experiments were performed for concentrations of probes and quencher for which the rheological properties of the material did not change.

The I/III ratios for pyrene in F127 and P104 hydrogels are very similar and much lower than the I/III ratio in water (1.6 ± 0.1 in 20% F127 gel and 1.5 ± 0.1 in 34% P104 gel) and this value is very close to I/III ratio for pyrene in liquid PPO block. The I/III ratios in P104 sol and gel were similar to each other. Additionally, the concentration ratio of P104 micelles to pyrene is high enough for me to conclude that all pyrene molecules entered into the P104 micelles and that pyrene is probably located in the hydrophobic region of P104 micelles as was also seen for F127 micelles. Moreover, there was no pyrene aggregate or excimer emission in the fluorescence emission plots of pyrene in P104 sol and gel. On the whole, in the presence of P104 micelles a higher concentration of pyrene molecules could get dissolved in aqueous polymer solution compared to water.

The lifetimes for singlet excited state pyrene in the presence of Pluronic micelles is longer compare to that in water, which is also an indication of the different microenvironment around the excited pyrene molecules. The lifetime for probe molecules when inserted into different micelles would differ due to the different environments around the probe. The lifetime of excited pyrene in P104 micellar system is close to the reported value in the literature.[45] Because of the different PPO/PEO ratios in F127 and P104, it was important to determine if the solubilization sites in these micelles have different properties. To further distinguish the number of regions in the P104 micellar system and compare this system with F127 micelles, pyrene was quenched with NM and NaI.

The evidence that quenching occurs through collisional quenching of pyrene with NM in 34% P104 hydrogel is the same as for the F127 hydrogel. In the case of both Pluronic micelles, dynamic quenching of the excited state pyrene with NM occurs. The constant I/III ratios for pyrene at different concentrations of NM in both P104 sol and gel shows that with increasing NM concentration, the microenvironment around excited pyrene probe did not change.

Quenching of pyrene with NM in both the P104 gel and sol revealed only one species of pyrene. Similar results were obtained in the case of 20% F127 gel at 30 °C, but there was one other pyrene species in 20% and 30% F127 at 20 °C. The reason that only one lifetime corresponding to excited state pyrene molecules in 34% P104 sol and gel (at 20 and 30 °C) was found, is the thinner corona shell for the P104 micelles compared to

F127 which is a consequence of the difference in PEO block lengths in these two polymers.[29, 177] In this respect, there is enough space in the hydrophilic region of the F127 micelle for the pyrene molecule at 20 °C to bind, but the hydrated PEO shell in P104 at 20 °C is not large enough compared to the hydrophobic segment of P104 micelles to accommodate pyrene molecules. Besides that, pyrene molecules due to their highly hydrophobic characteristics, prefer to stay in the hydrophobic region of P104 micelles. Finally, pyrene molecules exist in the hydrophobic region of P104 micelles when samples are in sol state or gel state. The k_q values for quenching pyrene in F127 and P104 gels are very similar such that it is possible to conclude that the PEs in the case of these Pluronic polymers for pyrene are very close.

The fluorescence quenching results for pyrene in P104 hydrogel with NaI as a quencher are very similar to the quenching results in F127 hydrogels. The mechanism of quenching was dynamic and I/III ratios for pyrene remained constant at different concentrations of quencher. One species of pyrene was found in both F127 and P104 sol and gel states.

In the case of the P104 polymer, even if NaI salt has the core enlarging effect that were observed for other salts, the thickness of PEO has not enough capacity to host pyrene molecules. Therefore, the relocation of excited pyrene in different regions of the micelle cannot happen in the presence of NaI. Additionally, both Pluronic polymers provide similar protection for excited pyrene from iodide quencher as supported by the similar k_q values.

Np was also quenched with iodide ions in the P104 gel. No emission corresponding to an excimer or aggregate was observed for Np in the P104 hydrogel. Np molecules due to their hydrophobicity, small size and also much lower concentration compared to P104 micelles concentration entered into the P104 micelles. Only one species of singlet excited state of Np was found in the P104 gel at different concentrations of NaI. The quenching rate constants in both P104 and F127 hydrogels were close to each other demonstrating similar protection for the singlet excited state of Np. In addition, the protection for excited state Np was higher compared to excited state pyrene molecules which is consistent with the results observed for the F127 hydrogel.

The fluorescence probing results provided enough evidence that F127 and P104 micelles provide similar protection to different probes from reactions with quenchers. As all the quenching cases studied were in the category of dynamic mechanism, diffusion plays the major role in determining quenching rate constants. From the Smoluchowski equation, the bimolecular rate constant is directly related to the diffusion coefficients of the fluorophore and quencher.[96] Based on the Stokes–Einstein equation, the diffusion coefficient depends on the temperature and viscosity of the sample.[181] Due to similar k_q values for different probes in F127 and P104 micelles, it is probable that the structure of these different micelles have no significant effect on the PE because the role of temperature and viscosity dominates in comparison to other possible factors. In this regard, the longer PEO lengths or in other words the thicker corona shell around F127 micelles, is not adequate to better protect probe molecules from quenchers.

4.4 Conclusions

Based on the fluorescence quenching experiments, only one solubilization site was found in P104 micelles with the same features as observed for the hydrophobic region in F127 micelles. Different PEO/PPO blocks ratios and the different hydrophilic content for F127 and P104 micelles, affected the location of excited pyrene molecule at 20 °C in these two different Pluronic micelles. Changing the Pluronic polymer from F127 to P104 did not affect the protection provided for probe molecules by these micelles highlighting the major role of temperature and viscosity on the bimolecular quenching rate constant. In summary, the findings of this study would be beneficial for designing polymers to solubilize small hydrophobic molecules and predict the interactions of guest molecules with polymeric host systems.

5 Chapter 5: Studying the Mobility of Small Molecules in F127 Hydrogel

Dr. Suma Thomas designed the experiments and helped me choose the probe molecules for this study. Moreover, she analyzed the decay profiles for quenching triplet excited probes in water-glycerol, 20% F127 sol and gel.

5.1 Introduction

5.1.1 Background

The solubilization sites in F127 hydrogel were characterized through fluorescence quenching method in chapter 3. To study the movements of guest molecules between different environments in F127 hydrogel, the fluorescence quenching technique is not a proper method because the lifetimes of singlet excites states are much shorter than the timescale for solute exchange between different environments.[105] For this reason, triplet excited state molecules become attractive due to their longer lifetimes which are on a similar timescale for the movements of small molecules between different environments of a hydrogel.

Some hydrogels having application in biomedical industry and cosmetics are important to study the dynamic behavior of solutes in gels which occurs in a short time scale.[182] For example, in some drug delivery applications, it is required that the solute have limited mobility inside the gel to obtain the sustained release of the drug in body.[183-184] Among many different techniques to study the mobility of solutes inside a gel, photophysical techniques have attracted much attention such as FSC which is a method allows to investigate the dynamics of a gel system at the molecular level.[185] The other photophysical technique to study the dynamics of hydrogels is fluorescence recovery after photobleaching using confocal microscopy.[182] Among all these methods to detect the diffusion of solutes inside hydrogels, using triplet excited state probes is of interest in the current project.

The mobility of probes inside hydrogels formed through crosslinking, depends on the crosslinking density and the porosity of the gel.[186] However, for Pluronic hydrogels formed with a network of micelles the interactions between solute and polymer nanoparticles are of interest which can affect the mobility of solutes in a micellar system. In this regard, different probe molecules have been chosen which have similar structure but different hydrophobicities. The probes are Np and its derivatives including NpOH and 2-NpC. Therefore, it is possible to investigate how the hydrophobicity of guest molecules can affect their interactions with Pluronic F127 micelles. The other possible parameter which can affect the mobility of the solute is the size of the solute molecules. For this purpose, Pht was used which is larger compared to Np molecules. Probe molecules are shown in chart 5.1.

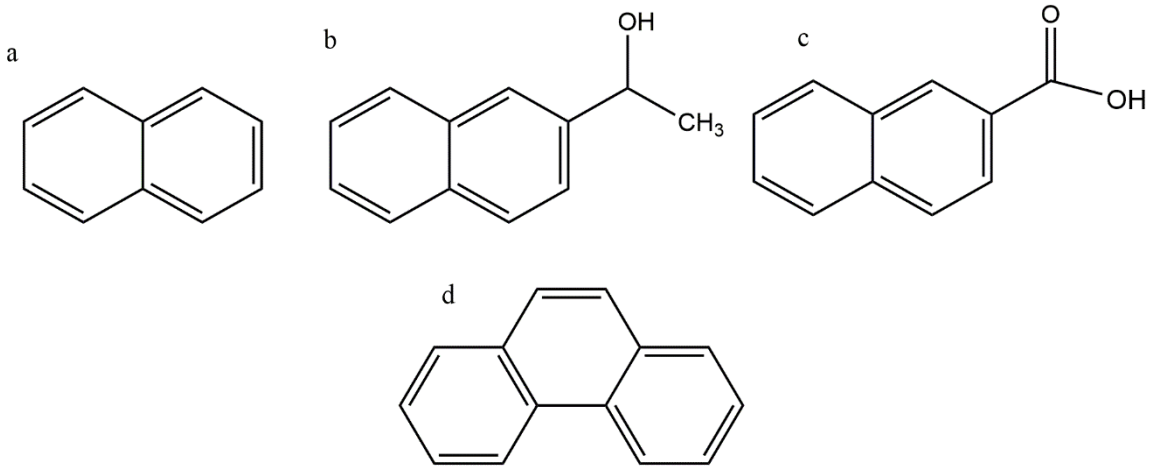

Chart 5.1. Probe molecules a) Np, b) NpOH, c) 2-NpC, d) Pht.

The quenching mechanism in a heterogenous system like a hydrogel is described in chapter 1 (Eq. 1.1-1.5). Hydrophobic molecules tend to stay inside the hydrophobic interior of Pluronic micelles rather than in aqueous phase of hydrogel but the quencher, which was nitrite in my case, due to their negative charge prefers the aqueous phase rather than the micellar phase of the gel. Accordingly, the micelles provide protection for excited state probes from the quencher.

The quenching plot which describes the dependence of k_{obs} with quencher concentration within a hydrogel is fit to equation 2.9. Increasing the concentration of the

quencher leads to a curvature in the quenching plots because dissociation of guest from host becomes rate limiting. Figure 5.1 shows an example of quenching plots in the absence and presence a micellar system. Triplet excited state Pht was used here as a guest molecule in F127 micellar system, and it was quenched with $NaNO_2$ in the presence and absence of F127 micelles. In the absence of micelles, the quenching plot is linear because there are no different microenvironments for the excited probe to be located in. Nevertheless, in the presence of micelles a curvature is observed (the curvature is emphasized in the inset figure). At high concentrations of quencher, the quenching plot becomes linear and the reason for this trend was described in chapter 2 (see section 2.5.6 and Eq. 2.9).

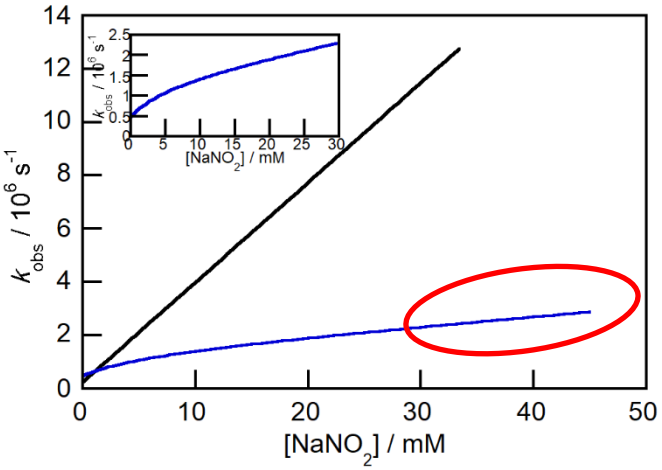

Figure 5.1. Quenching plots for quenching of the triplet excited state of Pth with $NaNO_2$ in the presence of F127 micelles at 20 °C (blue line), and in absence of micelles at 20 °C (black line). The red oval highlights the linear region of the plot. The inset expands the quenching plot in the presence of micelles at lower quencher concentrations.

5.1.2 Objectives

As described previously, studies of the quenching of triplet excited probes is a reliable method to determine the mobility of small molecules in a mesoscopic scale inside a hydrogel depending on the analyte size and shape and their interactions. I quenched Np derivatives and Pht with nitrite anions in water-glycerol mixture and in 20% F127 sol (at 20 °C) and gel (at 30 °C). Water-glycerol mixtures with the same viscosity of 20% F127 sol at 20 °C were used to represent the aqueous phase inside the F127 hydrogel. The protection provided by the micelles for different guest molecules were compared and also the exit and entry rate constants for different environments in a hydrogel were compared

for different guest molecules. This study gives information about the tendency of small molecules to reside in different environments of a hydrogel based on the structure and hydrophobicity of the small molecules.

5.2 Results

Before and after performing LFP experiments, the absorption spectra of samples were checked to find whether any degradation occurred during the irradiation of the samples with laser light. Some examples of the absorption spectra for different samples before and after the LFP experiments are shown in figures 7.6-7.9 (in the Appendix). The absorption spectra for different samples before and after doing LFP experiments are very similar, and no degradation was found.

All the triplet excited state guest molecules showed mono-exponential behavior in water-glycerol mixture and in 20% F127 sol and gel. The decay profiles for different triplet excited guests in 20% F127 gel at 30 °C in the absence and presence of $NaNO_2$ are illustrated in figures 5.2 and 5.3. Because all the transient decays of triplet excited guest molecules were mono-exponential I could fit the decay profiles to equation 2.8 (Fig 5.2-5.3).

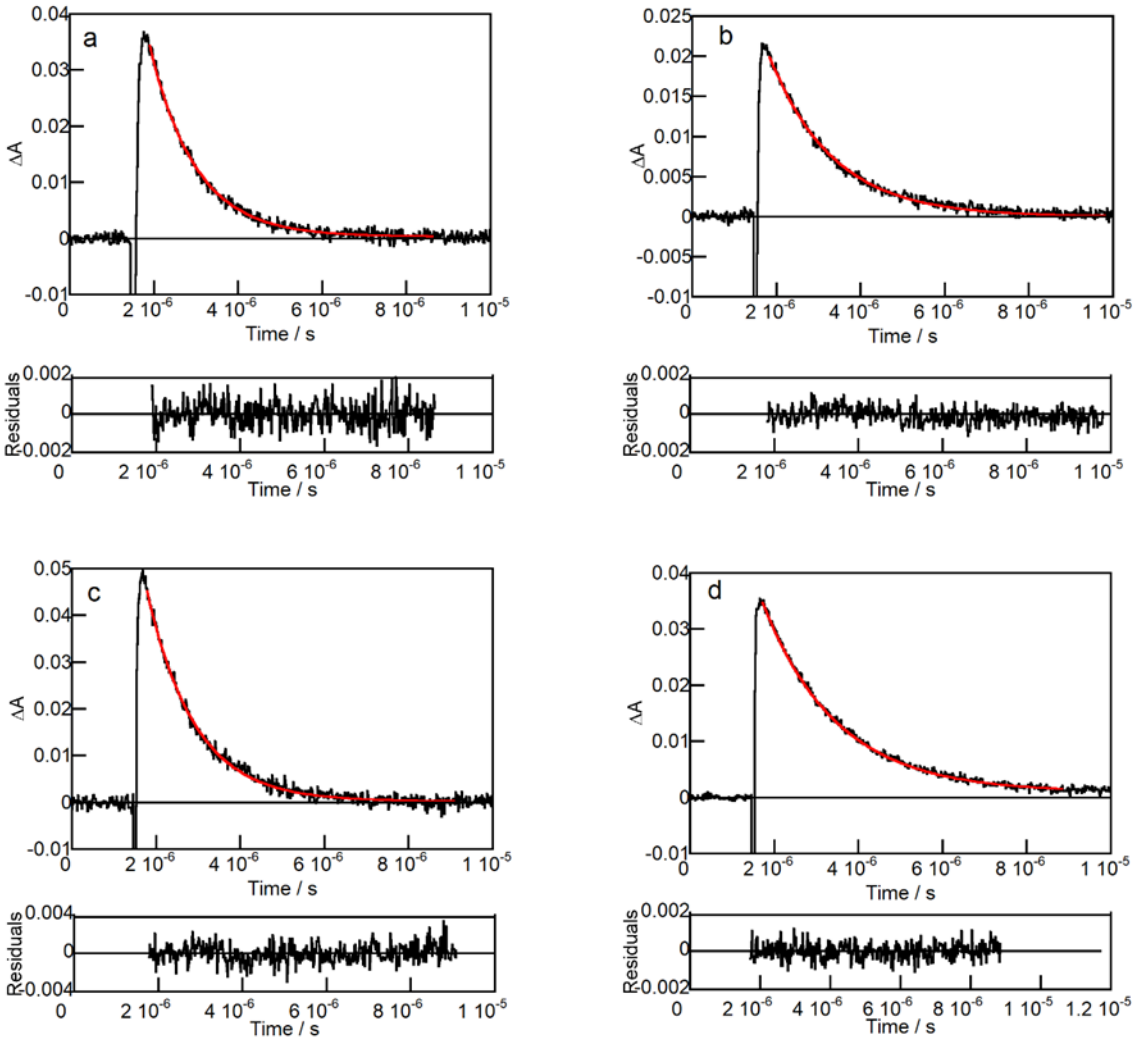

Figure 5.2. Triplet excited state decay for a) 80 μM Np, b) 80 μM NpOH, c) 50 μM Pht, and d) 80 μM 2-NpC in 20% F127 at 30 °C in the absence of $NaNO_2$ (black) fit to equation 2.9 (red). Residuals between calculated and experimental data are shown in the lower panels.

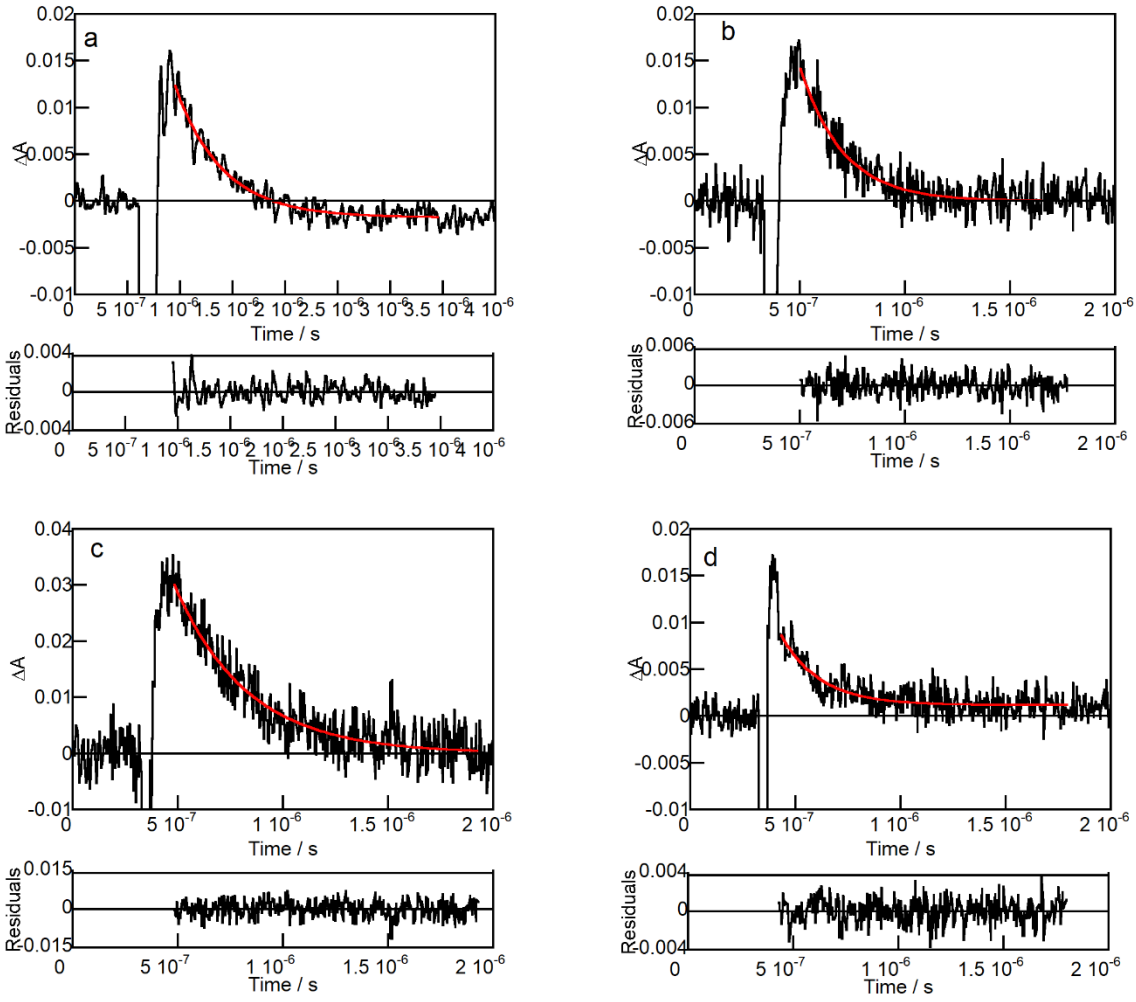

Figure 5.3. Triplet excited state decay for a) 80 μM Np, b) 80 μM NpOH, c) 50 μM Pht, and d) 80 μM 2-NpC in 20% F127 at 30 °C in the presence of 33 mM $NaNO_2$ (black) fit to equation 2.9 (red). Residuals between calculated and experimental data are shown in the lower panels.

The quenching plots for different triplet excited state molecules in a water-glycerol mixture, 20% F127 sol and gel are represented in figure 5.4. All the quenching plots in water-glycerol mixtures are linear but in 20% F127 sol and gel, these plots are nonlinear and have downward curvature. The quenching plots in the presence of F127 micelles were fit to equation 2.9 to obtain the different kinetic parameters. However, the quenching plots in the water-glycerol mixture were fit to equation 2.4 to determine the values for k_0 and k_q. There is a deviation between quenching plots in the absence and presence of F127 micelles.

The values of k_{obs} in 20% F127 sol and gel, are lower than in water-glycerol mixture for all triplet excited state guest molecules except 2-NpC (Fig 5.4). The deviation between quenching plots in water-glycerol mixtures and F127 hydrogels are more significant in the case of Np and Pht compared to NpOH and 2-NpC.

If the quenching reactions happen in both micellar and aqueous phases in the 20% F127 hydrogel, the last term in equation 2.9 becomes negligible and a linear relation would be observed between k_{obs} and quencher concentration. In this regard, to check if the proposed reactions are happening, I plotted k_{obs} versus high concentrations of $NaNO_2$ and the plots were linear. The slope of these plots correspond to the value of k_q^{F127}.[122] The protection efficiency (PE) as described in chapter 3, is the ratio of quenching rate constants in the absence and presence of quencher (k_q/k_q^{F127}). The highest PE is for Np molecules while 2-NpC molecules have the lowest PE value, table 5.1.

The known parameters, which were fixed in the fits of the quenching plot to obtain association and dissociation rate constants are listed in table 5.1 for different guest molecules. The values for k_{as}/N and k_{dis} for different guest molecules in 20% F127 sol and gel are shown in table 5.2. The value for k_{as} has not been calculated because there are different aggregation number values for F127 micelles in the literature,[29, 187] but it is still possible to compare k_{as} values for different triplet excited state guest molecules. The value for k_{dis} decreases with increasing the hydrophobicity of the guest molecules and from high to low values are ordered as: 2-NpC > NpOH > NP > Pht. On the other hand, the value for k_{as}/N increases with increasing the hydrophobicity of guest molecules (Table 5.2).

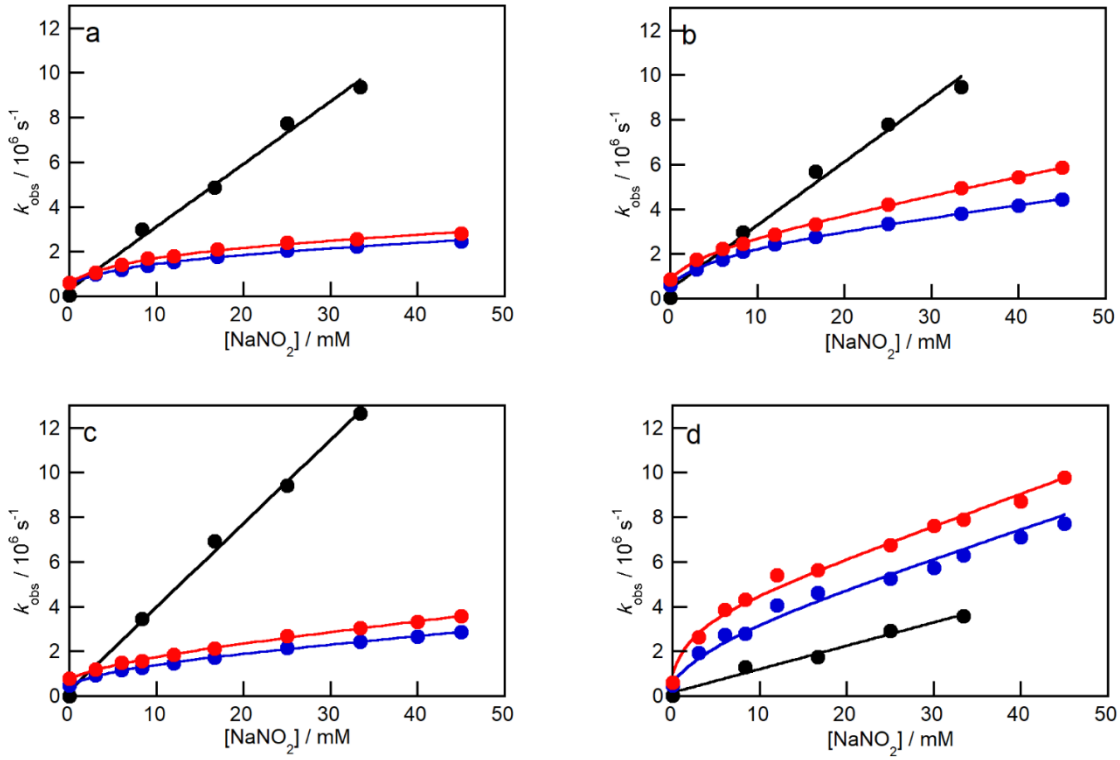

Figure 5.4. Quenching plots for a) 80 µM Np, b) 80 µM NpOH, c) 50 µM Pht, and d) 80 µM 2-NpC in 20% F127 at 20 °C (blue), at 30 °C (red) with $NaNO_2$ and for a) 80 µM Np, b) 80 µM NpOH, c) 30 µM Pht, and d) 80 µM 2-NpC in water-glycerol mixture at 20 °C with $NaNO_2$ (black).

Table 5.1. Rate constants for the quenching of different triplet excited guest molecules in a water-glycerol mixture in the absence and presence of $NaNO_2$ (k_0 and k_q) and in 20% F127 sol and gel in the absence and presence of $NaNO_2$ (k_0^{F127}, k_q^{F127}).[a]

Guest	[F127] / (w/v)	T / °C	$k_0^{F127}/10^5$ s^{-1}	$k_0/10^4$ s^{-1}	k_q^{F127} / 10^7 $M^{-1}s^{-1}$	$k_q/10^9$ $M^{-1}s^{-1}$	PE
Np	0	20		4.7±0.1		0.32±0.01	
	20%	20	6.0±0.2		3.1±0.3		10±1
	20%	30	6.4±0.3		3.4±0.1		9.4±0.4
NpOH	0	20		5.0±0.1		0.30±0.02	
	20%	20	5.7±0.4		4.8±0.6		6.3±0.9
	20%	30	8.4±0.7		7.6±0.5		4.0±0.4
Pht	0	20		0.84±0.01		0.39±0.01	
	20%	20	5.2±0.3		3.7±0.1		11±1
	20%	30	8.5±0.3		4.5±0.1		8.7±0.3
2-NpC	0	20		3.8±0.1		0.14±0.01	
	20%	20	5.1±0.1		8.7±0.4		1.6±0.1
	20%	30	5.9±0.1		13±1		1.1±0.1

[a]The errors for the parameters correspond to the average deviations from two experiments and standard deviations for three or more experiments.

Table 5.2. The association and dissociation rate constants for different guest molecules in 20% F127 sol and gel.[a]

Guest[b]	T / °C	k_{dis} / 10^6 s^{-1}	(k_{as}/N) / 10^8 $M^{-1}s^{-1}$
Np	20	1.0 ± 0.1	1.5 ± 0.2
	30	1.1 ± 0.1	1.2 ± 0.2
NpOH	20	1.9 ± 0.1	1.1 ± 0.1
	30	1.8 ± 0.1	0.96 ± 0.07
Pht	20	0.86 ± 0.02	1.7 ± 0.2
	30	0.97 ± 0.03	1.3 ± 0.2
2-NpC	20	3.9 ± 0.1	0.49 ± 0.06
	30	4.7 ± 0.1	0.44 ± 0.05

[a]The errors for the parameters correspond to the average deviations from two experiments and standard deviations for three or more experiments.
[b]Concentration of Np, NpOH, Pht, and 2-NpC are 80, 80, 50, and 80 μM, respectively.

5.3 Discussion

The guest molecules used in this study had almost similar structures (except Pht which is a larger molecule[188-189]), but different hydrophobicities. It is known that the PPO content in Pluronic copolymers affect the size of the core and solubilization of hydrophobic compounds.[190] In this respect, F127 was chosen due to its relatively large hydrophobic core and also its capability of solubilizing hydrophobic compounds.[150] The partitioning of compounds between the micellar and aqueous phases of Pluronic hydrogels depend on the

hydrophobicity of the small molecules that is a significant factor on the release of molecules from the micelles. More hydrophobic compounds have higher partition coefficient meaning that the concentration of the hydrophobic compound in the micellar phase is higher than the aqueous phase.[191] The other important factor affecting incorporation of a compound in micellar aggregates is the size of the compounds. The smaller the compounds, the easier to incorporate them inside aggregates.[160, 192]

The assumption to use equation 2.9 is that the concentration of probe molecules inside micellar phase is higher compared to the aqueous phase.[122] The quenching rate constants in the absence of micelles (k_q) are two order of magnitudes higher compared to the presence of micelles (k_q^{F127}) for all guest molecules, showing the faster accessibility of quencher to the excited state probes in the absence of micelles. The quenching rate constants in the presence of micelles increased for all guest molecules with increasing temperature. As described in chapters 3 and 4, the reason for higher values of quenching rate constants at elevated temperatures is because of faster diffusion of molecules at higher temperature. So, the increase in viscosity of hydrogel at higher temperature is not as effective as the influence of temperature and cannot decrease the diffusion of small molecules in Pluronic gel compared to the sol state.

The values of k_{dis} and k_{as}/N in F127 sol and gel are quite similar for all the guest molecules. The values of k_{dis} give insight into the residence time of the excited probe in the micellar phase. For more hydrophobic molecules, it is expected that their residence time in the micellar phase is longer than to stay in the aqueous phase. The comparison of k_{dis} values between different guest molecules shows that Pht has the lowest dissociation rate constant. The hydrophobicity of the guest molecules is in this order; Pht > Np > NpOH > 2-NpC. The values for k_{dis} decreases with increasing the hydrophobicity of guest molecules which is consistent with the expectation described above.

On the other hand, the value of k_{as}/N should increase with increasing hydrophobicity of the guest molecules because it represents the association rate constant and more hydrophobic guest molecules tend to enter the micelles more readily. There is a consistency between this expectation and the k_{as}/N values for the four different guest molecules.

The values for PE depend on both the structure and polarity of the guest molecules. Micelles can provide better protection for the more hydrophobic triplet excited probes; however, there is a discrepancy for Np and Pht. The more hydrophobic Pht molecule has a very similar PE value to that of the less hydrophobic Np molecule. The reason is the difference in the structure of these two guest molecules. Np, which is a smaller molecule showed a similar protection as Pht because it was easier for F127 polymers to surround smaller Np compared to Pht molecules.

The lowest protection for 2-NpC molecules and also the steeper quenching plots in the F127 sol and gel compared to water-glycerol mixture, indicate that 2-NpC molecules are not located in a hydrophobic environment and they have high accessibility to the quencher. The molecules of 2-NpC have highest hydrophilicity compared to the other guest molecules, thus the location for 2-NpC in the micellar phase should be different from other guest molecules and it should be located in more hydrophilic region of micellar phase or inside the aqueous phase of F127 hydrogel.

5.4 Conclusions

A kinetic model described the dynamics of guest molecules in F127 micellar hydrogel host. Based on the model, the interactions between host and guests, the entry and exit dynamics of guests in F127 hydrogel were determined. The interactions between different guest molecules and the micellar phase in F127 hydrogel were verified. Molecules with smaller size and more hydrophobicity are prone to get more protected inside the micellar phase because of the lower accessibility of quencher anions to the core of the micelles. In addition, the time that the more hydrophobic molecules spend in the micellar phase is higher than the aqueous one. On the other hand, the less efficient interaction was between 2-NpC and F127 micelles and was observed because of the high hydrophilicity of 2-NpC molecules. Lastly, the protection provided by micelles and the location of guest molecules inside the Pluronic hydrogel depend on the structure and hydrophobicity of guest molecules.

6 Chapter 6: Summary

This thesis describes different approaches using photophysical techniques to study the mobility of small molecules in a Pluronic triblock copolymer aqueous solutions and gels. Singlet excited states were used as immobile probes to study the mobility of quenchers that mainly reside in the aqueous phase. Triplet excited probes were used to study the mobility of these probes between the micelles and the aqueous phase of the sol and gel. The effect of quencher structure, charged vs. non-charged, of the change in polymer structure and of the change in hydrophobicity of the probes was investigated.

The fluorescence quenching studies on Pluronic F127 revealed different accessibility of quencher molecules to singlet excited probe which is due to the characteristic of the binding site for the probe molecules in F127 micelles. Quenchers based on their hydrophobicity had different accessibility to singlet excited state molecules and more hydrophobic quenchers had better access to excited state probe inside the micelle. Moreover, temperature had a key role on the number of different binding sites available for singlet excited state probe. Increasing the temperature led to changes to the binding sites from a hydrophilic region of the micelle to the more hydrophobic region of micelles for singlet excited pyrene when it was quenched with NM. The effect of the structure of the probe molecule on the accessibility of quencher to the probe in the F127 micellar system was investigated. The quenching results showed that the smaller probe was better protected inside the micelles against quenching as the unimers can form tighter aggregates around the smaller size probe molecule.

The microheterogeneity of another Pluronic copolymer with a different composition was investigated. Pluronic P104 has a lower number of hydrophilic blocks but similar hydrophobic blocks leading to thinner shell for P104 micelles when compared to F127 micelles. P104 forms hydrogels at elevated temperatures, but the structural difference impacted the binding sites for pyrene molecules as pyrene is only located in the hydrophobic region of P104 micelles in the solution or gel states. On the other hand, the compositional difference between F127 and P104 did not have an impact on the quenching rate constants of different probes at corresponding temperatures, suggesting that the mobility of the quenchers was not greatly affected by the change in structure of the micelle.

The addition of quenchers and probes did not affect the mechanical properties of F127 and P104 hydrogels and their micellar size. Also, the quenchers and probes did not change the temperature of gel formation of F127 and P104 which indicates that the additives concentrations were low enough to not change the structure of the Pluronic micelles.

In the last project, the binding dynamics of guest molecules with different hydrophobicity with the F127 micelles were measured. The dissociation process was slower for more hydrophobic guest molecules. The fastest binding dynamics observed for 2-NpC which is located in the more hydrophilic region of F127 micelles and due to higher hydrophilicity tends to not enter to the hydrophobic core of micelles.

The quenching studies with singlet and triplet excited states showed that this methodology can be effectively used to study the mobility of small molecules within gels, providing information that can then be correlated with the overall release kinetics of small molecules from the gel to a surrounding medium. This information will be valuable to achieve the overall goal to rationally design functional gels.

7 Bibliography

1. Ullah, F.; Othman, M. B. H.; Javed, F.; Ahmad, Z.; Akil, H. M., Classification, processing and application of hydrogels: A review. *Materials Science and Engineering: C* **2015,** *57*, 414-433.

2. Wichterle, O.; Lim, D., Hydrophilic gels for biological use. *Nature* **1960,** *185*, 117-118.

3. Chirani, N.; Gritsch, L.; Motta, F. L.; Fare, S., History and applications of hydrogels. *Journal of Biomedical Sciences* **2015,** *4*, 13-23.

4. Yoon, C.; Xiao, R.; Park, J.; Cha, J.; Nguyen, T. D.; Gracias, D. H., Functional stimuli responsive hydrogel devices by self-folding. *Smart Materials and Structures* **2014,** *23*, 094008.

5. Liu, H.; Rong, L.; Wang, B.; Xie, R.; Sui, X.; Xu, H.; Zhang, L.; Zhong, Y.; Mao, Z., Facile fabrication of redox/pH dual stimuli responsive cellulose hydrogel. *Carbohydrate Polymers* **2017,** *176*, 299-306.

6. Han, L.; Zhang, Y.; Lu, X.; Wang, K.; Wang, Z.; Zhang, H., Polydopamine nanoparticles modulating stimuli-responsive PNIPAM hydrogels with cell/tissue adhesiveness. *ACS Applied Materials & Interfaces* **2016,** *8*, 29088-29100.

7. Li, H.; Go, G.; Ko, S. Y.; Park, J.-O.; Park, S., Magnetic actuated pH-responsive hydrogel-based soft micro-robot for targeted drug delivery. *Smart Materials and Structures* **2016,** *25*, 027001.

8. Miyata, T.; Asami, N.; Uragami, T., A reversibly antigen-responsive hydrogel. *Nature* **1999,** *399*, 766-769.

9. Deng, W.; Yamaguchi, H.; Takashima, Y.; Harada, A., A chemical-responsive supramolecular hydrogel from modified cyclodextrins. *Angewandte Chemie International Edition* **2007,** *119*, 5236-5239.

10. Ebara, M.; Kotsuchibashi, Y.; Narain, R.; Idota, N.; Kim, Y. J.; Hoffman, J. M.; Uto, K.; Aoyagi, T., *Smart Biomaterials*. Springer Japan: 2014.

11. Peppas, N. A., *Biomedical applications of hydrogels handbook*. Springer Science & Business Media: 2010.

12. Caló, E.; Khutoryanskiy, V. V., Biomedical applications of hydrogels: A review of patents and commercial products. *European Polymer Journal* **2015,** *65*, 252-267.

13. Kopeček, J., Hydrogels: From soft contact lenses and implants to self-assembled nanomaterials. *Journal of polymer science Part A Polymer chemistry* **2009,** *47*, 5929-5946.

14. Terech, P.; Weiss, R. G., Low molecular mass gelators of organic liquids and the properties of their gels. *Chemical Reviews* **1997,** *97*, 3133-3160.

15. Van Esch, J.; Schoonbeek, F.; De Loos, M.; Marc Veen, E.; Kellogg, R. M.; Feringa, B. L., Low molecular weight gelators for organic solvents. In *Supramolecular Science: Where It Is and Where It Is Going*, Ungaro, R.; Dalcanale, E., Eds. Springer Netherlands: Dordrecht, 1999; pp 233-259.

16. Raeburn, J.; Zamith Cardoso, A.; Adams, D. J., The importance of the self-assembly process to control mechanical properties of low molecular weight hydrogels. *Chemical Society Reviews* **2013,** *42*, 5143-5156.

17. de Loos, M.; Feringa, B. L.; van Esch, J. H., Design and application of self-assembled low molecular weight hydrogels. *European Journal of Organic Chemistry* **2005,** *2005*, 3615-3631.

18. Jung, J. H.; Shinkai, S.; Shimizu, T., Spectral characterization of self-assemblies of aldopyranoside amphiphilic gelators: What is the essential structural difference between simple amphiphiles and bolaamphiphiles? *Chemistry – A European Journal* **2002,** *8*, 2684-2690.

19. Bao, C.; Lu, R.; Jin, M.; Xue, P.; Tan, C.; Liu, G.; Zhao, Y., l-Tartaric acid assisted binary organogel system: strongly enhanced fluorescence induced by supramolecular assembly. *Organic & Biomolecular Chemistry* **2005,** *3*, 2508-2512.

20. Chen, W.; Peng, J.; Su, Y.; Zheng, L.; Wang, L.; Jiang, Z., Separation of oil/water emulsion using Pluronic F127 modified polyethersulfone ultrafiltration membranes. *Separation and Purification Technology* **2009,** *66*, 591-597.

21. Mansur, C. R. E.; Barboza, S. P.; González, G.; Lucas, E. F., PLURONIC × TETRONIC polyols: study of their properties and performance in the destabilization of emulsions formed in the petroleum industry. *Journal of Colloid and Interface Science* **2004,** *271*, 232-240.

22. Bhardwaj, A.; Hartland, S., Applications of surfactants in petroleum industry. *Journal of Dispersion Science and Technology* **1993,** *14*, 87-116.

23. Kim, D. Y.; Kwon, D. Y.; Kwon, J. S.; Park, J. H.; Park, S. H.; Oh, H. J.; Kim, J. H.; Min, B. H.; Park, K.; Kim, M. S., Synergistic anti-tumor activity through combinational intratumoral injection of an in-situ injectable drug depot. *Biomaterials* **2016,** *85*, 232-245.

24. Bodratti, M. A.; Alexandridis, P., Formulation of Poloxamers for drug delivery. *Journal of Functional Biomaterials* **2018,** *9*, 11.

25. Pragatheeswaran, A. M.; Chen, S. B., Effect of chain length of PEO on the gelation and micellization of the Pluronic F127 copolymer aqueous system. *Langmuir* **2013,** *29*, 9694-9701.

26. Schmolka, I. R., A review of block polymer surfactants. *Journal of the American Oil Chemists' Society* **1977,** *54*, 110-116.

27. Singh-Joy, S. D.; McLain, V. C., Safety assessment of poloxamers 101, 105, 108, 122, 123, 124, 181, 182, 183, 184, 185, 188, 212, 215, 217, 231, 234, 235, 237, 238, 282, 284, 288, 331, 333, 334, 335, 338, 401, 402, 403, and 407, poloxamer 105 benzoate, and poloxamer 182 dibenzoate as used in cosmetics. *International Journal of Toxicology* **2008,** *27 Suppl 2*, 93-128.

28. Alexandridis, P.; Hatton, T. A., Poly(ethylene oxide) poly(propylene oxide) poly(ethylene oxide) block copolymer surfactants in aqueous solutions and at interfaces: thermodynamics, structure, dynamics, and modeling. *Colloids and Surfaces A: Physicochemical and Engineering Aspects* **1995,** *96*, 1-46.

29. Wanka, G.; Hoffmann, H.; Ulbricht, W., Phase diagrams and aggregation behavior of poly (oxyethylene)-poly (oxypropylene)-poly (oxyethylene) triblock copolymers in aqueous solutions. *Macromolecules* **1994,** *27*, 4145-4159.

30. Alexandridis, P., Amphiphilic copolymers and their applications. *Current Opinion in Colloid & Interface Science* **1996,** *1*, 490-501.

31. Xiong, X. Y.; Tam, K. C.; Gan, L. H., Polymeric nanostructures for drug delivery applications based on Pluronic copolymer systems. *Journal of Nanoscience and Nanotechnology* **2006,** *6*, 2638-2650.

32. Yong, C. S.; Choi, J. S.; Quan, Q.-Z.; Rhee, J.-D.; Kim, C.-K.; Lim, S.-J.; Kim, K.-M.; Oh, P.-S.; Choi, H.-G., Effect of sodium chloride on the gelation temperature, gel strength and bioadhesive force of poloxamer gels containing diclofenac sodium. *International Journal of Pharmaceutics* **2001,** *226*, 195-205.

33. Alexandridis, P.; Holzwarth, J. F.; Hatton, T. A., Micellization of poly (ethylene oxide)-poly (propylene oxide)-poly (ethylene oxide) triblock copolymers in aqueous solutions: thermodynamics of copolymer association. *Macromolecules* **1994,** *27*, 2414-2425.

34. Zhou, Z.; Chu, B., Light-scattering study on the association behavior of triblock polymers of ethylene oxide and propylene oxide in aqueous solution. *Journal of Colloid and Interface Science* **1988,** *126*, 171-180.

35. Tuzar, Z.; Kratochvíl, P., Block and graft copolymer micelles in solution. *Advances in Colloid and Interface Science* **1976,** *6*, 201-232.

36. Alexandridis, P.; Lindman, B., *Amphiphilic block copolymers: self-assembly and applications*. Elsevier: 2000.

37. Alexandridis, P.; Spontak, R. J., Solvent-regulated ordering in block copolymers. *Current Opinion in Colloid & Interface Science* **1999,** *4*, 130-139.

38. Chu, B., Structure and dynamics of block copolymer colloids. *Langmuir* **1995,** *11*, 414-421.

39. Alexandridis, P.; Holzwarth, J. F., Differential scanning calorimetry investigation of the effect of salts on aqueous solution properties of an amphiphilic block copolymer (Poloxamer). *Langmuir* **1997,** *13*, 6074-6082.

40. Kjellander, R.; Florin, E., Water structure and changes in thermal stability of the system poly(ethylene oxide)–water. *Journal of the Chemical Society, Faraday Transactions 1: Physical Chemistry in Condensed Phases* **1981,** *77*, 2053-2077.

41. Vadnere, M.; Amidon, G.; Lindenbaum, S.; Haslam, J. L., Thermodynamic studies on the gel-sol transition of some pluronic polyols. *International Journal of Pharmaceutics* **1984,** *22*, 207-218.

42. Li, L.; Lim, L. H.; Wang, Q.; Jiang, S. P., Thermoreversible micellization and gelation of a blend of pluronic polymers. *Polymer* **2008,** *49*, 1952-1960.

43. Wanka, G.; Hoffmann, H.; Ulbricht, W., The aggregation behavior of poly-(oxyethylene)-poly-(oxypropylene)-poly-(oxyethylene)-block-copolymers in aqueous solution. *Colloid and Polymer Science* **1990,** *268*, 101-117.

44. Armstrong, J. K.; Parsonage, J.; Chowdhry, B.; Leharne, S.; Mitchell, J.; Beezer, A.; Loehner, K.; Laggner, P., Scanning densitometric and calorimetric studies of poly (ethylene oxide)/poly (propylene oxide)/poly (ethylene oxide) triblock copolymers (poloxamers) in dilute aqueous solution. *The Journal of Physical Chemistry* **1993,** *97*, 3904-3909.

45. Nivaggioli, T.; Alexandridis, P.; Hatton, T. A.; Yekta, A.; Winnik, M. A., Fluorescence probe studies of pluronic copolymer solutions as a function of temperature. *Langmuir* **1995,** *11*, 730-737.

46. Brown, W.; Schillen, K.; Almgren, M.; Hvidt, S.; Bahadur, P., Micelle and gel formation in a poly(ethylene oxide)/poly(propylene oxide)/poly(ethylene oxide) triblock copolymer in water solution: dynamic and static light scattering and oscillatory shear measurements. *The Journal of Physical Chemistry* **1991,** *95*, 1850-1858.

47. Kostko, A. F.; Harden, J. L.; McHugh, M. A., Dynamic Light Scattering Study of Concentrated Triblock Copolymer Micellar Solutions under Pressure. *Macromolecules* **2009,** *42*, 5328-5338.

48. Mortensen, K.; Brown, W.; Joergensen, E., Phase behavior of poly(propylene oxide)-poly(ethylene oxide)-poly(propylene oxide) triblock copolymer melt and aqueous solutions. *Macromolecules* **1994,** *27*, 5654-5666.

49. Attwood, D.; Collett, J. H.; Tait, C. J., The micellar properties of the poly(oxyethylene) - poly(oxypropylene) copolymer Pluronic F127 in water and electrolyte solution. *International Journal of Pharmaceutics* **1985,** *26*, 25-33.

50. Liu, Y. C.; Chen, S. H.; Huang, J. S., Relationship between the microstructure and rheology of micellar solutions formed by a triblock copolymer surfactant. *Physical Review E* **1996,** *54*, 1698-1708.

51. Linse, P., Phase behavior of poly(ethylene oxide)-poly(propylene oxide) block copolymers in aqueous solution. *The Journal of Physical Chemistry* **1993,** *97*, 13896-13902.

52. Malmsten, M.; Linse, P.; Zhang, K. W., Phase behavior of aqueous poly(ethylene oxide)/poly(propylene oxide) solutions. *Macromolecules* **1993,** *26*, 2905-2910.

53. Wu, C.; Liu, T.; Chu, B.; Schneider, D. K.; Graziano, V., Characterization of the PEO−PPO−PEO triblock copolymer and its application as a separation medium in capillary electrophoresis. *Macromolecules* **1997,** *30*, 4574-4583.

54. Aniansson, E.; Wall, S.; Almgren, M.; Hoffmann, H.; Kielmann, I.; Ulbricht, W.; Zana, R.; Lang, J.; Tondre, C., Theory of the kinetics of micellar equilibria and quantitative interpretation of chemical relaxation studies of micellar solutions of ionic surfactants. *The Journal of Physical Chemistry* **1976,** *80*, 905-922.

55. Kositza, M. J.; Bohne, C.; Alexandridis, P.; Hatton, T. A.; Holzwarth, J. F., Dynamics of micro- and macrophase separation of amphiphilic block-copolymers in aqueous solution. *Macromolecules* **1999,** *32*, 5539-5551.

56. Hvidt, S., Pressure- and temperature-dependent micellization of a poly(ethylene oxide)-poly(propylene oxide) triblock copolymer in aqueous solutions. *Colloids and Surfaces A: Physicochemical and Engineering Aspects* **1996,** *112*, 201-207.

57. Hecht, E.; Hoffmann, H., Kinetic and calorimetric investigations on micelle formation of block copolymers of the poloxamer type. *Colloids and Surfaces A: Physicochemical and Engineering Aspects* **1995,** *96*, 181-197.

58. Mortensen, K.; Brown, W.; Nordén, B., Inverse melting transition and evidence of three-dimensional cubatic structure in a block-copolymer micellar system. *Physical Review Letters* **1992,** *68*, 2340-2343.

59. Alexandridis, P.; Zhou, D.; Khan, A., Lyotropic liquid crystallinity in amphiphilic block copolymers: temperature effects on phase behavior and structure for poly(ethylene oxide)-b-poly(propylene oxide)-b-poly(ethylene oxide) copolymers of different composition. *Langmuir* **1996,** *12*, 2690-2700.

60. Brown, W.; Schillen, K.; Hvidt, S., Triblock copolymers in aqueous solution studied by static and dynamic light scattering and oscillatory shear measurements: influence of relative block sizes. *The Journal of Physical Chemistry* **1992,** *96*, 6038-6044.

61. Wang, P.; Johnston, T. P., Kinetics of sol-to-gel transition for poloxamer polyols. *Journal of Applied Polymer Science* **1991,** *43*, 283-292.

62. Cabana, A.; Aït-Kadi, A.; Juhász, J., Study of the gelation process of polyethylene $oxide_a$–polypropylene $oxide_b$–polyethylene $oxide_a$copolymer (Poloxamer 407) aqueous solutions. *Journal of Colloid and Interface Science* **1997,** *190*, 307-312.

63. Jørgensen, E. B.; Hvidt, S.; Brown, W.; Schillén, K., Effects of salts on the micellization and gelation of a triblock copolymer studied by rheology and light scattering. *Macromolecules* **1997,** *30*, 2355-2364.

64. Osswald, T.; Rudolph, N., Polymer Rheology. In *Polymer Rheology*, Osswald, T.; Rudolph, N., Eds. Hanser: 2015; pp I-275.

65. Jalaal, M.; Cottrell, G.; Balmforth, N.; Stoeber, B., On the rheology of Pluronic F127 aqueous solutions. *Journal of Rheology* **2016,** *61*, 139-146.

66. Lau, B. K.; Wang, Q.; Sun, W.; Li, L., Micellization to gelation of a triblock copolymer in water: Thermoreversibility and scaling. *Journal of Polymer Science Part B: Polymer Physics* **2004,** *42*, 2014-2025.

67. Liu, S.; Li, L., Multiple Phase Transition and Scaling Law for Poly(ethylene oxide)–Poly(propylene oxide)–Poly(ethylene oxide) Triblock Copolymer in Aqueous Solution. *ACS Applied Materials & Interfaces* **2015,** *7* (4), 2688-2697.

68. Meyers, M. A.; Chawla, K. K., *Mechanical behavior of materials*. Cambridge University Press: 2008.

69. Ferry, J. D., *Viscoelastic properties of polymers*. John Wiley & Sons: 1980.

70. Stoeber, B.; Zhihao, Y.; Liepmann, D.; Muller, S. J., Flow control in microdevices using thermally responsive triblock copolymers. *Journal of Microelectromechanical Systems* **2005,** *14*, 207-213.

71. Hopkins, C. C.; de Bruyn, J. R., Gelation and long-time relaxation of aqueous solutions of Pluronic F127. *Journal of Rheology* **2019,** *63*, 191-201.

72. Bahadur, P.; Pandya, K.; Almgren, M.; Li, P.; Stilbs, P., Effect of inorganic salts on the micellar behaviour of ethylene oxide-propylene oxide block copolymers in aqueous solution. *Colloid and Polymer Science* **1993,** *271*, 657-667.

73. Pandit, N. K.; Kisaka, J., Loss of gelation ability of Pluronic® F127 in the presence of some salts. *International Journal of Pharmaceutics* **1996,** *145*, 129-136.

74. Pandit, N.; Trygstad, T.; Croy, S.; Bohorquez, M.; Koch, C., Effect of salts on the micellization, clouding, and solubilization behavior of Pluronic F127 solutions. *Journal of Colloid and Interface Science* **2000,** *222*, 213-220.

75. Pandit, N. K.; Wang, D., Salt effects on the diffusion and release rate of propranolol from poloxamer 407 gels. *International Journal of Pharmaceutics* **1998,** *167*, 183-189.

76. Damodaran, S.; Song, K. B., Effect of water structure makers and breakers on the adsorption of β-casein at the air—water interface. *Colloids and Surfaces* **1990,** *50*, 75-86.

77. Von Hippel, P. H., Effects of neutral salts on the structure and conformational stability of macromolecules in solution. *Structure and Stability of Biological Macromolecules* **1969,** *256*, 3394-3398.

78. Malmsten, M.; Lindman, B., Self-assembly in aqueous block copolymer solutions. *Macromolecules* **1992,** *25*, 5440-5445.

79. Almgren, M.; Bahadur, P.; Alsins, J., Fluorescence quenching and excimer formation to probe the micellization of a poly (ethylene oxide)-poly (propylene oxide)-poly (ethylene oxide) block copolymer, as modulated by potassium fluoride in aqueous solution. *Langmuir* **1991,** *7*, 446-450.

80. Desai, M.; Jain, N. J.; Sharma, R.; Bahadur, P., Temperature and salt-induced micellization of some block copolymers in aqueous solution. *Journal of Surfactants and Detergents* **2000,** *3*, 193-199.

81. Choi, H.-G.; Lee, M.-K.; Kim, M.-H.; Kim, C.-K., Effect of additives on the physicochemical properties of liquid suppository bases. *International Journal of Pharmaceutics* **1999,** *190*, 13-19.

82. Dumortier, G.; Grossiord, J. L.; Zuber, M.; Couarraze, G.; Chaumeil, J. C., Rheological study of a thermoreversible morphine gel. *Drug Development and Industrial Pharmacy* **1991,** *17*, 1255-1265.

83. Zhang, H.; Ding, J., Frequency- and temperature-dependent rheological properties of an amphiphilic block co-polymer in water and including cell-culture media. *Journal of Biomaterials Science, Polymer Edition* **2010,** *21*, 253-269.

84. Kadam, Y.; Yerramilli, U.; Bahadur, A., Solubilization of poorly water-soluble drug carbamezapine in Pluronic® micelles: Effect of molecular characteristics,

temperature and added salt on the solubilizing capacity. *Colloids and Surfaces B: Biointerfaces* **2009,** *72*, 141-147.

85. Dumortier, G.; Grossiord, J. L.; Agnely, F.; Chaumeil, J. C., A review of Poloxamer 407 pharmaceutical and pharmacological characteristics. *Pharmaceutical Research* **2006,** *23*, 2709-2728.

86. Boreham, A.; Brodwolf, R.; Walker, K.; Haag, R.; Alexiev, U., Time-resolved fluorescence spectroscopy and fluorescence lifetime imaging microscopy for characterization of dendritic polymer nanoparticles and applications in nanomedicine. *Molecules* **2017,** *22*, 17.

87. Kalyanasundaram, K., Photophysics of molecules in micelle-forming surfactant solutions. *Chemical Society Reviews* **1978,** *7*, 453-472.

88. Wehry, E. L., *Modern fluorescence spectroscopy*. Springer Science & Business Media: 2012.

89. Kalyanasundaram, K., *Photochemistry in microheterogeneous systems*. Elsevier: 2012.

90. Thomas, J. K., Radiation-induced reactions in organized assemblies. *Chemical Reviews* **1980,** *80*, 283-299.

91. Fendler, J. H., Microemulsions, micelles, and vesicles as media for membrane mimetic photochemistry. *The Journal of Physical Chemistry* **1980,** *84*, 1485-1491.

92. Grieser, F.; Drummond, C. J., The physicochemical properties of self-assembled surfactant aggregates as determined by some molecular spectroscopic probe techniques. *The Journal of Physical Chemistry* **1988,** *92*, 5580-5593.

93. Reeves, R. L., Nature of mixed micelles from anionic dyes and cationic surfactants. Kinetic study. *Journal of the American Chemical Society* **1975,** *97*, 6019-6024.

94. Paleos, C.; Stassinopoulou, C.; Malliaris, A., Comparative studies between monomeric and polymeric sodium 10-undecenoate micelles. *The Journal of Physical Chemistry* **1983,** *87*, 251-254.

95. Lianos, P.; Lang, J.; Strazielle, C.; Zana, R., Fluorescence probe study of oil-in-water microemulsions. 1. Effect of pentanol and dodecane or toluene on some properties of sodium dodecyl sulfate micelles. *The Journal of Physical Chemistry* **1982,** *86*, 1019-1025.

96. Lakowicz, J. R., *Principles of Fluorescence Spectroscopy*. Springer US: 2007.

97. Gehlen, M. H.; De Schryver, F. C., Time-resolved fluorescence quenching in micellar assemblies. *Chemical Reviews* **1993,** *93*, 199-221.

98. Rinco, O.; Nolet, M.-C.; Ovans, R.; Bohne, C., Probing the binding dynamics to sodium cholate aggregates using naphthalene derivatives as guests. *Photochemical & Photobiological Sciences* **2003,** *2*, 1140-1151.

99. Swain, J.; Mishra, A. K., Nile red fluorescence for quantitative monitoring of micropolarity and microviscosity of pluronic F127 in aqueous media. *Photochemical & Photobiological Sciences* **2016,** *15* (11), 1400-1407.

100. Kabanov, A. V.; Nazarova, I. R.; Astafieva, I. V.; Batrakova, E. V.; Alakhov, V. Y.; Yaroslavov, A. A.; Kabanov, V. A., Micelle formation and solubilization of fluorescent probes in poly (oxyethylene-b-oxypropylene-b-oxyethylene) solutions. *Macromolecules* **1995,** *28*, 2303-2314.

101. Jeon, S.; Granick, S.; Kwon, K.-W.; Char, K., Microviscosity in poly(ethylene oxide)-polypropylene oxide-poly(ethylene oxide) block copolymers probed by fluorescence depolarization kinetics. *Journal of Polymer Science Part B: Polymer Physics* **2002,** *40*, 2883-2888.

102. Grant, C. D.; DeRitter, M. R.; Steege, K. E.; Fadeeva, T. A.; Castner, E. W., Fluorescence probing of interior, interfacial, and exterior regions in solution aggregates of poly(ethylene oxide)− poly(propylene oxide)−poly(ethylene oxide) triblock copolymers. *Langmuir* **2005,** *21*, 1745-1752.

103. Kumbhakar, M.; Ganguly, R., Influence of electrolytes on the microenvironment of F127 triblock copolymer micelles: A solvation and rotational dynamics study of coumarin dyes. *The Journal of Physical Chemistry B* **2007,** *111*, 3935-3942.

104. Mohanty, M. E.; Rao, V. J.; Mishra, A. K., A fluorescence study on the interaction of telmisartan in triblock polymers pluronic P123 and F127. *Spectrochimica Acta Part A: Molecular and Biomolecular Spectroscopy* **2014,** *121*, 330-338.

105. Rharbi, Y.; Winnik, M. A., Solute exchange between surfactant micelles by micelle fragmentation and fusion. *Advances in Colloid and Interface Science* **2001,** *89-90*, 25-46.

106. Kirkeminde, A. W.; Torres, T.; Ito, T.; Higgins, D. A., Multiple diffusion pathways in Pluronic F127 mesophases revealed by single molecule tracking and fluorescence correlation spectroscopy. *The Journal of Physical Chemistry B* **2011,** *115*, 12736-12743.

107. Ghosh, S.; Mandal, U.; Adhikari, A.; Bhattacharyya, K., Study of diffusion of organic dyes in a triblock copolymer micelle and gel by fluorescence correlation spectroscopy. *Chemistry – An Asian Journal* **2009,** *4*, 948-954.

108. Nadiv, R.; Fernandes, R. M. F.; Ochbaum, G.; Dai, J.; Buzaglo, M.; Varenik, M.; Biton, R.; Furó, I.; Regev, O., Polymer nanocomposites: Insights on rheology, percolation and molecular mobility. *Polymer* **2018,** *153*, 52-60.

109. Nivaggioli, T.; Tsao, B.; Alexandridis, P.; Hatton, T. A., Microviscosity in pluronic and tetronic poly (ethylene oxide)-poly (propylene oxide) block copolymer micelles. *Langmuir* **1995,** *11*, 119-126.

110. Cau, F.; Lacelle, S., H NMR relaxation studies of the micellization of a poly(ethylene oxide)−poly(propylene oxide)−poly(ethylene oxide) triblock copolymer in aqueous solution. *Macromolecules* **1996,** *29*, 170-178.

111. Walderhaug, H.; Nyström, B., Anomalous diffusion in an aqueous system of a poly(ethylene oxide)−poly(propylene oxide)−poly(ethylene oxide) triblock copolymer

during gelation studied by pulsed field gradient NMR. *The Journal of Physical Chemistry B* **1997,** *101*, 1524-1528.

112. Ford, W. E.; Kamat, P. V., Photochemistry on surfaces. 3. Spectral and photophysical properties of monomeric and dimeric anthracenesulfonates adsorbed by colloidal alumina-coated silica particles. *The Journal of Physical Chemistry* **1989,** *93*, 6423-6428.

113. Wilkinson, F.; Willsher, C. J.; Warwick, P.; Land, E. J.; Rushton, F. A. P., Diffuse reflectance pulse radiolysis of opaque samples. *Nature* **1984,** *311*, 40-42.

114. Turro, N. J.; Zimmt, M. B.; Gould, I. R.; Mahler, W., Triplet energy transfer as a probe of surface diffusion rates: time-resolved diffuse reflectance transient absorption spectroscopy study. *Journal of the American Chemical Society* **1985,** *107*, 5826-5827.

115. Wilkinson, F.; Willsher, C. J.; Casal, H. L.; Johnston, L. J.; Scaiano, J. C., Intrazeolite photochemistry. IV. Studies of carbonyl photochemistry on the hydrophobic zeolite Silicalite using time-resolved diffuse reflectance techniques. *Canadian Journal of Chemistry* **1986,** *64*, 539-544.

116. Drake, J.; Levitz, P.; Turro, N. J.; Nitsche, K. S.; Cassidy, K. F., Benzophenone triplet quenching by oxygen at the gas/solid interface: a target annihilation reaction in the restricted pore geometry of silica. *The Journal of Physical Chemistry* **1988,** *92*, 4680-4684.

117. Kelly, G.; Willsher, C. J.; Wilkinson, F.; Netto-Ferreira, J. C.; Olea, A.; Weir, D.; Johnston, L. J.; Scaiano, J. C., Intrazeolite photochemistry. VI. Diffuse reflectance laser flash photolysis and product studies of diphenylmethyl radicals on solid supports. *Canadian Journal of Chemistry* **1990,** *68*, 812-819.

118. Liao, Y.; Bohne, C., Alcohol effect on equilibrium constants and dissociation dynamics of xanthone−cyclodextrin complexes. *The Journal of Physical Chemistry* **1996,** *100*, 734-743.

119. Bohne, C.; Barra, M.; Boch, R.; Abuin, E. B.; Scaiano, J. C., Excited triplet states as probes in organized systems. An overview of recent results. *Journal of Photochemistry and Photobiology A: Chemistry* **1992,** *65*, 249-265.

120. Elworthy, P. H.; Florence, A. T.; Macfarlane, C. B., *Solubilization by surface active agents and its applications in chemistry and biological sciences*. John Wiley & Sons, Incorporated: 1968.

121. Singleterry, C. R., Solubilization and Related Phenomena. Physical Chemistry. *Journal of the American Chemical Society* **1955,** *77*, 5453-5454.

122. Almgren, M.; Grieser, F.; Thomas, J. K., Dynamic and static aspects of solubilization of neutral arenes in ionic micellar solutions. *Journal of the American Chemical Society* **1979,** *101*, 279-291.

123. Barros, T. C.; Stefaniak, K.; Holzwarth, J. F.; Bohne, C., Complexation of naphthylethanols with β-cyclodextrin. *The Journal of Physical Chemistry A* **1998,** *102*, 5639-5651.

124. Infelta, P.; Gratzel, M.; Thomas, J., Luminescence decay of hydrophobic molecules solubilized in aqueous micellar systems. Kinetic model. *The Journal of Physical Chemistry* **1974,** *78*, 190-195.

125. Scaiano, J. C.; Paraskevopoulos, C. I., Comparison of the quenching of excited states by 5-DOXYL and 12-DOXYL-stearates in micellar solution. *Canadian Journal of Chemistry* **1984,** *62*, 2351-2354.

126. Miller, M.; Doran, M., Concentrated salt solutions. II. viscosity and density of sodium thiocyanate, sodium perchlorate and sodium iodide. *The Journal of Physical Chemistry* **1956,** *60*, 186-189.

127. Cheng, N.-S., Formula for the Viscosity of a Glycerol−Water Mixture. *Industrial & Engineering Chemistry Research* **2008,** *47*, 3285-3288.

128. Okano, L. T.; Barros, T. C.; Chou, D. T. H.; Bennet, A. J.; Bohne, C., Complexation dynamics of xanthone and thioxanthone to β-cyclodextrin derivatives. *The Journal of Physical Chemistry B* **2001,** *105*, 2122-2128.

129. Pace, T. C. S.; Bohne, C., Temperature effects on xanthone–β-cyclodextrin binding dynamics. *Canadian Journal of Chemistry* **2011,** *89*, 395-401.

130. Kalyanasundaram, K.; Thomas, J., Environmental effects on vibronic band intensities in pyrene monomer fluorescence and their application in studies of micellar systems. *Journal of the American Chemical Society* **1977,** *99*, 2039-2044.

131. Dong, D. C.; Winnik, M. A., The Py scale of solvent polarities. Solvent effects of the vibronic fine structure of pyrene fluorescence and empirical correlations with ET and Y values. *Photochemistry and Photobiology* **1982,** *35*, 17-21.

132. Birks, J. B.; Dyson, D. J.; Munro, I. H.; Flowers, B. H., 'Excimer' fluorescence II. Lifetime studies of pyrene solutions. *Proceedings of the Royal Society of London. Series A. Mathematical and Physical Sciences* **1963,** *275*, 575-588.

133. Xing, H.; Yan, P.; Xiao, J.-X., Unusual location of the pyrene probe solubilized in the micellar solutions of tetraalkylammonium perfluorooctanoates. *Soft Matter* **2013,** *9*, 1164-1171.

134. Binana-Limbele, W.; Zana, R., Fluorescence probing of microdomains in aqueous solutions of polysoaps. 2. Study of the size of the microdomains. *Macromolecules* **1990,** *23*, 2731-2739.

135. Grätzel, M.; Thomas, J., Dynamics of pyrene fluorescence quenching in aqueous ionic micellar systems. Factors affecting the permeability of micelles. *Journal of the American Chemical Society* **1973,** *95*, 6885-6889.

136. Tummino, P. J.; Gafni, A., Determination of the aggregation number of detergent micelles using steady-state fluorescence quenching. *Biophysical Journal* **1993,** *64*, 1580-1587.

137. Yihwa, C.; Kellermann, M.; Becherer, M.; Hirsch, A.; Bohne, C., Pyrene binding to persistent micelles formed from a dendro-calixarene. *Photochemical & Photobiological Sciences* **2007,** *6*, 525-531.

138. Alargova, R. G.; Kochijashky, I. I.; Sierra, M. L.; Zana, R., Micelle aggregation numbers of surfactants in aqueous solutions: A comparison between the results from steady-state and time-resolved fluorescence quenching. *Langmuir* **1998,** *14*, 5412-5418.

139. Olea, A. F.; Silva, P.; Fuentes, I.; Martínez, F.; Worrall, D. R., Probing solubilization sites in block copolymer micelles using fluorescence quenching. *Journal of Photochemistry and Photobiology A: Chemistry* **2011,** *217*, 49-54.

140. Alexandridis, P.; Nivaggioli, T.; Hatton, T. A., Temperature effects on structural properties of Pluronic P104 and F108 PEO-PPO-PEO block copolymer solutions. *Langmuir* **1995,** *11*, 1468-1476.

141. Almgren, M.; Bahadur, P.; Jansson, M.; Li, P.; Brown, W.; Bahadur, A., Static and dynamic properties of a (PEO-PPO-PEO) block copolymer in aqueous solution. *Journal of Colloid and Interface Science* **1992,** *151*, 157-165.

142. Gilbert, J. C.; Washington, C.; Davies, M. C.; Hadgraft, J., The behaviour of Pluronic F127 in aqueous solution studied using fluorescent probes. *International Journal of Pharmaceutics* **1987,** *40*, 93-99.

143. Robertson, J. M., The crystalline structure of naphthalene. A quantitative X-ray investigation. *Proceedings of the Royal Society of London. Series A, Containing Papers of a Mathematical Physical Character* **1933,** *142*, 674-688.

144. Camerman, A.; Trotter, J., The crystal and molecular structure of pyrene. *Acta Crystallographica* **1965,** *18*, 636-643.

145. Uchida, K.; Tanaka, M.; Tomura, M., Excimer emission of crystalline naphthalene. *Journal of Luminescence* **1979,** *20*, 409-414.

146. Mataga, N.; Tomura, M.; Nishimura, H., Fluorescence decay times of naphthalene and naphthalene excimers. *Molecular Physics* **1965,** *9*, 367-375.

147. Paterson, I. F.; Chowdhry, B. Z.; Leharne, S. A., Investigations of naphthalene solubilization in aqueous solutions of ethylene oxide-b-propylene oxide-b-ethylene oxide copolymers. *Langmuir* **1999,** *15*, 6187-6194.

148. Basak, R.; Bandyopadhyay, R., Encapsulation of hydrophobic drugs in Pluronic F127 micelles: Effects of drug hydrophobicity, solution temperature, and pH. *Langmuir* **2013,** *29*, 4350-4356.

149. Anand, U.; Mukherjee, S., Microheterogeneity and microviscosity of F127 micelle: The counter effects of urea and temperature. *Langmuir* **2014,** *30*, 1012-1021.

150. Kadam, Y.; Yerramilli, U.; Bahadur, A.; Bahadur, P., Micelles from PEO–PPO–PEO block copolymers as nanocontainers for solubilization of a poorly water soluble drug hydrochlorothiazide. *Colloids and Surfaces B: Biointerfaces* **2011,** *83*, 49-57.

151. Dey, J.; Kumar, S.; Nath, S.; Ganguly, R.; Aswal, V. K.; Ismail, K., Additive induced core and corona specific dehydration and ensuing growth and interaction of Pluronic F127 micelles. *Journal of Colloid and Interface Science* **2014,** *415*, 95-102.

152. El-Kamel, A. H., In vitro and in vivo evaluation of Pluronic F127-based ocular delivery system for timolol maleate. *International Journal of Pharmaceutics* **2002,** *241*, 47-55.

153. Jiang, J.; Li, C.; Lombardi, J.; Colby, R. H.; Rigas, B.; Rafailovich, M. H.; Sokolov, J. C., The effect of physiologically relevant additives on the rheological properties of concentrated Pluronic copolymer gels. *Polymer* **2008,** *49*, 3561-3567.

154. Li, Y.; Shi, T.; Sun, Z.; An, L.; Huang, Q., Investigation of sol−gel transition in Pluronic F127/D2O solutions using a combination of small-angle neutron scattering and Monte Carlo simulation. *The Journal of Physical Chemistry B* **2006,** *110*, 26424-26429.

155. Goodpaster, J. V.; Harrison, J. F.; McGuffin, V. L., Ab initio study of selective fluorescence quenching of polycyclic aromatic hydrocarbons. *The Journal of Physical Chemistry A* **2002,** *106*, 10645-10654.

156. Dowling, K. C.; Thomas, J. K., A novel micellar synthesis and photophysical characterization of water-soluble acrylamide-styrene block copolymers. *Macromolecules* **1990,** *23*, 1059-1064.

157. Chu, D. Y.; Thomas, J. K., Photophysical and photochemical studies on a polymeric intramolecular micellar system, PA-18K2. *Macromolecules* **1987,** *20*, 2133-2138.

158. Martinho, J. M. G.; Reis e Sousa, A. T.; Oliveira Torres, M. E.; Fedorov, A., Fluorescence quenching of pyrene monomer and excimer by CH3I. *Chemical Physics* **2001,** *264*, 111-121.

159. Thomas, J. K., Effect of structure and charge on radiation-induced reactions in micellar systems. *Accounts of Chemical Research* **1977,** *10*, 133-138.

160. Ju, C.; Bohne, C., Probing bile salt aggregates by fluorescence quenching. *Photochemistry and Photobiology* **1996,** *63*, 60-67.

161. Rassing, J.; Attwood, D., Ultrasonic velocity and light-scattering studies on the polyoxyethylene—polyoxypropylene copolymer Pluronic F127 in aqueous solution. *International Journal of Pharmaceutics* **1982,** *13*, 47-55.

162. Bohorquez, M.; Koch, C.; Trygstad, T.; Pandit, N., A study of the temperature-dependent micellization of pluronic F127. *Journal of Colloid Interface Science* **1999,** *216*, 34-40.

163. Watkins, A., Kinetics of fluorescence quenching by inorganic anions. *The Journal of Physical Chemistry* **1974,** *78*, 2555-2558.

164. Rasouli, M.; Tavassoli, S. H.; Mousavi, S. J.; Darbani, S. M. R., Measuring of naphthalene fluorescence emission in the water with nanosecond time delay laser induced fluorescence spectroscopy method. *Optik* **2016,** *127*, 6218-6223.

165. Jiang, J.; Lu, J., Impact of temperature on the linear viscoelastic region of wood. *Canadian Journal of Forest Research* **2009,** *39*, 2092-2099.

166. Zhang, M.; Djabourov, M.; Bourgaux, C.; Bouchemal, K., Nanostructured fluids from pluronic® mixtures. *International Journal of Pharmaceutics* **2013,** *454*, 599-610.

167. Lin, Y.; Alexandridis, P., Temperature-dependent adsorption of Pluronic F127 block copolymers onto carbon black particles dispersed in aqueous media. *The Journal of Physical Chemistry B* **2002,** *106*, 10834-10844.

168. Teng, Y.; Morrison, M. E.; Munk, P.; Webber, S. E.; Procházka, K., Release kinetics studies of aromatic molecules into water from block polymer micelles. *Macromolecules* **1998,** *31*, 3578-3587.

169. Focsaneanu, K.-S.; Scaiano, J. C., Potential analytical applications of differential fluorescence quenching: pyrene monomer and excimer emissions as sensors for electron deficient molecules. *Photochemical & Photobiological Sciences* **2005,** *4*, 817-821.

170. Kim, D.; Amos, R.; Gauthier, M.; Duhamel, J., Applications of pyrene fluorescence to the characterization of hydrophobically modified starch nanoparticles. *Langmuir* **2018,** *34*, 8611-8621.

171. Arık, M.; Çelebi, N.; Onganer, Y., Fluorescence quenching of fluorescein with molecular oxygen in solution. *Journal of Photochemistry and Photobiology A: Chemistry* **2005,** *170*, 105-111.

172. Jain, N. J.; Aswal, V. K.; Goyal, P. S.; Bahadur, P., Micellar structure of an ethylene oxide−propylene oxide block copolymer: A small-angle neutron scattering study. *The Journal of Physical Chemistry B* **1998,** *102*, 8452-8458.

173. Chowdhuri, S.; Chandra, A., Dynamics of halide ion−water hydrogen bonds in aqueous solutions: Dependence on ion size and temperature. *The Journal of Physical Chemistry B* **2006,** *110*, 9674-9680.

174. Seminario, J. M.; Concha, M. C.; Politzer, P., A density functional/molecular dynamics study of the structure of liquid nitromethane. *The Journal of Chemical Physics* **1995,** *102*, 8281-8282.

175. Alexandridis, P., Poly(ethylene oxide)/poly(propylene oxide) block copolymer surfactants. *Colloid & Interface Science* **1997,** *2*, 478-489.

176. Sharma, R.; Bahadur, P., Effect of different additives on the cloud point of a polyethylene oxide-polypropylene oxide-polyethylene oxide block copolymer in aqueous solution. *Journal of Surfactants and Detergents* **2002,** *5*, 263-268.

177. Foster, B.; Cosgrove, T.; Hammouda, B., Pluronic triblock copolymer systems and their interactions with ibuprofen. *Langmuir* **2009,** *25*, 6760-6766.

178. Parmar, A.; Singh, K.; Bahadur, A.; Marangoni, G.; Bahadur, P., Interaction and solubilization of some phenolic antioxidants in Pluronic® micelles. *Colloids and Surfaces B: Biointerfaces* **2011,** *86*, 319-326.

179. Khimani, M.; Verma, G.; Kumar, S.; Hassan, P. A.; Aswal, V. K.; Bahadur, P., pH induced tuning of size, charge and viscoelastic behavior of aqueous micellar solution of Pluronic® P104–anthranilic acid mixtures: A scattering, rheology and NMR study. *Colloids and Surfaces A: Physicochemical and Engineering Aspects* **2015,** *470*, 202-210.

180. Hvidt, S.; Keiding, K., Rheology and structures of EO-PO-EO block copolymers in aqueous solutions. *Annual Transactions of the Nordic Rheology Society* **2009,** *17*, 103-107.

181. Einstein, A., On the motion of particles suspended in still liquids, which is required by the molecular kinetic theory of heat. *Annals of Physics* **1905,** *4*, 208.

182. Cavalieri, F.; Chiessi, E.; Finelli, I.; Natali, F.; Paradossi, G.; Telling, M. F., Water, solute, and segmental dynamics in polysaccharide hydrogels. *Macromolecular Bioscience* **2006,** *6*, 579-589.

183. Burke, M. D.; Park, J. O.; Srinivasarao, M.; Khan, S. A., A novel enzymatic technique for limiting drug mobility in a hydrogel matrix. *Journal of Controlled Release* **2005,** *104*, 141-153.

184. Mealy, J. E.; Rodell, C. B.; Burdick, J. A., Sustained small molecule delivery from injectable hyaluronic acid hydrogels through host–guest mediated retention. *Journal of Materials Chemistry B* **2015,** *3*, 8010-8019.

185. Raccis, R.; Roskamp, R.; Hopp, I.; Menges, B.; Koynov, K.; Jonas, U.; Knoll, W.; Butt, H. J.; Fytas, G., Probing mobility and structural inhomogeneities in grafted hydrogel films by fluorescence correlation spectroscopy. *Soft Matter* **2011,** *7*, 7042-7053.

186. Schuster, E.; Sott, K.; Ström, A.; Altskär, A.; Smisdom, N.; Gebäck, T.; Lorén, N.; Hermansson, A.-M., Interplay between flow and diffusion in capillary alginate hydrogels. *Soft Matter* **2016,** *12*, 3897-3907.

187. Nagarajan, R., Solubilization of hydrocarbons and resulting aggregate shape transitions in aqueous solutions of Pluronic® (PEO–PPO–PEO) block copolymers. *Colloids and Surfaces B: Biointerfaces* **1999,** *16*, 55-72.

188. Trotter, J., The crystal and molecular structure of phenanthrene. *Acta Crystallographica* **1963,** *16*, 605-608.

189. Abrahams, S. C.; Robertson, J. M.; White, J. G., The crystal and molecular structure of naphthalene. I. X-ray measurements. *Acta Crystallographica* **1949,** *2*, 233-238.

190. Kozlov, M. Y.; Melik-Nubarov, N. S.; Batrakova, E. V.; Kabanov, A. V., Relationship between Pluronic block copolymer structure, critical micellization concentration and partitioning coefficients of low molecular mass solutes. *Macromolecules* **2000,** *33*, 3305-3313.

191. Sharma, P. K.; Bhatia, S. R., Effect of anti-inflammatories on Pluronic® F127: micellar assembly, gelation and partitioning. *International Journal of Pharmaceutics* **2004,** *278*, 361-377.

192. Li, G.; McGown, L. B., Model for bile salt micellization and solubilization from studies of a" polydisperse" array of fluorescent probes and molecular modeling. *The Journal of Physical Chemistry* **1994,** *98*, 13711-13719.

8 Appendix

Table 8.1. Fluorescence emission lifetimes and corresponding A values for 5 μM pyrene in the absence and presence of NM in 20% F127 at 30 °C (first experiment).

[NM] / mM[b]	τ_1/ns[a]	τ_2/ns[a]	τ_3/ns[a]	τ_4/ns[c]	A_1[c]	A_2[c]	A_3[c]	A_4[c]	χ^2
0	0.3	2.3	8.0	180±1	0.56±0.03	0.08±0.03	0.03±0.01	0.30±0.02	1.182
15.4±0.2	0.2	1.9	5.8	45±1	0.47±0.06	0.15±0.08	0.08±0.04	0.30±0.02	1.051
30.8±0.2	0.3	1.8	5.0	27±1	0.45±003	0.13±0.04	0.12±0.03	0.30±0.08	1.101
46.2±0.3	0.3	1.6	4.4	20±1	0.51±0.02	0.07±0.01	0.12±0.01	0.30±0.01	1.082
61.5±0.7	0.2	1.3	3.5	16±1	0.57±0.02	0.04±0.01	0.14±0.01	0.25±0.01	1.134

[a]Lifetimes correspond to F127 impurities were fixed.
[b]See 2.3.3 for method in the determination of the NM concentration.
[c]The errors represent the standard deviations calculated using the F900 software. The data correspond to one experiment.

Table 8.2. Fluorescence emission lifetimes and corresponding A values for 5 μM pyrene in the absence and presence of NM in 20% F127 at 30 °C (second experiment).

[NM] / mM[b]	τ_1/ns[a]	τ_2/ns[a]	τ_3/ns[a]	τ_4/ns[c]	A_1[c]	A_2[c]	A_3[c]	A_4[c]	χ^2
0	2.3	8.7	-	182±1	0.30±0.01	0.14±0.01	-	0.56±0.01	1.179
15.4±0.2	2.0	6.6	-	45±1	0.32±0.02	0.12±0.01	-	0.56±0.01	1.037
30.8±0.2	1.7	5.1	-	27±1	0.27±0.02	0.21±0.01	-	0.52±0.01	1.116
46.2±0.3	0.1	1.6	4.5	20±1	0.71±0.05	0.06±0.01	0.06±0.01	0.17±0.01	1.119
61.5±0.7	0.2	1.4	3.7	16±1	0.52±0.02	0.07±0.01	0.14±0.01	0.27±0.01	1.092

[a]Lifetimes correspond to F127 impurities were fixed.
[b]See 2.3.3 for method in the determination of the NM concentration.
[c]The errors represent the standard deviations calculated using the F900 software. The data correspond to one experiment.

Table 8.3. Fluorescence emission lifetimes and corresponding A values for 5 μM pyrene in the absence and presence of NM in 20% F127 at 20 °C (first experiment).

[NM] / mM[b]	τ_1/ns[a]	τ_2/ns[a]	τ_3/ns[c]	τ_4/ns[c]	A_1[c]	A_2[c]	A_3[c]	A_4[c]	χ^2
0	2.3	8.7	-	228±1	0.34±0.03	0.10±0.02	-	0.56±0.04	1.108
15.4±0.2	2.0	6.6	27±7	63±1	0.33±0.02	0.06±0.01	0.05±0.01	0.56±0.02	1.095
30.8±0.2	1.7	5.1	22±4	38±1	0.30±0.04	0.11±0.02	0.13±0.05	0.46±0.06	1.103
46.2±0.3	1.6	4.5	16±4	28±1	0.30±0.07	0.11±0.04	0.16±0.07	0.44±0.09	1.164
61.5±0.7	1.4	3.7	13±1	24±1	0.32±0.02	0.06±0.02	0.23±0.02	0.39±0.03	1.104

[a]Lifetimes correspond to F127 impurities were fixed.
[b]See 2.3.3 for method in the determination of the NM concentration.
[c]The errors represent the standard deviations calculated using the F900 software. The data correspond to one experiment.

Table 8.4. Fluorescence emission lifetimes and corresponding A values for 5 μM pyrene in the absence and presence of NM in 20% F127 at 20 °C (second experiment).

[NM]/mM [b]	τ_1/ns[a]	τ_2/ns[a]	τ_3/ns[c]	τ_4/ns[c]	A_1[c]	A_2[c]	A_3[c]	A_4[c]	χ^2
0	2.3	8.8	-	227±1	0.16±0.03	0.03±0.01	-	0.81±0.03	1.020
15.4±0.2	2.0	6.2	25±5	58±1	0.16±0.04	0.02±0.03	0.11±0.02	0.72±0.05	1.038
30.8±0.2	1.8	5.1	20±4	39±1	0.45±0.03	0.08±0.02	0.11±0.02	0.35±0.03	1.161
46.2±0.3	1.5	4.2	21±2	32±2	0.38±0.01	0.08±0.03	0.20±0.03	0.34±0.05	1.090
61.5±0.7	1.5	4.0	13±1	24±1	0.28±0.05	0.17±0.03	0.30±0.01	0.25±0.01	0.936

[a]Lifetimes correspond to F127 impurities were fixed.

[b]See 2.3.3 for method in the determination of the NM concentration.

[c]The errors represent the standard deviations calculated using the F900 software. The data correspond to one experiment.

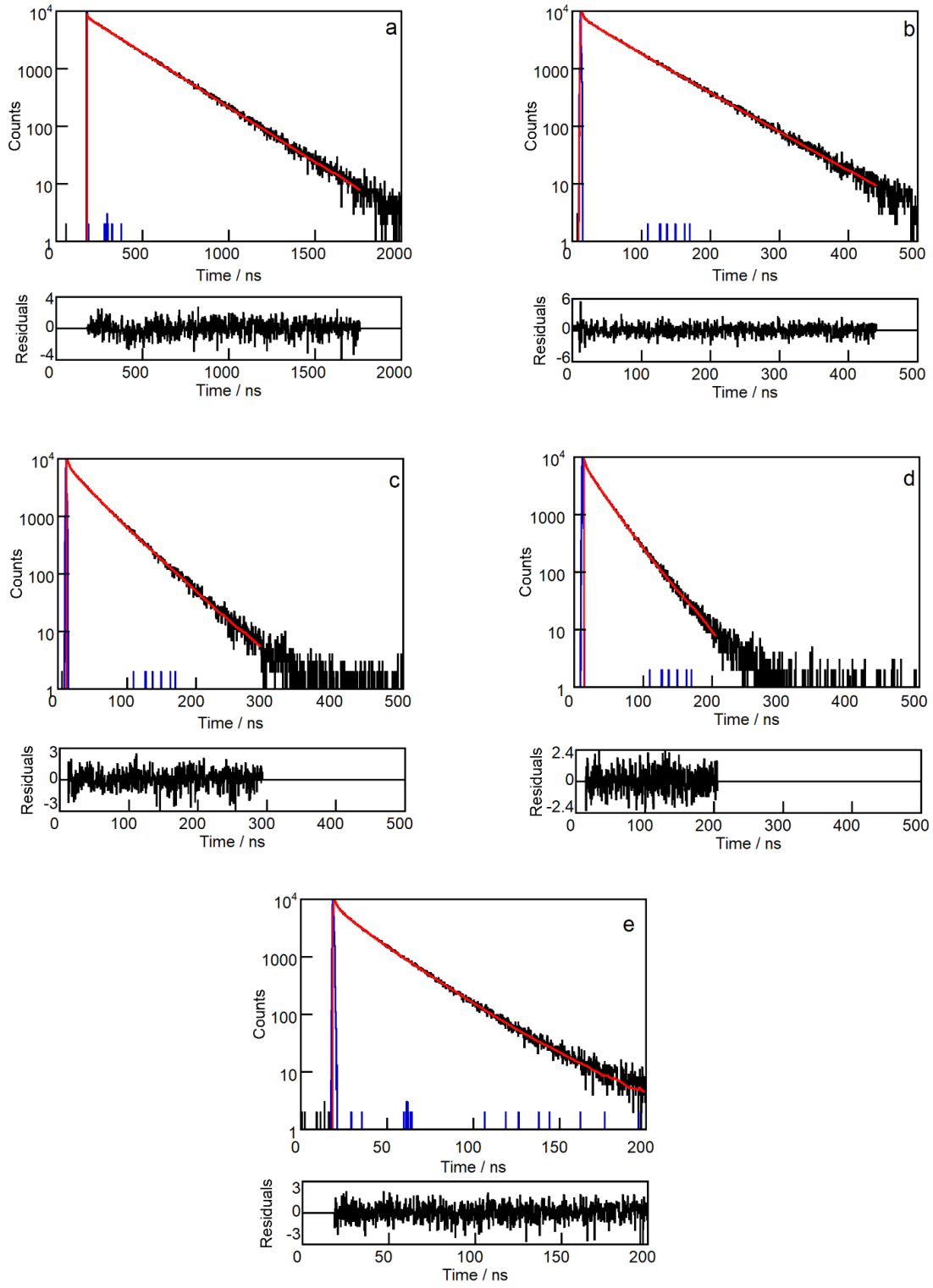

Figure 8.1. Fluorescence decay for 5 µM pyrene in 20% F127 at 20 °C (black) fit to a sum of exponentials decay (red). The IRF is shown in blue at different concentrations of NM a) 0 mM, b) 15.4 mM, c) 30.7 mM, d) 46.2 mM, and e) 62.5 mM. Residuals between calculated and experimental data are shown in the lower panels.

Table 8.5. Fluorescence emission lifetimes and corresponding A values for 5 μM pyrene in the absence and presence of NM in 30% F127 at 30 °C.

[NM] / mM[b]	τ_1/ns[a]	τ_2/ns[a]	τ_3/ ns[a]	τ_4/ns[c]	A_1[c]	A_2[c]	A_3[c]	A_4[c]	χ^2
0	0.3	2.3	8.0	197±1	0.60±0.03	0.05±0.01	0.15±0.01	0.20±0.01	1.110
15.4±0.2	0.2	1.9	5.8	46±1	0.6±0.1	0.13±0.02	0.05±0.01	0.21±0.02	1.125
30.8±0.2	0.3	1.8	5.0	28±1	0.6±0.1	0.12±0.02	0.09±0.01	0.24±0.02	1.129
46.2±0.3	0.3	1.6	4.4	21±1	0.60±0.03	0.06±0.01	0.14±0.01	0.20±0.01	1.181
61.5±0.7	0.2	1.3	3.5	16±1	0.52±0.05	0.08±0.01	0.14±0.01	0.26±0.01	1.148

[a]Lifetimes correspond to F127 impurities were fixed.
[b]See 2.3.3 for method in the determination of the NM concentration.
[c]The errors represent the standard deviations calculated using the F900 software. The data correspond to one experiment.

Table 8.6. Fluorescence emission lifetimes and corresponding A values for 5 μM pyrene in the absence and presence of NM in 30% F127 at 20 °C.

[NM] / mM[b]	τ_1/ns[a]	τ_2/ns[a]	τ_3/ns[a]	τ_4/ns[a]	A_1[c]	A_2[c]	A_3[c]	A_4[c]	χ^2
0	2.3	8.7	-	229±1	0.4±0.2	0.08±0.08	-	0.5±0.4	1.077
15.4±0.2	2.2	7.7	-	86±1	0.35±0.02	0.09±0.01	-	0.56±0.01	1.087
30.8±0.2	2.0	6.6	19±3	62±1	0.43±0.03	0.02±0.03	0.07±0.01	0.48±0.02	1.160
46.2±0.3	1.7	5.1	20±4	41±1	0.39±0.03	0.09±0.02	0.09±0.01	0.43±0.03	1.097
61.5±0.7	1.6	4.5	21±3	31±3	0.29±0.06	0.19±0.04	0.25±0.14	0.27±0.15	1.071

[a]Lifetimes correspond to F127 impurities were fixed.
[b]See 2.3.3 for method in the determination of the NM concentration.
[c]The errors represent the standard deviations calculated using the F900 software. The data correspond to one experiment.

Table 8.7. Fluorescence emission lifetimes and corresponding A values for 5 μM pyrene in the absence and presence of NM in 30% F127 at 10 °C.

[NM] / mM[b]	τ_1/ns[a]	τ_2/ns[a]	τ_3/ns[a]	τ_4/ns[a]	A_1[c]	A_2[c]	A_3[c]	A_4[c]	χ^2
0	2.3	8.7	-	261±1	0.8±0.8	0.03±0.02	-	0.14±0.09	1.094
15.4±0.2	2.2	7.7	37±6	112±1	0.43±0.02	0.03±0.02	0.06±0.01	0.48±0.02	0.944
30.8±0.2	2.0	6.6	32±6	80±1	0.43±0.03	0.06±0.02	0.07±0.01	0.44±0.02	0.993
46.2±0.3	1.7	5.1	21±2	54±1	0.42±0.02	0.08±0.02	0.10±0.01	0.40±0.01	1.069
61.5±0.7	1.6	4.5	19±2	38±1	0.34±0.03	0.17±0.02	0.12±0.02	0.37±0.02	1.047

[a]Lifetimes correspond to F127 impurities were fixed.
[b]See 2.3.3 for method in the determination of the NM concentration.
[c]The errors represent the standard deviations calculated using the F900 software. The data correspond to one experiment.

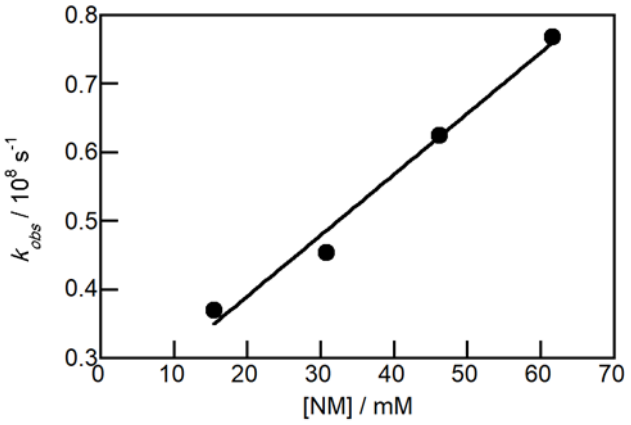

Figure 8.2. Quenching plot for 5 μM pyrene in 20% F127 at 20 °C quenched by NM (k_{obs} correspond to shorter lifetime of singlet excited pyrene). The data correspond to one experiment.

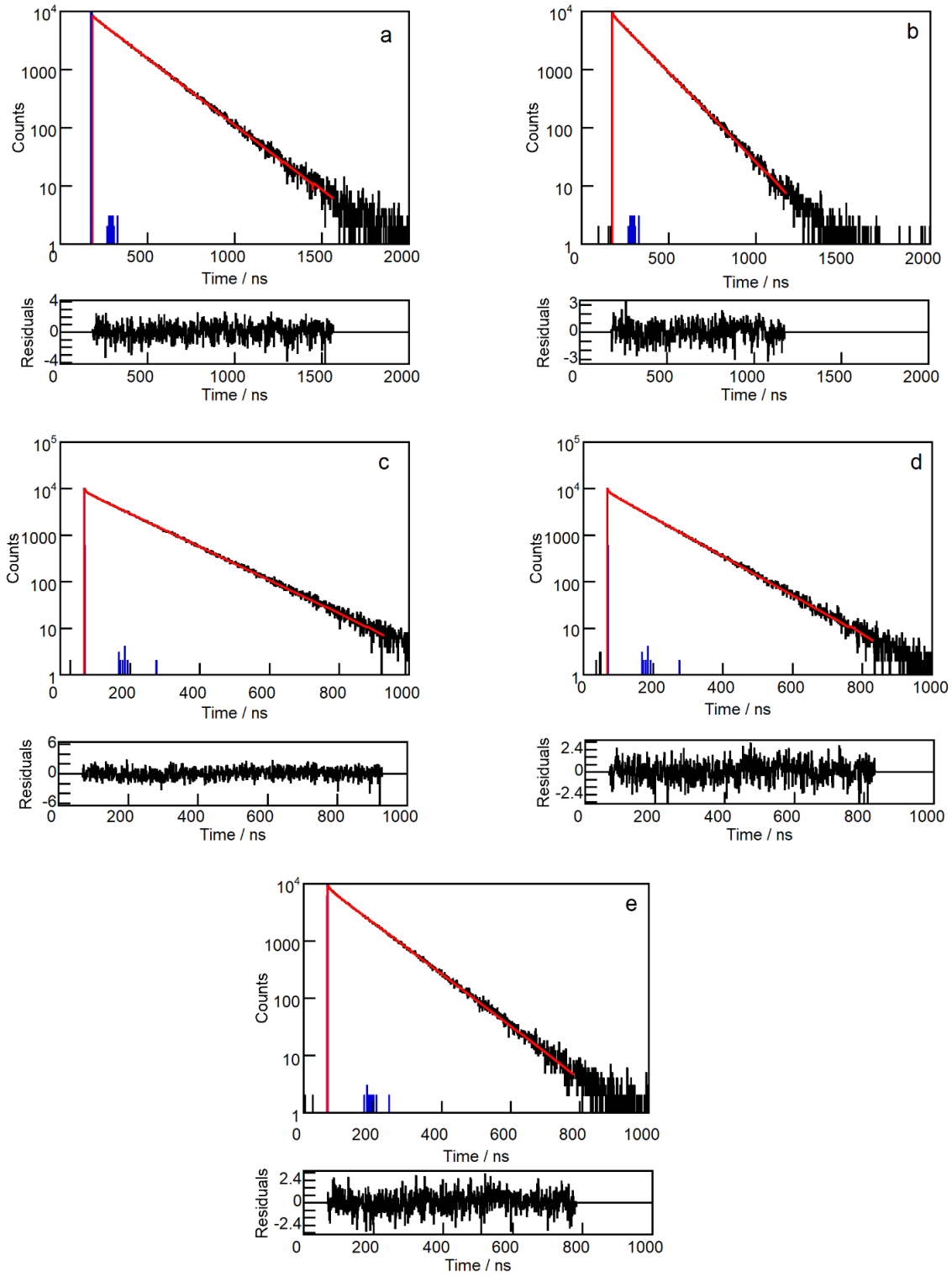

Figure 8.3. Fluorescence decay for 5 µM pyrene in 20% F127 at 30 °C (black) fit to a sum of exponentials decay (red). The IRF is shown in blue at different concentrations of NaI a) 0 mM, b) 14.9 mM, c) 30.8 mM, d) 45.7 mM, and e) 61.7 mM. Residuals between calculated and experimental data are shown in the lower panels.

Table 8.8. Fluorescence emission lifetimes and corresponding A values for 5 μM pyrene in the absence and presence of NaI in 20% F127 at 30 °C.

[NaI] / mM[b]	τ_1 / ns[a]	τ_2 / ns[a]	τ_3 / ns[c]	A_2[c]	A_3[c]	A_4[c]	χ^2
0	2.3	9.1	189.1±0.3	0.11±0.02	0.04±0.01	0.85±0.01	1.109
14.9±0.1	2.2	9.0	141.7±0.3	0.09±0.06	0.03±0.02	0.88±0.06	0.961
30.8±0.1	2.2	8.7	120.9±0.1	0.13±0.02	0.10±0.01	0.77±0.02	1.020
45.7±0.1	2.2	8.6	103.3±0.2	0.15±0.02	0.10±0.01	0.75±0.02	1.038
61.7±0.1	2.1	8.2	95.6±0.2	0.10±0.03	0.13±0.01	0.76±0.02	1.110

[a]Lifetimes correspond to F127 impurities were fixed.
[b]See 2.3.3 for method in the determination of the NaI concentration.
[c]The errors represent the standard deviations calculated using the F900 software. The data correspond to one experiment.

Table 8.9. Fluorescence emission lifetimes and corresponding A values for 5 μM pyrene in the absence and presence of NaI in 20% F127 at 20 °C.

[NaI] / mM[b]	τ_1 / ns[a]	τ_2 / ns[a]	τ_3 / ns[c]	A_2[c]	A_3[c]	A_4[c]	χ^2
0	2.3	9.1	227.6±0.3	0.5±0.2	0.2±0.3	0.3±0.6	1.101
14.9±0.1	2.2	9.0	165.0±0.3	0.18±0.06	0.08±0.02	0.74±0.05	1.011
30.8±0.1	2.2	8.7	135.9±0.2	0.23±0.02	0.10±0.01	0.67±0.02	1.077
45.7±0.1	2.2	8.6	120.4±0.2	0.24±0.02	0.10±0.01	0.66±0.02	1.141
61.7±0.1	2.1	8.2	109.9±0.2	0.22±0.02	0.13±0.01	0.65±0.02	1.148

[a]Lifetimes correspond to F127 impurities were fixed.
[b]See 2.3.3 for method in the determination of the NaI concentration.
[c]The errors represent the standard deviations calculated using the F900 software. The data correspond to one experiment.

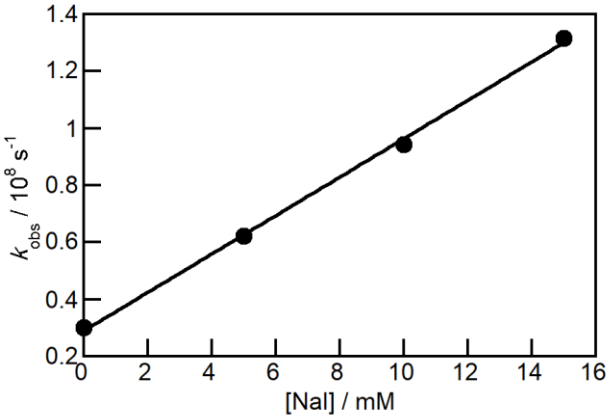

Figure 8.4. Quenching plot for 1 μM Np in water at 30 °C quenched by NaI. The data correspond to one experiment.

Table 8.10. Fluorescence emission lifetimes and corresponding A values of quenching impurities in 20% F127 with NaI at 30 °C (The excitation wavelength was 280 nm).

[NaI] / mM[b]	τ_1/ns[a]	τ_2 / ns[a]	τ_3 / ns[a]	A_1[a]	A_2[a]	A_3[a]	χ^2
0	0.4±0.1	4.1±0.1	12.1±0.2	0.84±0.01	0.14±0.01	0.02±0.01	1.073
4.8 ±0.1	0.4±0.1	4.1±0.1	11.7±0.3	0.84±0.01	0.14±0.01	0.02±0.01	0.992
10.2±0.1	0.4±0.1	3.9±0.1	11.0±0.2	0.84±0.01	0.14±0.01	0.02±0.01	1.001
14.9±0.1	0.4±0.1	3.8±0.1	10.9±0.2	0.84±0.01	0.14±0.01	0.02±0.01	1.059
19.9±0.1	0.4±0.1	3.8±0.1	11.0±0.2	0.84±0.01	0.14±0.01	0.02±0.01	1.025

[a]The errors represent the standard deviations calculated using the F900 software. The data correspond to one experiment.
[b]See 2.3.3 for method in the determination of the NaI concentration.

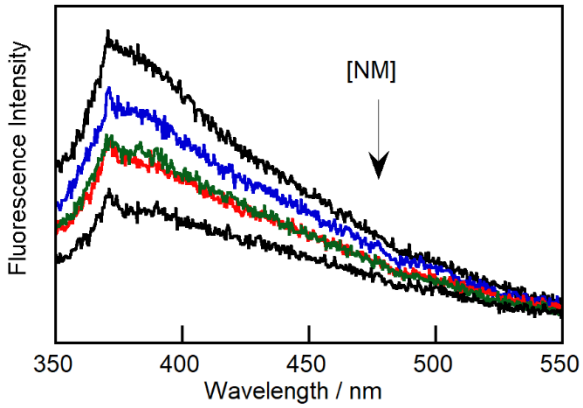

Figure 8.5. Fluorescence emission spectra of impurities in 34% P104 quenched with NM ([NM] = 0-61.5 mM).

Table 8.11. Fluorescence emission lifetimes and corresponding A values for 5 μM pyrene in the absence and presence of NM in 34% P104 at 30 °C.

[NM] / mM[b]	τ_1 / ns[a]	τ_2 / ns[a]	τ_3 / ns[c]	A_1[c]	A_2[c]	A_3[c]	χ^2
0	2.2	8.9	204±1	0.32±0.09	0.05±0.02	0.63±0.05	1.183
15.4±0.2	2.0	5.6	51±1	0.35±0.02	0.12±0.01	0.53±0.01	1.140
30.8±0.2	1.7	4.4	29±1	0.31±0.02	0.19±0.01	0.50±0.01	1.129
46.2±0.3	1.6	4.3	22±1	0.34±0.01	0.15±0.01	0.51±0.01	1.106
61.5±0.7	1.3	3.3	17±1	0.17±0.01	0.25±0.01	0.58±0.01	1.164

[a]Lifetimes corresponding to P104 impurities were fixed.
[b]See 2.3.3 for method in the determination of the NM concentration.
[c]The errors represent the standard deviations calculated using the F900 software. The data correspond to one experiment.

Table 8.12. Fluorescence emission lifetimes and corresponding A values for the quenching of impurities in 34% P104 with NM at 20 °C.

[NM] / mM[b]	τ_1 / ns[a]	τ_2 / ns[a]	τ_3 / ns[a]	A_1[a]	A_2[a]	A_3[a]	χ^2
0	0.3±0.1	2.2±0.1	7.7±0.2	0.50±0.04	0.45±0.02	0.05±0.01	1.009
15.4±0.2	0.4±0.1	2.0±0.1	6.1±0.3	0.49±0.03	0.46±0.02	0.05±0.01	0.931
30.8±0.2	0.3±0.1	1.8±0.1	4.9±0.2	0.53±0.06	0.40±0.02	0.07±0.01	0.988
46.2±0.3	0.2±0.1	1.5±0.1	4.0±0.1	0.54±0.08	0.37±0.03	0.09±0.01	0.928
61.5±0.7	0.2±0.1	1.5±0.1	3.9±0.2	0.61±0.09	0.33±0.03	0.06±0.01	0.990

[a]The errors represent the standard deviations calculated using the F900 software. The data correspond to one experiment.
[b]See 2.3.3 for method in the determination of the NM concentration.

Table 8.13. Fluorescence emission lifetimes and corresponding A values for 5 μM pyrene in the absence and presence of NM in 34% P104 at 20 °C.

[NM] / mM[b]	τ_1/ns[a]	τ_2/ns[a]	τ_3/ns[c]	A_1[c]	A_2[c]	A_3[c]	A_4[c]	χ^2
0	2.2	7.7	238±1	0.22±0.04	0.07±0.01	-	0.71±0.03	0.997
15.4±0.2	2.0	6.1	65±1	0.37±0.02	0.12±0.01	-	0.51±0.01	1.075
30.8±0.2	1.8	4.9	38±1	0.31±0.03	0.19±0.02	-	0.50±0.02	1.189
46.2±0.3	1.5	4.0	28±1	0.25±0.01	0.27±0.01	-	0.48±0.01	1.053
61.5±0.7	1.5	3.9	22±1	0.57±0.07	0.07±0.01	0.12±0.01	0.24±0.01	1.155

[a]Lifetimes corresponding to P104 impurities were fixed.
[b]See 2.3.3 for method in the determination of the NM concentration.
[c]The errors represent the standard deviations calculated using the F900 software. The data correspond to one experiment.

Table 8.14. Fluorescence emission lifetimes and corresponding A values for 5 μM pyrene in the absence and presence of NaI in 34% P104 with NaI at 30 °C.

[NaI] / mM[b]	τ_1 / ns[a]	τ_2 / ns[a]	τ_3 / ns[c]	A_1[c]	A_2[c]	A_3[c]	χ^2
0	2.7	9.2	206±1	0.21±0.03	0.06±0.01	0.73±0.03	1.072
4.8±0.1	2.8	8.9	176±1	0.21±0.03	0.06±0.01	0.73±0.03	1.046
10.2±0.1	2.8	8.3	155±1	0.22±0.03	0.05±0.02	0.73±0.03	1.007
14.9±0.1	2.7	8.1	143±1	0.25±0.08	0.06±0.03	0.69±0.01	0.977
19.9±0.1	2.6	7.4	132±1	0.16±0.04	0.11±0.02	0.73±0.03	0.990

[a]Lifetimes correspond to P104 impurities were fixed.
[b]See 2.3.3 for method in the determination of the NaI concentration.
[c]The errors represent the standard deviations calculated using the F900 software. The data correspond to one experiment.

Table 8.15. Fluorescence emission lifetimes and corresponding A values for 5 μM pyrene in the absence and presence of NaI in 34% P104 with NaI at 20 °C.

[NaI] / mM[b]	τ_1 / ns[a]	τ_2 / ns[a]	τ_3 / ns[c]	A_1[c]	A_2[c]	A_3[c]	χ^2
0	2.7	9.2	239±1	0.27±0.03	0.04±0.01	0.69±0.02	1.048
4.8±0.1	2.8	8.9	204±1	0.18±0.03	0.08±0.01	0.74±0.03	1.011
10.2±0.1	2.8	8.3	180±1	0.28±0.03	0.02±0.01	0.70±0.03	0.961
14.9±0.1	2.7	8.1	166±1	0.18±0.04	0.10±0.02	0.72±0.03	1.059
19.9±0.1	2.6	7.4	156±1	0.23±0.04	0.08±0.02	0.69±0.03	1.178

[a]Lifetimes corresponding to P104 impurities were fixed.
[b]See 2.3.3 for method in the determination of the NaI concentration.
[c]The errors represent the standard deviations calculated using the F900 software. The data correspond to one experiment.

Table 8.16. Fluorescence emission lifetimes and corresponding A values of quenching 5 μM naphthalene with NaI in 34% P104 at 30 °C.

[NaI] / mM[b]	τ_1/ns[a]	τ_2/ns[a]	τ_3/ns[a]	τ_4/ns[c]	A_1[c]	A_2[c]	A_3[c]	A_4[c]	χ^2
0	0.5	2.7	9.2	73±1	0.33±0.04	0.01	0.02	0.64±0.03	1.073
4.8±0.1	0.6	2.8	8.9	63±2	0.48±0.03	0.01	0.01	0.50±0.02	1.095
10.2±0.1	0.6	2.8	8.3	58±3	0.51±0.03	0.01	0.01	0.47±0.01	1.183
14.9±0.1	0.6	2.7	8.1	53±1	0.24±0.01	0.01	0.03	0.72±0.01	0.993
19.9±0.1	0.4	2.6	7.4	49±1	0.26±0.02	0.01	0.03	0.70±0.01	1.020

[a]Lifetimes corresponding to P104 impurities were fixed.
[b]See 2.3.3 for method in the determination of the NaI concentration.
[c]The errors represent the standard deviations calculated using the F900 software. The data correspond to one experiment.

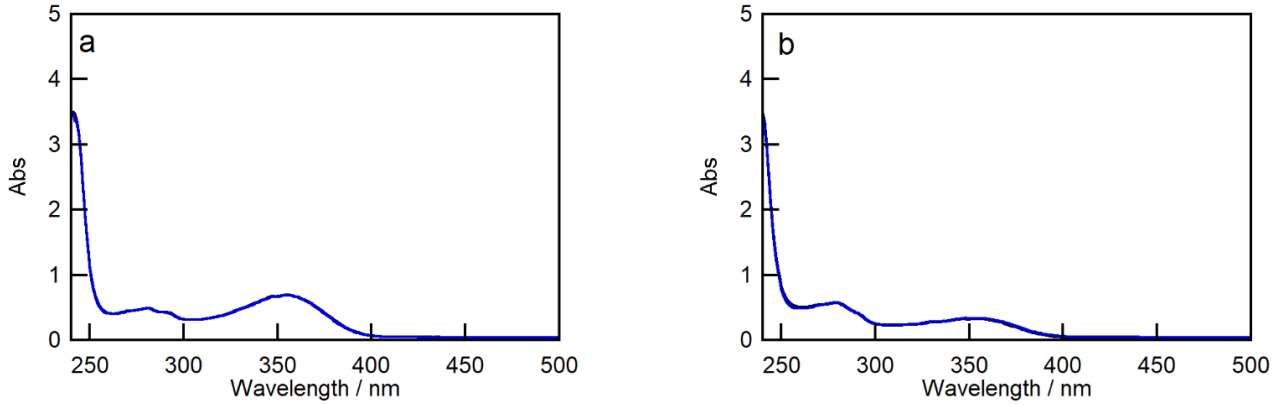

Figure 8.6. The absorption spectra of 80 μM 2-NpC in a) water-glycerol mixture, b) 20% F127 at 20 °C in the presence of 33 mM $NaNO_2$ before (black line) and after (blue line) performing LFP experiments.

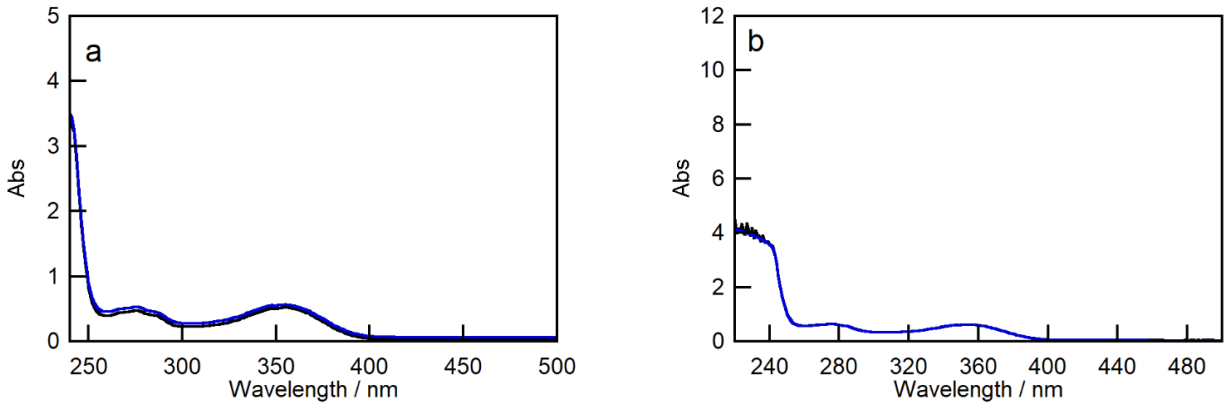

Figure 8.7. The absorption spectra of 80 μM NpOH in a) water-glycerol mixture, b) 20% F127 at 20 °C in the presence of 33 mM $NaNO_2$ before (black line) and after (blue line) performing LFP experiments.

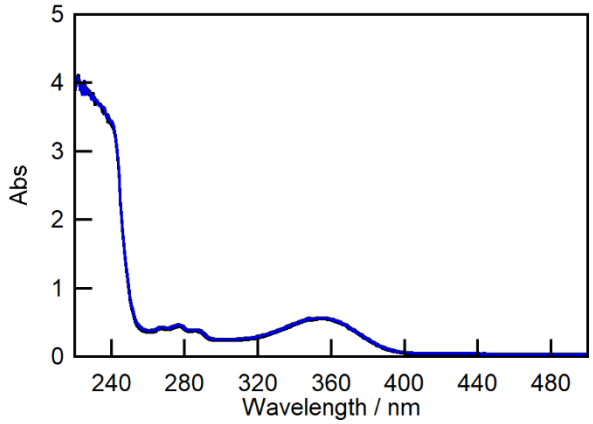

Figure 8.8. The absorption spectra of 80 μM Np in water-glycerol mixture at 20 °C in the presence of 33 mM $NaNO_2$ before (black line) and after (blue line) performing LFP experiments.

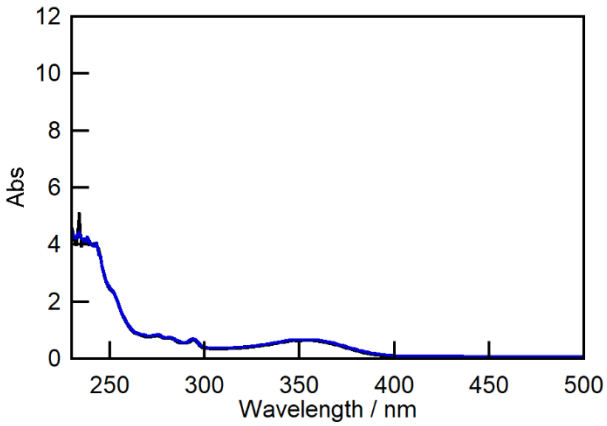

Figure 8.9. The absorption spectra of 30 μM Pht in 20% F127 at 20 °C in the presence of 33 mM $NaNO_2$ before (black line) and after (blue line) performing LFP experiments.